Finite Element Analysis of Carbon Nanotube (CNT)-Reinforced Composites having a Broken CNT

A Thesis Submitted in

Partial Fulfillment of the Requirements

for the Degree of

DOCTOR OF PHILOSOPHY

by

Sushen Kirtania

Department of Mechanical Engineering

Indian Institute of Technology Guwahati

Guwahati - 781039, India

August 2016

Department of Mechanical Engineering
Indian Institute of Technology Guwahati
Guwahati - 781039, India

Certificate

It is certified that the work contained in this thesis entitled " **Finite Element Analysis of Carbon Nanotube (CNT)-Reinforced Composites having a Broken CNT**" submitted by **Sushen Kirtania (Roll no. 07610305)** to Indian Institute of Technology Guwahati for the award of the degree of **Doctor of Philosophy** has been carried out under my supervision in the Department of Mechanical Engineering. The contents of this thesis, in full or parts have not been submitted elsewhere for a degree.

.

Debabrata Chakraborty
Professor, Mechanical Engineering Department
Indian Institute of Technology Guwahati
Guwahati - 781039, Assam, India

Dedicated to my family
for
their love and support

Acknowledgments

I would like to express my gratitude to my supervisor, Dr. Debabrata Chakraborty for his guidance and extensive support throughout my PhD thesis work. I am obliged for being introduced to such a relevant area of research. His valuable suggestions and constant encouragement helped me a lot in completing my PhD thesis work successfully.

I would like to express my sincere gratitude to my doctoral committee members, Prof. Sashindra K. Kakoty, Prof. K. S. R. Krishna Murthy and Prof. Anjan Dutta for reviewing my entire work with furnishing their valuable comments and suggestions.

I am thankful to all the faculty and staff members of the Mechanical Engineering Department and many individuals who were directly and indirectly helped me at IIT Guwahati.

I would like to thank all my friends, particularly Dr. Bitta Gopal Mondal, Dr. Bidyut Kr. Patra, Dr. Sachin Kr. Singh, Mr. Pranjol Paul, Mr. Purnendu Kr. Mondal, Dr. Jagannath Sardar, Mr. Rakesh Bhadra, Mr. Arpan Kr. Mondal, Mr. Biplab Das and many more with whom I have come into contact during my PhD study.

I would like to extend my sincere thanks to my colleagues Mr. Polash Pratim Dutta, Mr. Paragmoni Kalita, Dr. Ratul Baruah, all the colleagues in the Mechanical Engineering Department and many others at Tezpur University for their help and support in different ways during my PhD study.

I would like to express my deepest appreciation to my wife Smt. Soma Kirtania for her understanding and patience during my entire course of time. Without her it would not have been possible on my part to complete the work successfully. I would like to extend my love to our beautiful son master Souhrid Kirtania who served as an inspiration in pursuing this undertaking.

Finally, I am grateful to my parents, elder brother and all of my family members for their love, patience and support.

Above all, I am thankful to the Almighty.

Sushen Kirtania

ABSTRACT

The present thesis deals with three dimensional (3D) finite element (FE) analysis of carbon nanotube (CNT)-reinforced composites starting with determination of thermoelastic properties to failure analysis of such composites having a defect in the form of broken CNT fiber. Owing to the fact that experimental determination of thermoelastic properties of CNT composites are difficult, FE analysis has been performed on a representative volume element (RVE) of the CNT-reinforced composites to determine thermoelastic properties and to understand not only the effect of important parameters on the properties but also the effect of types of modeling on the estimated properties. Eight noded solid elements have been used to develop the FE model and appropriate properties of matrix and the CNT are input. Different types of matrix materials viz. polymer, metal and ceramic; and nonlinear stress strain relation of the CNT has been considered in the analysis. Considering the fact that CNTs are the main load bearing member and volume fraction of CNTs in CNT-reinforced composites are much lower compared to that in conventional fiber (like glass or carbon) reinforced composites, it is important to understand the consequence of having one or more CNTs defective which may break during loading. Therefore, FE analysis of CNT-reinforced composite having one CNT broken has been performed, first to study the stress redistribution near the vicinity of such break especially the induction of interfacial stresses at the interface of the broken CNT and the matrix which might lead to debonding of the fiber from the matrix and to determine the ineffective length of the broken CNT. Secondly, strain energy release rate (SERR) components near the vicinity of the broken CNT have been determined to understand the propensity of fiber matrix debonding from such break using linear elastic fracture mechanics (LEFM). At the end an attempt has been made to numerically determine the critical SERR of a broken CNT composite using LEFM and stress based failure criterion.

Based on the results of FE analysis, some important conclusions have been drawn. It has been observed that even a very small volume fraction (~3%) of CNT increases the elastic modulus of matrix substantially, and leads to a very low coefficient of thermal expansion of the resulting composite thus improving the thermal stability of the composite. Ineffective length of a broken CNT in a CNT-reinforced composite is also observed to be dependent on the matrix material and for stiffer matrix material it is low thus enabling a major length of the broken CNT to actively participate in the load bearing. Mode-II SERR component is observed to be also dependent on the matrix materials and volume fraction. Mode-II SERR of CNT/epoxy composite is approximately three times more compared to that in conventional carbon fiber/epoxy composites. Critical SERR determined using the FE analysis and LEFM shows qualitative agreement with available results and could be used to decide the growth of debonding from a fiber break in a CNT-reinforced composite.

भारतीय प्रौद्योगिकी संस्थान गुवाहाटी
Indian Institute of Technology Guwahati

Table of Contents

भारतीय प्रौद्योगिकी संस्थान गुवाहाटी
Indian Institute of Technology Guwahati

List of Figures

भारतीय प्रौद्योगिकी संस्थान गुवाहाटी
Indian Institute of Technology Guwahati

List of Tables

भारतीय प्रौद्योगिकी संस्थान गुवाहाटी
Indian Institute of Technology Guwahati

List of Symbols

a	Length of unit vector / Crack length
$2a$	Thickness (or width) of the square representative volume element (RVE)
$\mathbf{a}_1$ and $\mathbf{a}_2$	Unit vectors
A_c	Cross sectional area
ΔA	Virtual extension area of the crack
Δa	Virtual extension length of the crack
$\mathbf{C}_h$	Chiral vector
E_1	Axial Young's modulus of composite
E_2	Transverse Young's modulus of composite
E_{nt}	Young's modulus of the CNT
E_m	Young's modulus of matrix material
E_f	Young's modulus of fiber
F_a	Total axial force
F_{ms}	Matrix shear strength
F_6	Inplane shear strength of the composites based on matrix shear failure
G_I	Mode-I strain energy release rate (SERR)
G_{II}	Mode-II SERR
G_{III}	Mode-III SERR
G_c	Critical SERR
G_{IIc}	Critical more-II SERR
G_{12}	Longitudinal shear modulus of composites
G_{23}	Transverse shear modulus of composite
G_f	Shear modulus of fiber
G_{12f}	Fiber axial shear modulus
G_m	Matrix shear modulus
G_T	Total SERR
L	Circumference of the CNT
L_a	Initial axial length of the model

ΔL_a	Elongation in axial direction
L_t	Initial transverse length of the model
ΔL_t	Elongation in transverse direction
n, m	Number of steps along the zigzag carbon bonds
P_y	Constant pressure load applied along y-direction
r_i	Inner radius of the CNT
r_0	Outer radius of the CNT
S_{rr}	Interfacial normal strength for σ_{rr} stress
S_{rz}	Interfacial shear strength for τ_{rz} stress
S_{rr}	Interfacial shear strength for τ_{rs} stress
t	Thickness of CNT
ΔT	Change in temperature
V_f	Fiber volume fraction
V_m	Matrix volume fraction
V_{nt}	Volume fraction of CNT
θ	Chiral angle
α_1	Axial coefficient of thermal expansion (CTE) of composite
α_2	Transverse CTE of composite
α_{nt}	CTE of CNT
α_m	CTE of matrix materials
ν_{nt}	Poisson ratio of CNT
ν_m	Poisson ratio of matrix material
ν_{12}	Effective Poisson's ratio / Longitudinal (major) Poisson's ratio of composite
ν_{23}	Transverse Poisson's ratio of composite
ν_f	Poisson's ratio of fiber
κ_t	Shear stress concentration factor
σ_n	Normal stress

σ_{rr}	Interfacial normal stress components ahead of the debonding responsible for mode-I
τ_{rz}	Interfacial shear stress components ahead of the debonding responsible for mode-II
$\tau_{rs} / \tau_{r\theta}$	Interfacial shear stress components ahead of the debonding responsible for mode-III
σ_{zz}	Axial normal stress along *z*-direction
$\varepsilon / \varepsilon_n$	Normal strain

भारतीय प्रौद्योगिकी संस्थान गुवाहाटी
Indian Institute of Technology Guwahati

List of Acronyms and Abbreviations

Al	Aluminium
Al_2O_3	Alumina
ANS	Axial normal stress
C-C bond	Carbon-carbon bond
CF	Carbon fiber
CMCs	Ceramic matrix composites
CNT	Carbon nanotube
CTE	Coefficient of thermal expansion
Cu	Copper
DOF	Degree of freedom
FE	Finite element
FRC	Fiber reinforced composite
GPa	Gigapascal
HA	Hydroxyapatite
IFNS	Interfacial normal stress
IFSS	Interfacial shear stress
IPS	In-plane shear
LEFM	Linear elastic fracture mechanics
MD	Molecular dynamics
MM	Molecular mechanics
Mg	Magnesium
MMCs	Metal matrix composites
MPa	Megapascal
MWCNT	Multi-walled CNT
PAN	Polyacrylonitrile
PMCs	Polymer matrix composites
PP	Polypropylene
PS	Polystyrene
QSC	Quadratic stress criterion

ROM	Rule of mixture
RVE	Representative volume element
SCF	Stress concentration factor
SERR	Strain energy release rate
SWCNT	Single-walled CNT
TEEP	Thermoelastic extremum principle
Ti	Titanium
TPa	Terapascal
VCCI	Virtual crack closure integral
3D	Three dimensional

Chapter 1

Introduction

1.1 History and background

The concepts of nanoscience and nanotechnology started with a talk entitled "There's Plenty of Room at the Bottom" delivered by American physicist Richard Feynman [1] at the annual meeting of the American Physical Society at the California Institute of Technology in December, 1959, which is considered as a seminal event in the history of nanotechnology. In his talk, he described a process in which scientists would be able to manipulate and control individual atoms and molecules. He also predicted that future science and technology would be focused on miniaturization and every machine, structure and instruments would be designed start from atomic scale. This talk was the first inspirational talk to work in the field of nanotechnology and hence physicist Feynman is known as father of nanotechnology. Professor Taniguchi [2] of the Tokyo Science University first defined the term "Nanotechnology" in 1974. He defined Nano-technology as "the processing of separation, consolidation, and deformation of materials by one atom or one molecule". Nanoscience and nanotechnology are the study and application of extremely small things and can be used in all the fields, such as chemistry, biology, physics, materials science and engineering.

Among many potential applications of nanotechnology, nanocomposites have been one of the recent important research areas. Carbon nanotubes (CNTs) are believed to be ideal reinforcing materials for high performance structural composites due to their inherent advantages like high strength-to-weight ratio, high aspect ratio along with superior thermal, electrical and mechanical properties. These CNTs are also chemically inert and are able to sustain a high strain without breakage. Due to these superior properties, CNT-reinforced nanocomposites have been one of the important research areas for last twenty years. The main constituent in a CNT-reinforced composite is CNT and therefore it is important to understand the basic characteristic of CNT.

1.2 Carbon nanotubes (CNTs)

Nanotubes were discovered by Iijima [3] in 1991 and after that a revolution started on research on nanotechnology in different directions. Nanotubes belong to a class of materials which exhibit a variety of fascinating properties and offer a diversity of issues for research in both fundamental issues and practical interest. Carbon nanotubes are molecular-scale tubes of graphitic carbon with outstanding properties. They are among the stiffest and strongest fibers known, and have remarkable unique characteristics. It is as stiff as diamond. It has been estimated that the CNTs could be designed as a longest cable in the world i.e. a 23000 miles cable from space station to the Earth without suffering a high gravitation force due to its own weight at that length [4]. Carbon nanotubes exhibit extraordinary properties [4-5] having Young's modulus of the order of 1 TPa, tensile strength of 200 GPa and strain 10-30% without breakage. These are also thermally stable up to 2800 ^{0}C in vacuum and have thermal conductivity about two times higher than that of diamond and electrical-current-carrying capacity 1000 times higher than that of copper wires.

Large aspect ratio makes them extremely suitable for use in miniature electronics, advanced composites, and as biological molecules in various biotechnological applications. In particular, owing to their extraordinary thermal conductivity, mechanical and electrical properties, carbon nanotubes find applications as additives and reinforcements to various structural materials. Properties like very high modulus of elasticity exceeding that of steel, high tensile strength, very low density, high chemical inertness, negative coefficient of longitudinal thermal expansion and very high toughness make CNT to be used as fiber in high performing materials in the field of aerospace, sports, automobile, military and many other applications. Due to these superior properties they have attracted huge academic and industrial interest with potential structural applications.

1.2.1 Atomic arrangement of CNTs

Before analysis of CNT-reinforced composites, it is important to understand the physics of an isolated CNT. Depending on the direction of hexagons, nanotubes can be classified into three types viz. zigzag, armchair and chiral. Figure 1.1 shows the different types of CNTs formed from a hexagonal graphene sheet. If a rectangle (*ABCD*) is cut from the graphene

sheet and rolled up in such a way that the tip (*B*) of the chiral vector ($\mathbf{C}_h$) touches its tail (*A*), chiral CNT is produced.

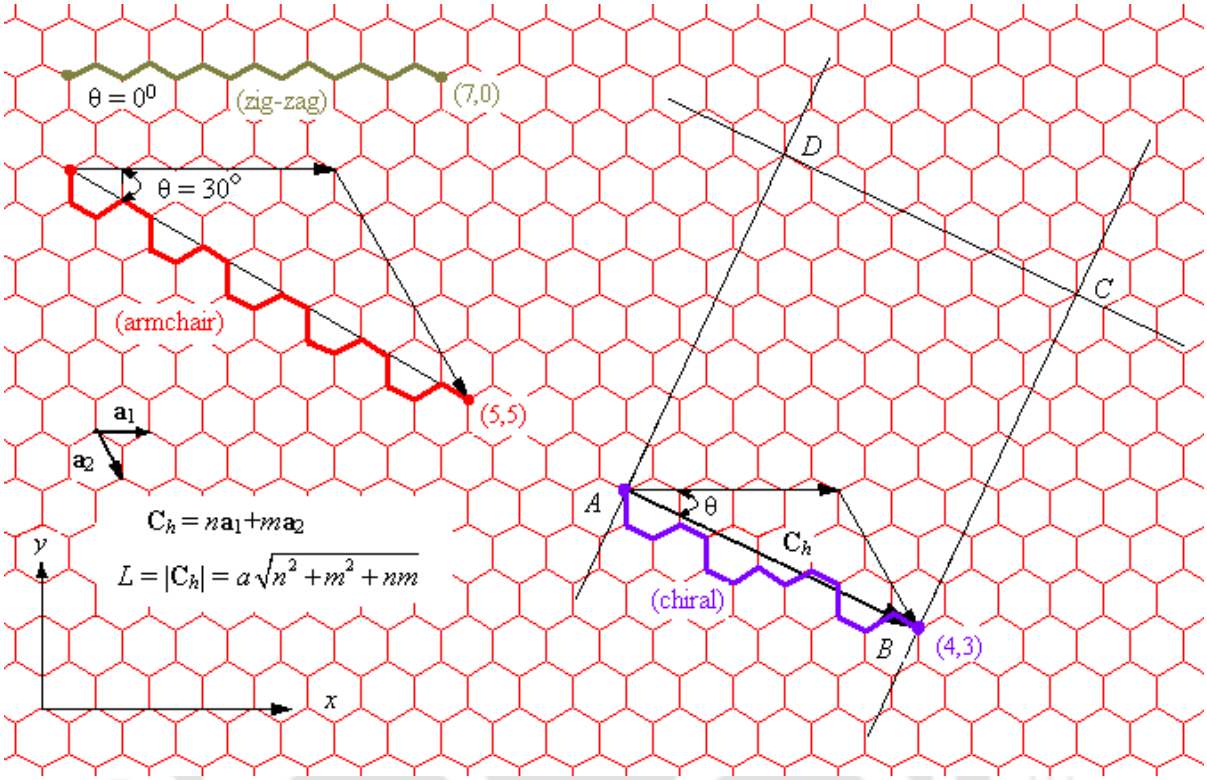

Figure 1.1 Formation of different types of CNTs [zigzag (7,0), armchair (5,5) and chiral (4,3)] by rolling up a hexagonal graphene sheet.

The atomic arrangement of CNTs can be described by the tube chiral vector and chiral angle (θ). The chiral angle determines the amount of twist in the tube. If $\theta = 0^0$ and 30^0 it will form zigzag and armchair CNTs, respectively and for $0^0 < \theta < 30^0$, it will form chiral CNT. The chiral vector is also known as the roll-up vector and it can be described by the following equation [6].

$$\mathbf{C}_h = n\mathbf{a}_1 + m\mathbf{a}_2 \tag{1.1}$$

where the integers (*n*, *m*) are the number of steps along the zigzag carbon bonds and $\mathbf{a}_1$ and $\mathbf{a}_2$ are unit vectors as shown in Fig. 1.1.

The circumference of the CNTs is also determined by the following equation [6]

$$L = |\mathbf{C}_h| = a\sqrt{n^2 + m^2 + nm} \tag{1.2}$$

where *a* is the length of unit vector.

Figures 1.2 shows the front view and pictorial view of an armchair (10,10) single-walled CNT (SWCNT) . SWCNT can be formed by rolling up a graphene sheet as shown in Fig. 1.1.

1.2.2 Types of CNTs

Depending on the direction of hexagons, nanotubes can be classified as zigzag, armchair and chiral as described in the previous section 1.2.1. CNTs can also be classified on the basis of number of CNT layers i.e. SWCNT and multi-walled CNT (MWCNT). The distance between two layers for MWCNT is equal to 0.34 nm [6-7]. Figure 1.3 shows a MWCNT with five numbers of layers [8].

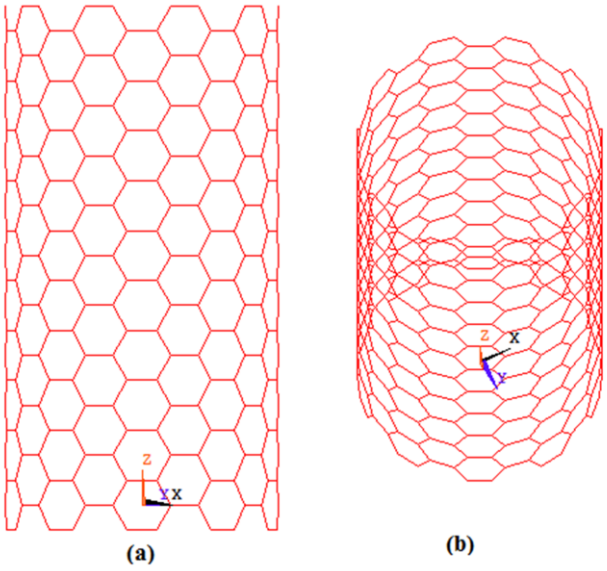

Figure 1.2 An armchair SWCNT (10,10) (a) front view and (b) pictorial view.

1.2.3 Advantages and applications of CNTs

Since discovery of CNT in 1991, researches on CNTs have been given much attention due to their remarkable properties and potential applications. It has been reported that the CNTs could be used as reinforcing element for light weight and high structural composites. Therefore, researchers have been trying to apply CNT in real life application since CNT have lots of advantages and applications.

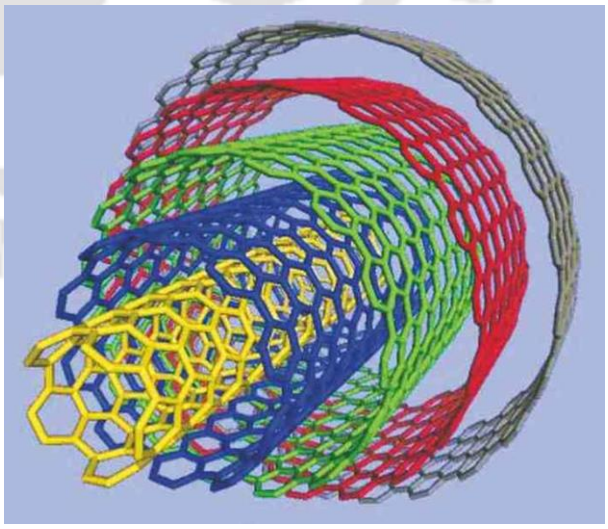

Figure 1.3 A MWCNT with five layers [8].

1.2.3.1 Advantages of CNTs

Some of the important advantages of CNT are listed below

- High strength to weight ratio
- High mechanical strength (at least 10 - 100 times stronger than steel)
- High aspect ratio (1000 - 100000)
- High specific surface area (1315 m^3/g)
- Light weight/Low density (1800 Kg/m^3)
- High strain (10% – 30% without breakage)
- Very high toughness
- Chemical inertness
- High electrical and thermal conductivuty
- Low coefficient of thermal expansion (CTE)

1.2.3.2 Applications of CNTs

The outstanding properties of CNTs make them potential candidate to be used in different fields. Some of the important applications of CNTs are listed below

- The important potential applications of such CNTs are their use as reinforcement in structural composites leading to the CNT fiber reinforced composites.
- Energy storage and environment (lithium ion batteries for notebook computer and mobile phones, supercapacitors, solar cell, portable water filter)
- Multifunctional coating materials (paint/MWCNT mixtures can reduce bio fouling of ship hull)
- Artificial muscles (CNT sheet)
- Tribological application
- Fuel cell, solar cell (SWCNT sheet)
- Sensors and actuators
- Capacitor
- Nanoelectronic devices (since low defect density of SWCNT)
- Electrode or light emitting diode (MWCNT or SWCNT sheet)
- Microelectronics (memory cell, transistors, high power amplifiers to enhanced thermal dissipation)

- Atomic force microscopy (AFM) probe tips: Single-walled carbon nanotubes have been attached to the tip of an AFM probe to make the tip sharper. This allows much higher resolution imaging of the surface under investigation.

1.3 Composites materials

In studying the potential applications of CNTs as reinforcements in CNT-reinforced composites, it is essential to understand some of the important fundamentals of conventional fiber composites. Composite materials are made by combining two or more materials at microscopic scale often ones that have very different properties. As in the case of alloys, combining metals dissolve into each other and forms a different material, but within the composite materials the constituting materials do not dissolve or blend into each other.

Metals are the most commonly used materials in these domains. In the last two-three decades, there have been specific requirements on the properties of these materials. It is impossible for any material to fulfill all these properties. Therefore, there is an intense need for new materials with improved desired properties. The properties like strength, stiffness, toughness, high corrosion resistance, high wear resistance, high chemical resistance, reduced weight, high fatigue life, thermal insulation, conductivity, reduced cost, attractiveness are few of an in-exhaustive list of desired properties which are required to be fulfilled by a material to be selected for any application. All the desired properties are difficult to find in a single material. Many of the above properties could be achieved in composites materials.

The most important characteristics of composite materials are that their properties can be tailored (one can design the required properties). The biggest advantage of modern composite materials is that they are light as well as strong. By choosing an appropriate combination of matrix and reinforcement material, a new material can be made that exactly meets the requirements for a particular application. The need for application based properties can only be fulfilled by the composite materials. Approximately all machines and structures are striving for light weight, high strength and economically affordable materials. Composites also provide design flexibility because many of them can be molded into complex shapes. Although the resulting product is more efficient, the raw materials are often expensive. Therefore, scientist and researchers are giving special attention towards the development of cheaper composite materials.

1.3.1 Fiber-reinforced composites

There are various reasons because of which the reinforcement is made in thin fiber form. An experiment by Leonardo da Vinci on the tensile strength of iron wires of various lengths showed that the wires of same diameter with shorter length showed higher tensile strength than those with longer lengths [9]. The reason for this is the fact that the number of flaws in a shorter length of wire is less as compared to longer length wire. Further, it is well known that the strength of a bulk material is much less than the strength of the same material in wire form. The same concept also applies behind the strength of composites with reinforcement in fiber form. As the fibers are made of thin diameter, the inherent flaws in the material decrease. Hence, the strength of the fiber increases as the fiber diameter decreases. Typically, composite material has two constituents. One of the constituent acts as a reinforcement and other acts as a matrix. Composites materials can be classified based on the different form of reinforcement are –

- particle reinforced composites,
- flake reinforced composites and
- fiber reinforced composites

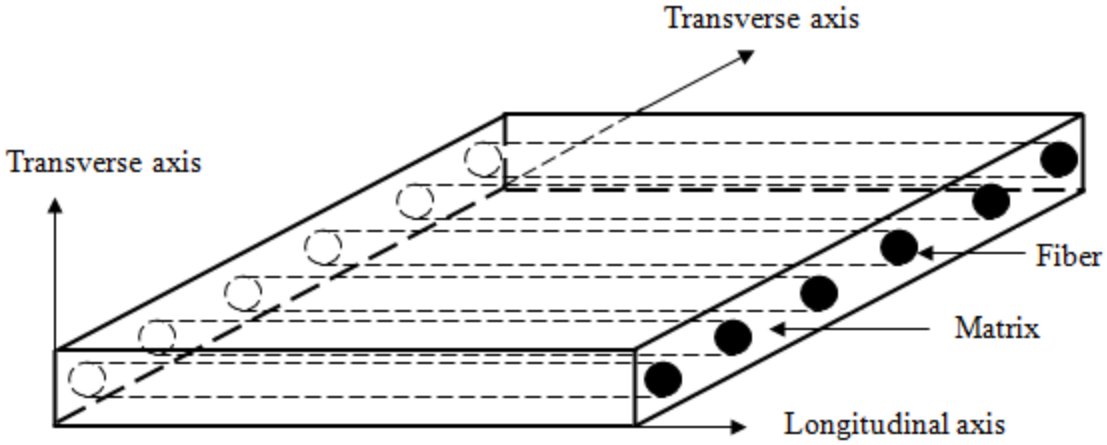

Figure 1.4 A unidirectional lamina.

In a fiber reinforced composites (FRC), fibers are the main source of strength and the function of the fiber is to carry the load along their longitudinal direction. The matrix hold all the fibers together and the function of the matrix are to transfer stress between the reinforcing

fiber. Fibers can be placed in any orientation/direction. Fiber in a lamina may be aligned, random or woven. A unidirectional fiber reinforced lamina is shown in Fig. 1.4.

In a fiber reinforced composites, a laminate is fabricated by adding lamina in different stacking sequence. Laminas are stacked together by adding a thin layer between those laminas and this thin layer is known as interface. Therefore, a FRC consists of three components – fibers, matrix materials and interface region. Figure 1.5 shows the development of a laminate from different stacking sequence of laminas. Different orientations of fibers in lamina provide different directional strength and stiffness. Combination of such lamina provides the desired directional strength and stiffness of the composite.

1.3.2 Different types of fibers used in composite materials

The strength of the FRC depends on the properties of the fibers, the matrix and the interfacial bond between them. The properties of fiber-reinforced composite materials are anisotropic. It has high specific strength and high specific modulus. The longitudinal tensile strength is higher than that of transverse tensile strength. Even the transverse tensile strength is less than that of the matrix tensile

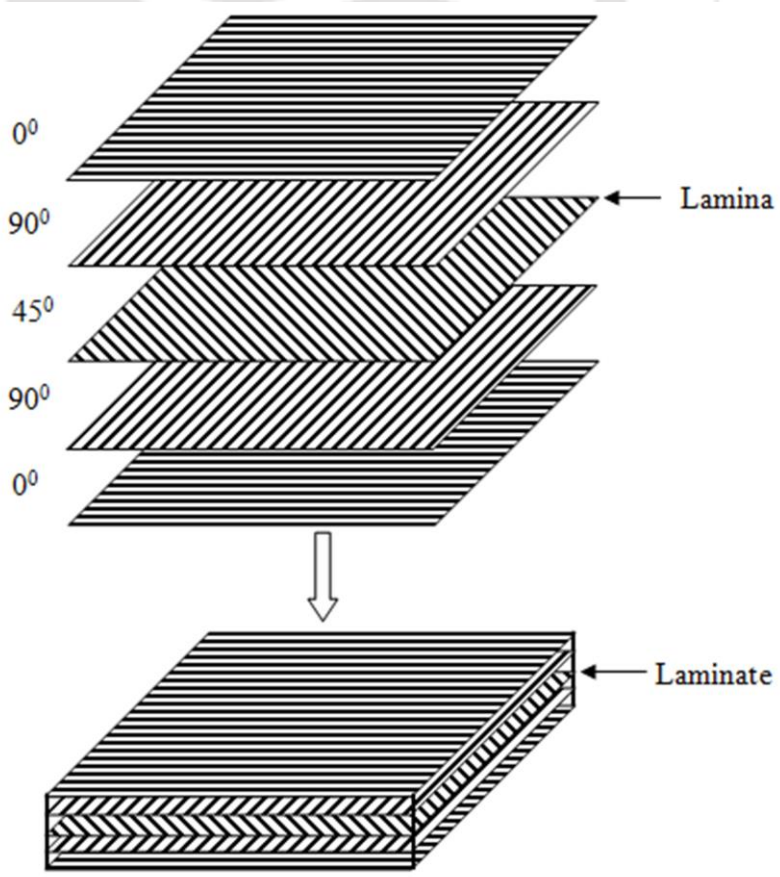

Figure 1.5 Laminae stacked to form a laminate.

strength. There are different types of fibers used as reinforced element in matrix (mainly polymer). The most common fibers are –

- Carbon fibers,
- Glass fiber,
- Boron fiber and
- Aramid fiber

These different types of fibers have their own advantages and limitations. Depending upon the type of applications, a laminate may be made either from a single type of fiber or sometimes may comprise more than one type of fibers leading to hybrid laminates.

Depending upon the type of the matrix, fiber reinforced composites are classified as

- polymer matrix composites (PMCs),
- metal matrix composites (MMCs),
- ceramic matrix composites (CMCs) and
- carbon-carbon composites (CCCs).

1.3.3 Advantages and applications of composite materials

1.3.3.1 Advantages of composite materials

Composites parts have many advantages compared to metals parts. Some of the important advantages of composites materials are listed below -

- High specific stiffness and specific strength
- High impact strength
- High strength to weight ratio
- Hugh fatigue life
- Dimensional stability
- High resistance to corrosion
- Durable
- Design flexibility: A large set of design parameters are available to choose from which desired properties can be obtained in the final product. Some available design parameters are - choice of materials (fiber/matrix), volume fraction of fiber and matrix, fabrication method, layer orientation.

- Cost effective fabrication: Since lesser wastage of the raw materials as the product is fabricated to the final product size unlike in metals.
- Thermal conductivity: Low thermal conductivity which can be used as insulator (glass/polyesters) or a high thermal conductivity (copper matrix material).

1.3.3.2 Applications of composite materials

Composite materials are extensively used worldwide in every field. Some of the applications are listed below under different group -

- Aerospace like - satellites, rockets, space telescopes, space shuttle helicopters and its parts etc.
- Missile like - silicon carbide ceramic matrix composite are used in high temperature and hot structures etc.
- Transportation and infrastructure like - railway coaches (doors, interior walls, interior furnishing and seating) and composite brake-blocks, bridges, ships and boats, truck bodies and floors, dams etc.
- Sports equipment like - bicycle frame, base-ball bats, tennis racquets, cricket bats, fishing rods, arrows in archery etc.
- Automotive parts like - drive shafts, fan blades, springs, bumpers, interior panels, tires, brake shoes, clutch plates, gaskets, hoses, belts etc.
- Medical like - artificial muscles, wheelchairs, hip joints, heat valves, dentistry, surgical equipment, stretcher etc.
- Electronic applications like - integrated circuits, processors, RAM/ROM hard disk CD drive, interconnection, heat sinks etc.
- Military applications like - helmets, bullet proof vests, impact resistant vehicles, composite soldier etc.

1.4 Carbon nanotube-reinforced composites

There has been a continuous drive to improve the efficiency of current technology by incorporating the new technologies. The CNT-reinforced composites give a better solution to this problem in terms of strength and effectiveness. Researchers and scientist are constantly working with the CNTs and are coming up with new solutions and materials to combat this

problem. Behavior of nanocomposites depends entirely on the size of the fibers added. For the past several years, automobile companies have been using nanocomposites instead of plastic to make certain parts. The development of a new manufacturing process of CNT-reinforced composites with high purity, geometrical identity, productivity, and low cost is an important factor in bringing the CNT-reinforced nanocomposites to be more acceptable to the society. Recently, CNT-reinforced composites have been used in many engineering components and in future CNT-reinforced composite will play a significant role in developing future space vehicles and could be used to manufacture different goods which are being used in our daily life. Therefore CNT-reinforced composites have been termed by experts as the "material of the 21st century".

1.4.1 Advantages of CNT-reinforced composites

Some of the important advantages of CNT-reinforced composites over conventional fiber-reinforced composites are listed below -

1.4.1.1 Advantages of CNT/polymer matrix composites

- High stiffness and strength
- High interfacial shear strength
- High thermal and electrical conductivity
- High thermal and chemical stability
- Low coefficient of thermal expansion
- High fracture toughness
- Low solar absorptive
- High optical transparency
- High thermal emissivity and stability

1.4.1.2 Advantages of CNT/metal matrix composites

- High strength and toughness
- High elastic modulus
- Light weight/Low density
- Low coefficient of thermal expansion

- High thermal conductivity
- Good electrical conductivity
- Ni-P-CNT composites coating exhibited higher wear resistance and lower friction coefficient than Ni-P-SiC and Ni-P-graphite composites coating
- Lower wear rate and coefficient of friction of CNT/copper (Cu) composites compared to pure copper

1.4.1.3 Advantages of CNT/ceramic matrix composites

- High temperature stability
- Improved wear resistance and lower friction coefficient [CNT/hydroxyapatite (HA)]
- Enhanced fracture toughness and flexural strength (CNT/HA composites)
- Enhancement of compressive strength
- High creep resistance
- Improve abrasion resistance

1.4.2 Potential uses of CNT-reinforced composites

Depending upon the matrix, CNT-reinforced composites may be

- CNT-reinforced polymer matrix composites (CNT/PMCs),
- CNT-reinforced metal matrix composites (CNT/MMCs) and
- CNT-reinforced ceramic matrix composites (CNT/CMCs) each are having their specific advantages to be used as structural composites.

Some of the important potential applications of CNT-reinforced composites are presented next.

1.4.2.1 Application of CNT/polymer matrix composites

A thermoset resin such as epoxy or other thermoset or thermoplastic polymers, such as polyester, vinyl ester or nylon are sometimes used in the CNT-reinforced epoxy composites. Some common applications of the CNT/PMCs are given below -

- Space applications (ultra-light weight space structures, thermal optical coating, multi-layer thermal insulation blanket materials)

- Sports goods (Tennis racquets, baseball bats, bicyle frame) since CNT/polymer contact can increase materials damping
- Bullet proof vests [SWCNT/poly(vinyle alcohol)]
- Wind blades (CNT/polyurethane)
- CNT sheet and yarn used as lightweight data cables electromagnetic shielding materials
- Composite gear (CNT/nylon) less than 1 nm in diameter
- Lightweight CNT-fiber composites boat hull for maritime security boats
- Oil mining (CNT/rubber composites)
- Electronics applications (Sensors and actuators)
- Supercapacitors or electrochemical capacitors (SWCNT/polyacylonitrile)

1.4.2.2 Application of CNT/metal matrix composites

CNT-metal matrix composites are emerging class of new materials that are being developed to take advantage of the high tensile strength and electrical conductivity of CNTs. A homogeneous dispersion of CNTs in the metal matrix provides a strong interfacial adhesion between matrix and CNTs. Some of the applications of CNT/MMCs are given below -

- Automobile (Break shoes, cylinder liner, piston rings, gears)
- Aerospace (Aircraft breaks, landing gear)
- Sports goods (Lightweight bicycles, tennis and badminton rackets)
- Heat sink (CNT/Cu composite)
- Lightweight structure
- Micro-electro-mechanical system (MEMS) and sensor (micro-beams and micro-gears)
- Electronic [Solder, electronic packaging materials (CNT/aluminum (Al))]
- Tribological applications for higher wear resistance and lower coefficient of friction

1.4.2.3 Application of CNT/ceramic matrix composites

In ceramic matrix CNT reinforced nanocomposite main part of the volume is occupied by a ceramic such as oxides, nitrides, borides, silicide etc. and the dispersant phase is CNTs. Studies on CNT/CMCs are few as compared to those on CNT/PMCs and CNT/MMCs. However, ceramics have many advantages over metal such as under harsh conditions, the CNT-reinforced MMCs cannot be used effectively. Therefore, from structural point of view, ceramics have many advantages over metals even though it is more brittle than metals. Alumina-coated CNTs were found to be best suited for interfacial adhesion with the ceramic matrix. Some of the important applications of CNT/CMCs are -

- Thermal barrier coating on turbine blade (since turbine blade operate at extremely high temperature and mechanical loading conditions)
- Light weight armor made of CNT/boron carbide nanocomposites
- Biomedical engineering such as CNT/HA nanocomposites for hard tissue replacement.
- Bearings, valves and other wear resistance machine parts (CNT/alumina composites are highly resistance to contact damage)
- Coating materials for biomedical implants under high load bearing conditions (CNT/HA composites)
- Aero-engine (Combustor liner, acoustic liner, turbine airfoil system, transistor duct)
- Nonlinear optic application (CNT/silica)

1.4.3 Modeling and analysis of CNT-reinforced composites

In order to design components made of CNT-composite, it is important to understand the analysis of such components. Therefore a proper design of CNT-reinforced composites is required. But due to their small sizes and fabrication process, conducting tests for such CNT-reinforced composites are extremely difficult and are not economical. On the other hand, modeling and simulation of nanocomposites can be easily performed by a modern day computer. Therefore, computational approach played a significant role in the development of the CNT-reinforced composites by providing simulation results to help understanding, analyzing and designing of such nanocomposites.

1.4.3.1 Modeling of CNT-reinforced composites

Modeling of CNT-reinforced composites is also an important task from the analysis point of view. Different types of modeling techniques of CNT-reinforced composites have been reported by earlier researchers which include analytical model, finite element (FE) model, micromechanics model etc.

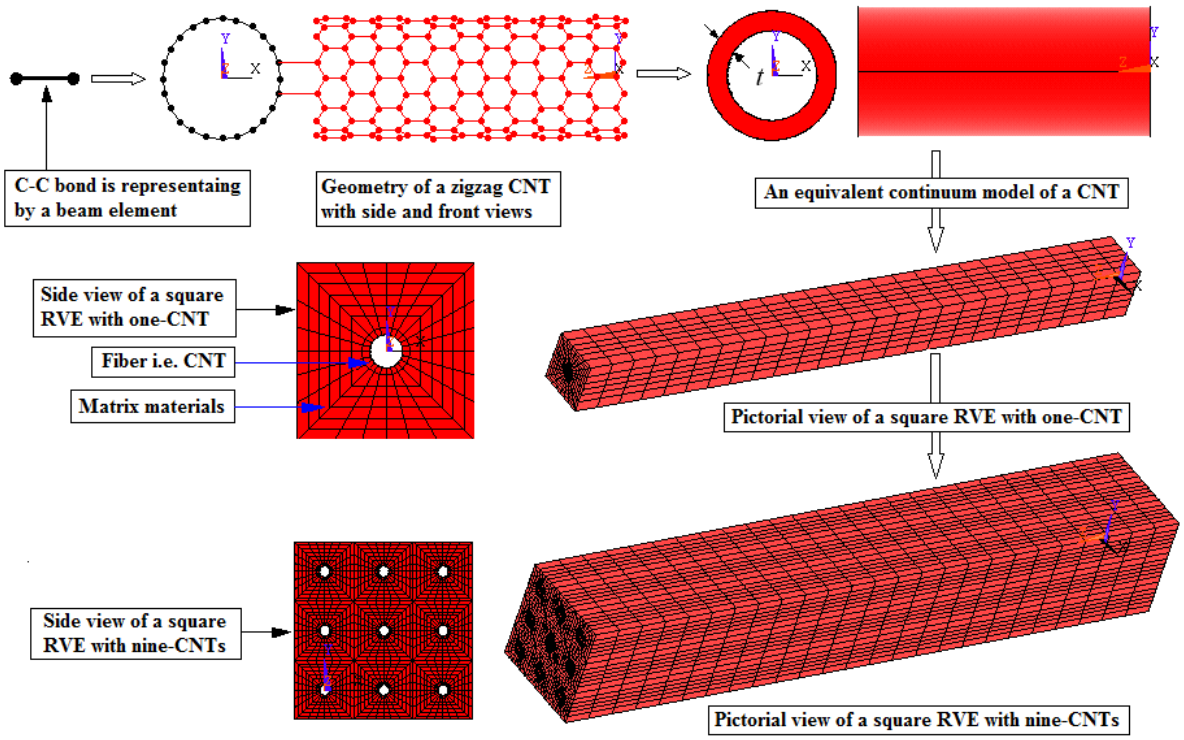

Figure 1.6 A square RVE with nine CNTs is modeled successively from a C-C bond.

A graphene sheet is modeled as a continuous plate with finite thickness termed as equivalent plate model and SWCNTs have been formed by rolling this equivalent plate model. Therefore, the SWCNT is considered as equivalent-continuum tube**.** The development and the parameters of equivalent-continuum model have been described by Odegard et al. [10]. The first part of the Fig. 1.6 described the development of equivalent continuum model of SWCNT from a carbon-carbon (C-C) bond via the geometry of a zigzag SWCNT. Figure 1.6 shows a square RVE with nine CNTs modeled successively from a C-C bond. The square RVE with nine CNTs modeled successively as follows: C-C bond → CNT → equivalent CNT → RVE with one CNT → RVE with nine CNTs. In the present work, it has been

assumed that SWCNT is aligned inside the matrix materials and FE analysis of CNT-reinforced composites has been carried out.

1.4.3.2 Analysis of CNT-reinforced composites

In order to design components made of CNT-composite, it is important to understand the characterization of such composites in terms of load deflection (stress-strain) behavior and to determine the critical load to failure. Different types of analysis of CNT-reinforced composites have been reported in earlier literatures for determination of different important properties of CNT-reinforced composites. Three main types of analysis of CNT-reinforced composites are listed below –

- Experimental,
- Numerical and
- Theoretical

Experimental studies of CNT-reinforced composites are found more compared to numerical and theoretical analysis. The CNT-reinforced composites can be experimentally analyzed to obtain desired properties by performing tensile test, bending test, impact test, shear test etc. Two types of important numerical studies namely FE simulation and molecular dynamics (MD) simulations are also reported by earlier researchers. Finite element method has been extensively used in the analysis of CNT-reinforced composites. Finite element method is a numerical technique for finding approximate solutions and it is a powerful tool which is used to solve any complex geometrical structure. Finite element analysis is used for new product design or to refine an existing product to ensure performance and reliability of such product prior to manufacturing. In this way FE analysis helps to reduce material usage, physical prototyping and testing. The advantages of FE analysis are (i) relatively low investment cost and (ii) rapid analysis can be performed for different models based on applications. The disadvantages of FE analysis are (i) difficulty in creating complex models and (ii) the model needs to be refined repeatedly to obtain accurate result. Molecular dynamics simulations provide detail information on molecular motions and conformational changes. This method is used to investigate the thermodynamics and structure of chemical and biological molecules. Very small time steps in the order of femtosecond are used in this simulation method therefore huge computational time required to perform MD simulation.

Though there are different types of theoretical analysis available in literature but many literatures were published using molecular mechanics, molecular structural mechanics and shear lag model of CNT-reinforced composites. In molecular mechanics (MM) the bonded interactions are treated as springs and atoms are considered as balls. The fundamental to MM is to mathematically model a molecule as a collection of balls which are held together by springs. The magnitude of energy of molecules is expressed as a function of its resistance to bond stretching, bond bending and atom crowding. The main advantage of MM is less computational tasks. The shear-lag method is used for analysis of stress transfer from matrix to fiber or vice-versa by means of interfacial shear stresses in composites. The model is based on considering the radial variation of shear stress in the matrix and at the interface. Shear lag models have been used extensively for stress analysis of unidirectional fiber reinforced composite. There are certain limitations in usage of this model which includes low fiber volume fraction and does not provide detailed information about the spatial variation of stresses and displacements within the composite. They capture the average stress filed over fiber and matrix cross-section accurately enough for purpose of material failure.

Analytical methods are also used in the study of CNT-reinforced composites. Analytical model is simply a mathematical modeling technique that describes relationships among variables. Analytical models are used for simulation and explanation to study the effects of different components and to predict the behavior. Analytical models are extensively used by physicists, engineers, statisticians, operations research analysts and economists. Analytic models are more cost effective and less expensive than simulation. The limitations of analytical model are (i) lots of assumptions are considered and (ii) mathematically challenging to obtain solution.

1.4.3.2.1 Determination of thermoelastic properties

Mechanical and thermal properties of CNT-reinforced composites decide whether the CNT can be used effectively as reinforcement in matrix materials or not. There have been some works [4-5] which confirmed the use of CNT as reinforcement in matrix materials instead of conventional glass and carbon fibers. Therefore, prediction of thermoelastic properties of CNT-reinforced composites is an important issue. Thermoelastic properties of CNT-reinforced composites have been evaluated numerically, theoretically and experimentally by earlier researchers.

1.4.3.2.2 Stress analysis

The strength of CNT-reinforced composites could be determined by appropriate stress analysis of CNT-reinforced composites. Therefore, stress analysis is one of the important tasks of CNT-reinforced composites which needs to be addressed properly. Considering the fact that experimental stress analysis of CNT-reinforced composites is difficult and due to inherent advantages of FE method, many researchers used FE method for stress analysis. Stress analyses of CNT-reinforced composites have been investigated numerically, theoretically as well as experimentally by earlier researchers.

1.4.3.2.3 Fracture mechanics and failure analysis

Looking at the huge potential of CNT-reinforced composites as materials for structural components, it is important from design point of view to understand different failure possibilities of such structure and to perform an analysis. Failure analysis of CNT-reinforced composites is one of the important tasks which need to be addressed properly. Failure of CNT-reinforced composites could be predicted based on –

- CNT pullout,
- CNT breaks and
- Matrix cracking

Due to variability of fiber strength, it is possible that one or more fiber may break in the nanocomposites during loading. In such a case, the location of fiber break becomes the weakest link of the nanocomposites. Once a fiber breaks, stress redistribution occurs in the vicinity of the break and depending upon the magnitude of the stress at the interface, fiber matrix debonding may take place. It is therefore important to study the behavior of a CNT composite in presence of a fiber break. Fracture behavior and failure analysis of CNT-reinforced composites have also been reported by earlier researchers.

1.5 Motivation for the present thesis work

In view of the fact that CNTs are very useful components in engineering applications and CNT-reinforced composites are potential candidate for high performance structural applications, it is extremely important to study the design and analysis of such composites. In general determination of linear elastic properties of such CNTs is essential for

characterization in aiding the failure analysis of such CNT composites in particular. Whereas difficulties in experimental characterization are already explained, there is enough scope of numerical analysis for characterization, stress and failure analysis of such composites. This has motivated to undertake this thesis work in general. Again due to variability of strength of CNT fibers it is possible that one or more fibers in a CNT composite may break during application. The fact that volume fraction of CNTs in CNT composites are low (compared to conventional fiber composite), it is important to study the effect of such fiber break on the behavior of the composite and to study the chances of failure of the composite as a result of this fiber break. With this motivation, a thorough literature review has been done in the broad area of CNT composites to understand the state of the art in this area and to decide the objectives of the present work. This literature review is presented in the next chapter.

भारतीय प्रौद्योगिकी संस्थान गुवाहाटी
Indian Institute of Technology Guwahati

Chapter 2

Literature Review

This chapter presents the work published in the broad area of CNTs and CNT-reinforced composites in general and stress analysis of CNT-reinforced composites in particular. Exhaustive literature review has been performed to understand the potential of CNT-reinforced composites and thus arriving at the specific objectives of the present thesis work. Literatures have been classified according to the nature of work and presented in separate sections of this chapter. A flow chart highlighting the classification of literature review is shown in Fig. 2.1.

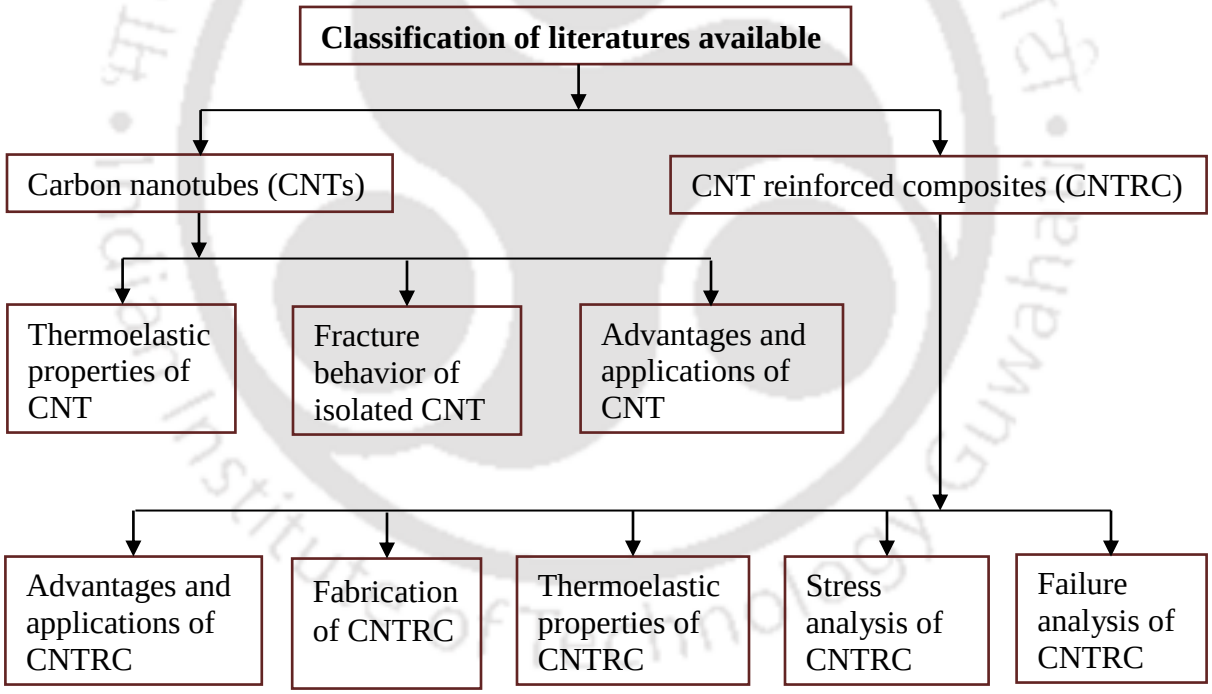

Figure 2.1 A flow chart highlighting the classification of literature review.

2.1 Carbon nanotubes

In 1991, a Japanese electron microscopist Iijima [3] prepared a new type of finite carbon structure consisting of needle-like tubes using an arc-discharge evaporation method. Each

needle comprises coaxial tubes of graphitic sheets, ranging in number from 2 up to about 50. On each tube, the carbon-atom hexagons are arranged in a helical fashion about the needle axis where the diameter of needles range from 4 nm to 30 nm and length up to 1 μm. These needle-like tubes are the multi-walled CNTs (MWCNTs). The discovery of CNT has opened the door to numerous nanoscale research fields. Lau and Hui [4] presented a compressive review on production, physics properties and applications of CNTs and their composites. Their review predicted that in the future, the nanotechnology would be one of the emerging technologies that would play a significant role in developing future space vehicles. Thostenson et al. [5] also presented a compressive review on recent advances in CNTs and their composites. This review paper has reported the atomic structure, morphology, fabrication, characterization and mechanics of CNTs. They also reported the processing and characterization of CNT-reinforced composites. The overall conclusions of these two review papers are that the CNTs offer tremendous opportunities for the development of fundamentally new material systems for their unique electronic, thermal and mechanical properties where the stiffness, strength and resilience exceed any current materials. In particular, the exceptional mechanical properties of CNTs, combined with their low density, offer scope for the development of a new class of nanocomposites. Dresselhaus et al. [6] have reviewed and presented fundamental parameters of CNTs along with the basic relation governing these parameters and typical numerical values of these parameters. The authors specified the CNTs in term of the tube diameter and chiral angles. A framework was given for the symmetric properties of CNTs. There are lots of literatures published on mechanical, thermal and electrical properties, fracture behavior as well as application of CNTs. Some of the important literatures of CNTs are presented here

Lu [7] investigated elastic properties of nanotubes and nanoropes using an empirical force constant model. The author reported that the elastic properties of single-walled CNTs (SWCNTs) and MWCNTs were insensitive to the radius, the chirality, and the number of walls. He also reported that the tensile Young's modulus (~1 TPa) and the torsion shear modulus (~0.5 TPa) of tubes are comparable to those of the diamond, while the bulk modulus is smaller. The author also reported that the nanoropes composed of SWCNTs made them ideal materials for composite and nano scale engineering due to their usual properties like light, flexible and stiff. Odegard et al. [10] proposed a method for developing structure-

property relationships of nano-structural materials. This method serves as a link between computational chemistry and solid mechanics by substituting discrete molecular structures with equivalent-continuum models. Li and Chou [11] presented a structural mechanics approach for modeling the deformation of CNTs. They reported that the Young's moduli of both armchair and zigzag CNTs increase with the increase in tube diameter and approach the Young's modulus of graphite. Tserpes and Papanikos [12] proposed a three dimensional (3D) finite element (FE) model of SWCNTs. They investigated the influence of tube wall thickness, diameter and chirality on the elastic moduli of SWCNTs and reported that the choice of wall thickness significantly affects the values of Young's modulus. The authors found that the elastic moduli of the SWCNTs increased with the increase in tube diameter. They concluded that the proposed FE model might provide a valuable tool for studying the mechanical behavior of carbon nanotubes and their integration in nano-composites. Kirtania and Chakraborty [13] evaluated the Young's modulus, shear modulus and coefficient of thermal expansion (CTE) of graphene sheet and SWCNTs using FE method. They reported that the Young's modulus of graphene sheet was observed to increases with the increase in the size of the graphene sheet. It was also reported that the elastic moduli of both armchair and zigzag CNTs increase monotonically with the increase in diameter of SWCNTs and approach the Young's modulus of graphene sheets for large diameter. They also found that the Young's modulus of both armchair and zigzag SWCNTs proportionally decreases with the increase in the wall thickness of SWCNT. It has been reported that with the increase in the size of the graphene sheets and diameter of CNT, the coefficient of thermal expansion of graphene sheets and both the CNTs were increased uniformly. The variation of CTE with the size of the graphene sheet and the diameter of the CNTs has been observed to be negligible. Lu and Hu [14] developed an improved 3D finite element model of armchair, zigzag and chiral SWCNTs based on molecular mechanics for predicting mechanical behaviors of SWCNTs. They investigated the effects of diameters, chirality and wall thickness on elastic stiffness (Young's modulus and shear modulus) of SWCNTs. Their computational simulation results have been compared with both experimental and theoretical results from the earlier literatures and good agreements have been reported. Kwon et al. [15] performed molecular dynamics simulations to study shape changes of carbon fullerenes and nanotubes with temperature. Jiang et al. [16] developed an analytical method to determine the CTE of

SWCNTs. This analytical method provides a simple and straightforward way to investigate the temperature and helicity dependence of the CTE of CNTs. Their results showed that, the CTE of CNTs is negative at low and room temperature, but becomes positive at high temperature. The CTE in radial direction of the CNT is less than that in the axial direction for armchair CNTs, but the opposite holds for zigzag CNTs. The radial CTE is independent of the CNT helicity, while the axial CTE shows strong helicity dependence. Maniwa et al. [17] determined the CTE of SWCNT bundles as $-0.15 \pm 0.20 \times 10^{-5}$ K^{-1} by means of X-ray scattering between the temperature ranges from 300 K to 950 K. They reported that the tube with small diameter formed a strong carbon-carbon bond comparable to that of graphite. The authors also reported that the CTE for the intertubule gap is equal to $4.2 \pm 1.4 \times 10^{-5}$ K^{-1} which is larger than that of graphite.

Very recently, Yengejeh et al. [18] presented a review on the response of structural and atomically modified CNTs. This review highlights the most prominent literature available for mechanical investigation of imperfect CNTs and concluded that any type of imperfection, either atomic or structural modification, influences the mechanical behavior of nanotubes and reduces the stiffness and structural stability of nano-structures. There are some studies on the fracture behavior of isolated CNT in literatures [19-23] on the nano scale. Belytschko et al. [19] performed molecular mechanics simulation and reported that the failure stress and strain of a defect-free CNT to be 65-93 GPa and 10% - 15%, respectively. Reduction in strength has also been observed when a defect was introduced by removing one atom and associated bonds from the structure of CNTs and reported that strength was reduced about 25% with the removal of a single atom. They have also predicted the brittle character of the fracture behavior of CNTs. Tserpes et al. [20] proposed an atomistic-based progressive fracture model for simulation the mechanical performance of SWCNTs. Finite element analysis of defective SWCNT has been performed by applying axial tension. They compared the predicted stress-strain curves of SWCNT with that obtained from theoretical and experimental work and a well agreement was reported. Fracture mechanism in CNT-reinforced composites was briefly discussed by Thostenson and Chou [21]. Vaez and Jalili [22] performed *ab initio* calculations on the perfect and defected SWCNT with Stone Wales (SW) defects and concluded that SW defects can drastically change the electronic structures and transport properties of SWCNTs. Molecular dynamics simulations of defected SWCNTs

have been performed by Feng and Liew [23] reported that the vacancies in the nanorings are more insensitive to their fracture than that in the straight nanotubes. Molecular dynamics simulations have been used by Talukdar and Mitra [24] and observed that bundle formation led to significant changes in breaking behavior and mechanical properties of the SWCNTs. Tuzun and Erkoc [25] investigated the structural and electronic properties of unusual carbon nanorods by quantum chemical methods. Moelhave et al. [26] demonstrated the onset of nanotube damage in ambient conditions with accelerated rate at higher bias voltages. Xiao et al. [27] developed molecular structural mechanics model of defect free CNTs and predicted the Young's moduli, Poisson's ratios and non-linear stress–strain relationships of defect free CNTs under tension and torsion loading conditions. Yu et al. [28] performed several tensile experiments of MWCNTs and plotted the stress-strain curves of their experimental results.

Advantages and applications of CNTs have been reported in earlier literatures and listed in Chapter 1 (section 1.2.3). High specific surface area, strength and remarkable physical properties of CNTs make them very unique material for applications in all the fields. Practical application of CNTs in the fields of electrochemical systems, nanocomposites, and medical devices have been described by Endo et al. [29] and predicted that CNTs would play an important role for the development of nanotechnology in the near future. Volder et al. [30] reviewed on the most promising present and future commercial applications of CNTs. Literatures in [29-36] discuss varied advantages and applications of CNTs in general and in particular Harris [36] provided a detailed description on synthesis, properties and applications of CNTs.

2.2 Carbon nanotubes-reinforced composites

There have been lots of literatures available on the analysis of CNT-reinforced composites and some of the important literatures are described here

Compressive reviews on CNTs and CNT-reinforced composites have been presented by earlier literatures [4-5]. Nahas MN [37] has described about the fundamentals of FE modeling of CNT and CNT-reinforced composite. He has also reported regarding the different types of analysis, applications and future prospects of CNT and CNT-reinforced composites. Lau and Hui [38] reported that the use of MWCNTs as intrinsic reinforcements for composite structures might not allow the maximum strength to be achieved due to non-

uniform axial deformation inside the MWCNTs and hence the use of SWCNTs might be more beneficial for advanced composites structures. Jia et al. [39] explained the reasons and possibility of strong (C-C) bond between the CNTs and matrix, as well as described the importance of interface in CNT-reinforced composites. Recently, Pal and Kumar [40] reviewed various modeling techniques for predicting the strength, stiffness, fatigue behavior, fracture and damage resistance of CNT/polymer composites. They reported that the conventional materials for both structural and non-structural applications could be substituted by the advanced lightweight and high strength CNT/polymer nanocomposites. They suggested that the factors such as the CNT type, aspect ratio, quality, concentration, orientation, degree of dispersion and interfacial adhesion with the matrix should be taken into account in the modeling for predicting the performance of CNT/polymer nanocomposites. They also highlighted the current challenges and future prospect of CNT/polymer composites.

Advantages of CNT-reinforced composites have been reported in earlier literatures and listed in Chapter 1 (section 1.4.1). Bakshi et al. [41] presented comprehensive reviews on CNT reinforced MMCs including processing techniques, mechanical properties, interfacial phenomena, potential applications and scope of future studies of CNT-reinforce MMCs. Cho et al. [42] presented a comprehensive review on CMCs containing CNTs. They reviewed the latest processing technique, mechanical and functional properties and possible toughening mechanisms of CNT-reinforced ceramics matrix composites. There is a recent book on carbon nanotube reinforced metal and ceramic matrices composites edited by Tjong [43] describing different types of CNT-reinforced MMCs and CMCs. The same book also provided a detailed description on the importance, preparation, physical properties, mechanical properties, future prospects and potential applications of CNT-metal and CNT-ceramic nanocomposites. Advantages of CNT reinforced composites are also reported in [44-48]. Shimizu Y [49] published a book chapter where they have provided the fabrication techniques, mechanical properties and possible application of CNT-reinforced magnesium (Mg) composite in future. In addition, applications of CNT-reinforced composites have also been reported in earlier literatures [50-58] and listed in Chapter 1 (section 1.4.2).

2.3 Fabrication of CNT-reinforced composites

There are also some literatures available describing the manufacturing processes of CNT-reinforced composites as these has significant learning on the properties of such composites. Some of the important literatures on fabrication of CNTs-reinforced composites are presented here -

Nam et al. [59] developed stretching and pressing techniques to fabricate superior CNT sheets with high alignment and dense packing of CNTs. They fabricated aligned CNT/epoxy composites with high CNT volume fraction using hot-melt prepreg processing with the vacuum assisted system. They reported that the tensile strength and elastic modulus of composite fabricated by stretch and pressed technique were increased by 32% and 27% compared with pristine composites, respectively. Thostenson and Chou [60] fabricated and evaluated the mechanical properties of aligned CNT/polystyrene composites. The authors reported that the improvement of elastic modulus with align nanotube composites is five times greater than that of the randomly oriented composites. Cheng et al. [61] fabricated CNT/epoxy composites with controllable alignment of CNT using resin transfer molding process to find out mechanical and electrical properties of the nanocomposites. Jin et al. [62] fabricated CNT/polymer composites with aligned CNTs. The alignments of CNTs in polymer matrix were performed by mechanical stretching. The orientation and degree of alignment of CNTs were determined by X-ray diffraction. The dispersion and the alignment of the CNTs were also studied by transmission electron microscopy. Wardle et al. [63] fabricated high volume fraction aligned CNT/polymer composites using mechanical densification techniques. The author fabricated up to 20% volume fraction of CNT in CNT/polymer composites. Bradford et al. [64] developed a novel shear pressing method to fabricate high volume fraction (27%) CNT/epoxy composites with long aligned CNTs.

Kwon et al. [65] fabricated CNT/aluminum (Al) composites by combining the processes of spark plasma sintering and hot extrusion. Esawi et al. [66] fabricated CNT/Al composites by ball milling to investigate the effect of CNT content on the mechanical properties of CNT/Al composites. Isaza et al. [55] developed a new technique called sandwich technique for fabrication of CNT/Al composites with less damage of CNTs compared to other technique reported in earlier. They reported that the CNTs in the composite were uniformly distributed and aligned and predicted that their fabrication technique opens the door for

future research on the topic of lightweight materials for applications in aeronautics, aerospace, and automotive industries. Chen et al. [67] fabricated SWCNT/Cu matrix composites by electrochemical co-deposition method and reported that this method is a good approach for achieving good interfacial bonding between CNTs and a metallic matrix. They reported the enhanced fracture toughness of CNT/Cu composite which proof good interfacial bonding between a SWCNT and a copper matrix. Goh et al. [68] fabricated CNT/Mg composite using the disintegrated melt deposition technique followed by hot extrusion. Uddin et al. [69] fabricated CNT/Cu and CNT/Cu alloy composites using hot-press sintering method to find out mechanical and electrical properties of the nanocomposites. Chai et al. [70] fabricated CNT/Cu nanocomposite by the electrochemical co-deposition process. Kuzumaki et al. [71] prepared the CNT-reinforced titanium (Ti) composites by mechanical mixing and conventional powder metallurgy method.

Pal et al. [72] synthesized CNT-reinforced alumina (Al_2O_3) matrix nanocomposites by two different techniques. In the first process they used sol-gel method to prepare 3 wt% CNT/Al_2O_3 composites after sintering. The second method was chemical mixing process and using this method they fabricated 10 wt% CNT/Al_2O_3 composites after sintering. Zhan et al. [73] fabricated dense nanocomposites of SWCNTs with nanocrystalline alumina matrix to evaluate fracture toughness by spark plasma sintering. Zhang et al. [74] synthesized CNT/Al_2O_3 nanocomposites to evaluate fracture toughness by chemical vapor deposition and spark plasma sintering.

2.4 Evaluation of thermoelastic properties of CNT-reinforced composites

Evaluation of thermoelastic properties is essential first step for design and analysis of components made of such materials. Therefore there has been number of works reported on determination of such properties using different methods.

Qian et al. [75] reported that with the addition of 1 wt% CNT in polystyrene, elastic modulus and breaking stress could be increased by ~ 40% and ~25%, respectively, indicating a significant load transfer across the nanotube-matrix interface. Andrews et al. [45] reported that the tensile strength, elastic modulus and electrical conductivity of a pitch composite fiber

with 5 wt% of purified SWCNTs could be enhanced by ~90%, ~150%, and 340% respectively, as compared to the corresponding values in unmodified isotropic pitch fibers. Cheng et al. [61] reported a significant improvement of mechanical and electrical properties of CNT/epoxy composites. The authors reported that the Young's modulus, tensile strength of the composites could be increased by 716% and 160%, respectively compared to pure epoxy. They also reported the electrical conductivity of composite along the direction of the CNT alignment was reached up to 1.3×10^4 S/m. Liu and Chen [76], and Chen and Liu [77] evaluated **e**ffective mechanical properties of CNT-based composites using a three dimensional nanoscale representative volume element (RVE) based on the 3D elasticity theory and solved by the FE method. They reported that with the addition of 3.6 vol% CNTs in a matrix, axial Young's modulus of the composites increased by 33% for the case of long CNT fibers. Alamry et al. [78] reported a significant improvement in mechanical and fracture properties by addition of a small percentage of MWCNT in epoxy. They reported that with the addition of only 0.3 wt% MWCNT in epoxy the mechanical properties have increased by 75%. They have also reported that with the addition of just 0.1 wt% CNT in epoxy, there is increase in elastic modulus and toughness by 56.2% and 32.7%, respectively. Nahas and Alzahrani [79] conducted FE analysis of nanocomposites and reported that addition of 0.2% to 2% volume fractions of grapheme sheets led to the increase in stiffness of the nanocomposite by 33% to 185% respectively higher than those of the epoxy. Zuberi and Esat [80] proposed a cylindrical RVE model of SWCNT/epoxy composite by using FE technique. They have used two approaches named non-bonded interaction and perfect bonding for modeling the interface between SWCT and epoxy to investigate mechanical properties of SWCNT/epoxy composites. They concluded that the perfect bonding approach is better than non-bonded approach for evaluating the effects of chirality and size of SWCNTs on the mechanical properties of single-walled chiral CNT-reinforced epoxy composite. Han and Elliott [81] performed molecular dynamics simulation (MD) to calculate elastic properties of CNT/polymer composites using constant-strain energy minimization technique for different volume fraction of CNTs and reported that interfacial bonding effect is important. Lau et al. [82] evaluated micro-hardness and flexural properties of CNT/epoxy composites pre-treated at different temperatures and their variation with volume fraction of CNT.

Lusti and Gusev [83] performed FE analysis of CNT-reinforced composites for calculation of Young's modulus and CTE of CNT/epoxy composites for different orientation of CNTs in matrix, and concluded that CNTs could be more efficient as compared to conventional glass or carbon fibers. Sul et al. [84] determined the thermo-mechanical properties of CNT/epoxy composite with and without addition of CNT in epoxy using atomistic modeling and MD simulations. They reported that with the addition of CNT in epoxy the elastic modulus increase moderately with the reduction of coefficient of thermal expansion. Sul et al. [85] experimentally determined the thermo-mechanical properties of CNT/epoxy composite and reported that both the glass transition temperature and thermal stability of the CNT/epoxy composites increase with the addition of CNT in epoxy. They have also explained about the reason for the same. It is due to the presence of CNT which act as an obstruction due to the crosslink orientation of CNTs in epoxy. Kundalwal and Meguid [86] investigated the influence of CNT waviness, and the interphase between CNT and the polymer matrix on the thermoelastic response of a nano-tailored composite. They reported that the interphase between a CNT and the surrounding polymer matrix plays a crucial role in the modelling of the thermoelastic properties of the CNT-reinforced composite. They also reported that for the particular planar orientation of CNT waviness and the value of CNT wave frequency, the effective CTEs of the hybrid nano-tailored composite become zero, making the nanocomposite a "super-insulator". Dong C [87] studied thermo-mechanical properties of CNT/polymer composite with the aid of Mori–Tanaka method. The effects of CNT volume fraction, aspect ratio, and orientation on thermo-mechanical properties of CNT/polymer composites have been investigated. They concluded that the effective stiffness linearly increases and longitudinal CTE decreases with volume fraction of CNT from 1% to 5%. But in case of the transverse stiffness and transverse CTE shows little change with CNT volume fraction. They reported that the longitudinal stiffness increases with the aspect ratio but in case of transverse stiffness changes are less. It has been reported that the longitudinal CTE decreases and transverse CTE increases with the increase in aspect ratio. It has also been reported that the changes in stiffness and CTE become negligible when the aspect ratio is greater than 100. The Young's modulus, CTE and electrical conductivity of SWCNT/polyacrylonitrile (PAN) composites film were determined experimentally by Guo et al. [88] and reported that Young's modulus of composites above glass transition temperature

is 40 times than the Young's modulus of PAN. It this work, they showed significant reduction of CTE at higher temperature of composite film as compared to PAN film and reported that there was good interaction between PAN and SWCNT.

Alian et al. [89] developed a multi-scale modeling technique to determine the elastic properties of any advanced nanocomposites containing either align or randomly dispersed CNTs. They carried out MD simulations to determine the transversely isotropic properties of nanocomposite containing either an individual CNT or CNT bundles embedded in an epoxy matrix. They investigated the influence on the orientation and agglomeration of the dispersed CNTs and reported that randomly oriented CNTs or their bundles have significant influence on the elastic properties of the CNT/epoxy composites. They reported that the effective elastic properties of the nanocomposite decrease with increase the number of CNTs in the bundle for the same volume fraction of CNT. They also reported that transverse Young's modulus, axial shear, and transverse shear moduli of nanocomposites reinforced with aligned CNTs are less than those of the randomly dispersed CNTs. Recently, Chwal and Muc [90] derived five elastic material constants of CNT/polymer composite having aligned and uniformly distributed long CNTs using FE method and homogenization theory for the 3D square RVE. In this study, the behavior of the reinforcement and the matrix was assumed to be isotropic, homogenous and linearly elastic.

Si-nian et al. [91] conducted experiment and reported that by adding 0.67 wt% CNT in Mg, the tensile strength and elongation percentage of CNT/Mg composite could be increased by 150% and 30% respectively. Thotsaphon et al. [92] fabricated and evaluated the friction and wear behavior of MWCNT-reinforced composite. They reported that the hardness of composite increases but coefficient of friction decreases with the addition of CNT in titanium. Effect of CNT content on the mechanical properties of CNT/Al composites were investigated by Esawi et al. [66] and reported that tensile strength and stiffness of CNT/Al composite could be increased up to 50% and 23%, respectively compared to pure aluminum. Hassan et al. [93] investigated the effect of CNT damage on the mechanical properties of CNT/Al composites. They reported that CNT/Al composite with mildly damaged CNTs have 97.5% higher strength and 14.2% higher modulus than pure aluminum but in the case of severely damaged CNTs, CNT/Al composites have 71% higher strength and 3.3% higher modulus than pure aluminum. It could be concluded that enhancement of strength and

Young's modulus is more significant in the case of the mildly damaged CNTs than severely damaged CNTs because the mildly damaged CNTs retained their tubular structure and high aspect ratio. They also reported that enhancement in strength due to matrix strengthening mechanisms and enhancement of Young's modulus due to load transfer to the CNT. It is important to note that even severely damaged CNTs were found to strengthen the aluminum matrix but their properties were lower than the mildly damaged CNTs composites due to agglomerations of CNTs. Kwon et al. [65] experimentally showed that with the addition of 5 vol% CNTs in Al, the tensile strength of CNT/Al could be increased about thrice that of pure aluminum. Tang et al. [56] reported that with the addition of 15 vol% CNTs in Al, the CTE of CNT/Al composites could be decreased up to 65%. Therefore, the CNT/Al composites may be used as electronic packaging materials. Uddin et al. [69] found that by adding 0.1 wt.% of MWCNT in copper the hardness of CNT/Cu composites improved up to 47% compared to pure copper. They concluded that the hardness of highly-conductive low-strength copper metals can be improved by using CNT as reinforcement in composites materials. Kaewsai et al. [94] prepared CNT/stainless steel (SS) composite coatings by a flame spray technique reported that the hardness of the CNT/SS composite coating could be increased by 58%. They also reported that the CNT/SS composite coating had higher hardness and lower coefficient of friction which in turn resulted in a lower wear rate compared to that of the pure stainless steel coating. In this study, it has also been reported that the coefficient of friction of the SS/CNT coating was almost 3 times lower than that of stainless steel coating which resulted in reduction of sliding wear rate of nearly 2 times.

Mechanical properties of CNT/Al_2O_3 nanocomposites have been determined by Zhang et al. [74] They reported that with the addition of 7.39 wt% CNT in alumina, the hardness and fracture toughness of CNT/Al_2O_3 nanocomposites were observed to increase by 8.4% and 21.1%, respectively, compared to those of the pure alumina. They also reported that higher or lower concentration of CNTs in the composites will compromise the mechanical properties of ceramics. Therefore, the optimal concentration of CNTs in the composites in between 5 to 8 wt.%. Guo et al. [47] studied the effect of plasma surface modification on interfacial behavior in CNT/Al_2O_3 nanocomposites. They found that the strength of the CNT/Al_2O_3 nanocomposites could be significantly enhanced from 4.3 MPa (uncoated) to 97.8 MPa (coated) which more than 20 times higher by the plasma-polymerized coating method at the

surface of CNT and alumina nanoparticles. They reported that a stronger interfacial bonding and significant enhancement of thermal stability of CNT/Al_2O_3 composites were achieved due to surface coating. Fan et al. [48] reported that with the addition of 1 wt% SWCNT in alumina, the fracture toughness and flexure strength of SWCNT/Al_2O_3 nanocomposites were 103% and 20%, respectively higher than that of unreinforced alumina.

2.5 Stress analysis of CNT-reinforced composites

The stress-strain behavior, stress distribution and stress transfer characteristics in CNT-reinforced composites have been investigated by experimentally, numerically and theoretically in some earlier works. Some of the important literatures on stress analysis of CNT-reinforced composites are described below. Load transfer depends on the interfacial shear stress (IFSS) between the fiber and matrix and the performance of a composite materials system is critically controlled by the interfacial characteristics of the reinforcement and the matrix material. There are three main mechanisms of load transfer from matrix to fiber – micromechanical interlocking, chemical bonding, and weak van der Waals bonding between the CNTs and the matrix materials. The interfacial characteristics of CNT-reinforced composite system have been reported in some earlier works and suggested that the IFSS stress of the CNT-reinforced composite was observed to be significantly higher than that of most carbon fiber reinforced composite systems. Some of the important literatures on interfacial characteristic and mechanical properties of CNT-reinforced composites are described below.

An interfacial characteristic between CNT and polymer was critically reviewed by Rahmat and Hubert [95]. They concluded that an optimal CNT/polymer interaction is a key factor to use CNT as reinforcement in nanocomposites. Wagner et al. [44] reported the shear stress transfer ability of MWCNT/polymer interface to be more than that of current advanced composites and was of the order of 500 MPa. Liao and Li [96] performed a pull out test in a SWCNT/polystyrene (PS) system using MD simulation and reported that the interfacial bond strength could be up to 160 MPa, even without considering the chemical bond between CNT and matrix. On the basis of pull out experiment conducted, Cooper et al. [97] reported that the interfacial shear stress between a MWCNT and epoxy ranges from 35 to 375 MPa. Barber et al. [98] performed pullout experiment using atomic force microscopy and found

that the separation strength between CNT and polymer matrix to be remarkably high, indicating that CNTs are effective as reinforcement in polymer. Chowdhury and Okabe [99] performed MD simulation and studied the effect of the matrix density, chemical cross-links in the interface, and geometrical defect in the CNTs on the CNT pull-out from polyethylene. They have also evaluated the interfacial shear strength with the change of total potential energy. Montazeri et al. [100] investigated the mechanical properties of MWCNT/epoxy composites and concluded that acid-treated MWCNT was more efficient as reinforcement in epoxy matrix than untreated MWCNT. Schadler et al. [101] studied the mechanical behavior of MWCNT/epoxy composites in both tension and compression and reported that the compression modulus is higher than the tensile modulus. They attributed the reason for the same to the fact that during compression all the layers respond but in case of tension only the outer layer responds. Zhu et al. [102] reported that at first the bending strength of CNTs/epoxy composites increased with the increase of the CNT volume fraction, attained the maximum value at a certain CNT volume fraction and then decreases with further increase in the CNT volume fraction. Wang et al. [103] studied the stress transfer characteristics at the interface between CNTs and the polymer matrix, and reported that the use of SWCNT might be more beneficial than the use of MWCNT in CNT-reinforced composite structures. They also predicted that matrix with higher modulus may be more beneficial for the interface stress transfer characteristics of CNT-reinforced composites. Romanov et al. [104] developed a 3D FE model to predict stress distribution in a unidirectional carbon fiber composite reinforced with CNT, where CNT can exist in four different configurations. This model is applied to investigate whether CNTs can be used for re-distribution and suppression of stress concentrations in composites on the micro-level. They reported that stress concentration reduces in the matrix close to the fiber surface due to growth of CNTs on fibers but agglomerated CNTs behave as stiff microscopic particles leading to additional stress magnification. The interfacial mechanical characteristics such as interfacial shear stress, pull-out force of CNT and van der Waals interaction energy between the CNT and the surrounding epoxy matrix of CNT/epoxy composite have been investigated using MD simulations by Xiong and Meguid [105]. They reported that the interfacial shear strength of the CNT/epoxy composite increases linearly with the increase in the epoxy density and decreases for greater values of length and diameter of CNT. The maximum values of pull-out

force increases with the increase in the epoxy density, the diameter of CNT but decreases with the increase in the interfacial thickness between CNT and matrix. They also reported the maximum value of the pull-out forces do not depend on the length of CNT.

Frankland et al. [106] generated the stress-strain curves of CNT/polyethylene composites using MD simulation by applying load in both the axial and transverse direction. They concluded that the short, discontinuous fiber composites, upon loading in either direction showed no appreciable load transfer from the polymer to the CNTs. But stiffer behavior was observed for long continuous CNT-reinforced composites with longitudinal load. Tzeng and Tsai [107] investigated the stress distribution in CNT/polyimide composites using molecular dynamics simulation. They reported that the surface modification on CNTs to be an effective procedure to improve the load transfer efficiency as well as the modulus of nanocomposite. They also reported that if there were no surface modification on CNTs then the load transfer efficiency only depends on the intensities of the van der Waals interaction which is relatively very low. Mora et al. [108] performed tensile and compression tests of CNT/epoxy composites and reported that CNT-fibers provided a good reinforcement in compression as well as tension.

Xiao and Zhang [109] investigated the effects of nanotube length and diameter on the distributions of tensile stress and interfacial shear stress at the interface of SWCNT/epoxy composites. They predicted that CNTs with smaller diameter are more effective as reinforcement and there exist an optimal CNTs length at which reinforcement was maximum. They also found that a CNT has greater stress transfer efficiency than a solid fiber, providing flexibility for toughness and tensile strength optimization. Gao and Li [110] developed a shear-lag model for predicting the interfacial stress transfer in CNT-reinforced polymer composites using a multi-scale approach. They investigated the distribution of average axial normal stress in the CNT as well as in the matrix materials along the nanotube length. The variation of interfacial shear stress along the CNTs axis has also been studied. They reported that the nanotube aspect ratio plays a critical role in designing the CNT-reinforced composites; therefore the nanotubes with sufficiently high aspect ratio should be used to achieve better reinforcements. Li and Saigal [111] developed a micromechanical model for assessing the interfacial shear stress transfer in CNT-reinforced polymer composites. The RVE considered was composed of three concentric cylinders with different length. The

innermost cylinder is a hollow CNT which is surrounded by matrix cylinder and matrix cylinder is surrounded by composites cylinder. The variation of average axial normal stress in the nanotube and interfacial shear stress at the interface of CNT/matrix composite along the CNTs axis have also been presented. They reported that a small volume fraction of nanotube improved the efficiency of interfacial stress transfer in CNT-reinforced polymer composites. Meguid and Sun [112] investigated the influences of debonding and shear characteristic at the interfaces of nanocomposites at different volume fractions. They reported that beyond a certain wt% CNT the interfacial strength of nanocomposite was observed to have reduced.

Ci and Bai [113] investigated reinforcement effect on the matrix materials with different stiffness. The stress-strain curves have been plotted for the composites and a significant reinforcement and fracture strain of CNT were observed for soft and ductile composites. Mohammadpour et al. [114] proposed an effective model for CNT/polypropylene (PP) composites based on nonlinear FE modeling. Their FE model was capable of predicting the stress-strain behavior of CNT/PP composites under tensile loading at large strain. The nonlinear RVEs of CNT/PP composites were developed to investigate the effect of CNT length and interfacial strength on the mechanical response of the composites. These RVEs consist of CNT, PP matrix and non-bonded interface. The interface between CNT and matrix was simulated using contact elements. They observed that the CNT/PP interface has significant influence on the tensile strength of the composites and reported that CNT length also plays an important role on the strength of the composites. Li and Chou [115] examined the interfacial shear stress distribution, axial normal stress concentrations in the nanotube as well as matrix material, and the effect of nanotube aspect ratio on load transfer in CNT/polymer composite under tension by combining the atomistic molecular structural mechanics approach and continuum FE methods. Haque and Ramasetty [116] developed an analytical model to study the axial stress and interfacial shear stress along the CNT length in SWCNT reinforced polymer matrix composites. The effects of aspect ratio, fiber volume fractions and matrix modulus on the axial stress and interfacial shear stress distribution along the CNT length were studied. Finite element analysis was carried out to validate the result generated from the analytical model. A reasonable agreement was observed between the

results obtained from analytical model and finite element analysis at higher aspect ratio of CNT.

Multi-scale modeling is required to simulate and assess the true response of CNT-reinforced nanocomposites. Tserpes et al. [117] proposed a multi-scale RVE for modeling and analysis of the tensile behavior of CNT/polymer composites and reported a significant enhancement in stiffness of polymer with the addition of CNT. They found the generalized stress-strain curves of CNTs and relation between the stress and strain of CNTs by fitting the data of the curves using third-order polynomials. The continuum FE method was used for building the RVE. They also reported the stress-strain curves of CNT-polymer composites for different interfacial shear strength and nanotubes volume fraction, and observed that at low strain the stress-strain curve coincides with the linear behavior given by the rule-of-mixtures and at larger strain the stress-strain curves deviated due to non-linear behavior of CNTs. They also reported a significant improvement of tensile strength with the increase in volume fraction of CNTs. Shokrieh and Rafiee [118] performed FE analysis of CNT/polymer composites. A full 3D multi-scale FE model of CNT, non-bonded interphase region and its surrounding polymer was constructed on the basis of multi-scale modeling approach. They reported a non-linear stress-strain behavior of CNT/polymer composites and reported that the length of the CNT plays an important role on the load transfer efficiency. Spanos et al. [119] investigated the stress transfer in CNT-reinforced composites using a multi-scale FE approach. The authors reported that the stress transfer depends on the CNT volume fraction, interfacial stiffness and elastic modulus of matrix materials.

Goh et al. [68] performed tensile test on CNT/Mg composite and plotted stress-strain curves of pure magnesium as well as CNT/Mg composites for different volume fraction. They observed from those stress-strain curves that the maximum improvement of ductility was 69% with the addition of 1.3 wt% CNT. Boesl et al. [120] performed tensile test of CNT/Al composite and reported that with the addition of 1 vol% CNT in aluminum the elastic modulus and tensile strength of CNT/Al composite increased by 65% and 40% higher than pure aluminum. In this study, they investigated that the failure of CNT/Al was occurred due to CNT pullout from aluminum. They also reported that longer CNTs (25-30 μm) at lower concentration are beneficial for improving the strength and stiffness of CNT/Al composites. Recently, Choi et al. [121] conducted molecular dynamic simulation, and

reported that Young's modulus and toughness of CNT/Al composite could be increased up to 39% and 100%, respectively compared to pure aluminum. They concluded that a small fraction of CNT can play a significant role in enhancing the mechanical properties of CNT/Al composites. In this study, the stress-strain curves of CNT/Al composite have also been plotted under tensile loading. Choi et al. [122] investigated the reinforcing effect of CNT in aluminum matrix composites. They reported that the values of the yield strength and fracture toughness of CNT/Al composite were increased by 15 and 7 times higher than those of the pure Al. The stress-strain curves of the specimens with different volume fractions have also been plotted and reported that yield strength of composites observes to increase with the increase in volume fraction. Chai et al. [70] fabricated CNT/Cu nanocomposite and performed tensile test for both the CNT/Cu composite and pure Cu for comparison purpose, and both the stress-strain curves have been plotted together. It has been observed from stress-strain curve that the fracture strain of the CNT/Cu nanocomposite is larger than 4% which indicate the CNT/Cu also produces considerable ductility. They reported that the yield strength and ultimate tensile strength of the CNT/Cu nanocomposite were five times and three times greater than those of pure copper, respectively. They also reported that good interfacial bonding between CNT and copper could be attributed by uniform distribution of CNTs in copper matrix. Guo et al. [47] plotted the stress-strain curves of coated and uncoated samples of CNT/Al_2O_3 composites and reported higher yield stress for coated sample than that of uncoated sample.

2.6 Failure analysis of CNT-reinforced composites

In view of their potential use as high performance structural components, it is important to understand different failure mechanisms of CNT composites. Fracture behaviors and failure analysis of CNT-reinforced composites have been reported in some earlier works.

Fereidoon et al. [123] built a 3D FE model of a representative volume element near the crack tip for fracture behavior of CNT/epoxy composites. The authors studied the effect of length and chirality of SWCNT in epoxy matrix on the fracture behavior. They reported that the crack resistance could be improved by increase in the length and chirality of CNTs. They showed that bridging condition has minimum stress intensity factor. They also showed that CNT/epoxy with 10 wt.% CNTs has lower stress intensity factor compared to

epoxy/halloysite for same wt.% CNTs as well as loading condition. They reported that fracture toughness of CNT/epoxy composites could be improved by increasing the weight percentage of SWCNT. Ayatollahi et al. [124] studied fracture toughness of MWCNT/epoxy composites under mode-I and mode-II loading conditions. They reported that strength and mode-II fracture toughness of composite were increased with the increase in volume fraction of CNTs. They also reported that the presence of CNT had a greater effect on fracture toughness of nanocomposites under shear loading compared to normal loading. A 3D FE model of SWCNT/polymer composite has been constructed by Rafiee et al. [125] to study the effect of CNTs on fracture properties of composites. In the 3D FE model CNT is modeled as a lattice structure using beam elements, the interface region is considered as non-bonded van der Wall interactions and the surrounding polymer is constructed using solid elements. They reported that the lattice structure of CNT and non-bonded interphase region should not be neglected in the modeling procedures. A combined numerical and experimental study was performed by Kuronuma et. al. [126] to understand the fracture behavior of cracked CNT/polycarbonate composites at room temperature as well as liquid nitrogen temperature under tension. Joshi et al. [127] analyzed the crack propagation and fracture in CNT-based composites using extended FE method. Jia et al. [128] performed FE analysis to simulate single CNT pullout to understand its bridging effect in CNT/polymer composites. They reported that the specific pullout energy increases with the increase in embedded length of CNT but the same has been independent on the radius of CNT. Therefore, it could be concluded that the fiber bridging effect could be enhanced by increasing the embedded length of CNT without changing the radius of CNT. They also reported that the debonding force cannot be continuously increased by increasing the embedded length of CNT and a saturated debonding force exists corresponding to a critical embedded length of CNT. The higher saturated debonding force can be achieved with CNT having larger radius or with stronger interfacial bonding at the interface between the CNT and the matrix. Zhan et al. [73] investigated a significant improvement of fracture toughness of CNT/Al_2O_3 nanocomposites and they reported that with the addition of 10 vol% SWCNT in alumina, the fracture toughness increased three times that of pure alumina. Lei et al. [129] reported that with the addition of 2 wt% CNT in alumina, the fracture toughness and flexural strength of CNT/Al_2O_3 nanocomposites reached 6.35 $\mathrm{MPa}\sqrt{\mathrm{m}}$ and 331 MPa, respectively, which were

respectively 68% and 10% higher than those of the pristine alumina. Fan et al. [48] determined the fracture toughness of SWCNT/Al_2O_3 composites is twice as high as that of unreinforced alumina and predicted that the main toughening mechanism is crack bridging of SWCNTs. Fracture toughness of SWCNT/Al_2O_3 has also been determined by Zhang et al. [74].

Li and Chou [130] studied the failure analysis of CNT/polymer composites by using a micromechanics model and conducting FE simulation. They reported that the nanotube waviness tends to reduce the elastic modulus and tensile strength but enhanced the ultimate strain of the composite. They also reported that randomness of nanotube distribution tends to reduce both the composite elastic modulus and tensile strength. They have analyzed the damage initiation and evaluation in composites with random wavy nanotubes and reported that the evaluation of damage was strongly influenced by the waviness, distribution and aspect ratio of nanotubes. Chen et al. [131] performed failure analysis and the optimal toughness design of CNT-reinforced composites. The three-level failure analysis on the basis of atomistic simulation, shear-lag theory and facture mechanics have been carried out for fracture toughness enhancement of CNT-reinforced composites. Chen et al. [132] investigated the effect of CNT diameter on the fracture toughness of CNT reinforced composites based on the three-level failure analysis. They reported that the CNTs with smaller diameter do not confer a better fracture toughness on their reinforced composites, and the optimal CNT diameter may exist in the transition between failure modes, especially from interfacial debonding to CNT break. The optimal CNT diameter is determined by CNT content, matrix modulus, and interface strength. They also reported that reducing CNT diameter can cause a sudden drop in fracture toughness of composites due to the transition of dominant failure mode. This study can provide guiding reference for CNT reinforced composite design. Chen et al. [133] fabricated wall-bridged MWCNT/Al composite and investigated the fracture behavior of MWCNT during tensile failure of CNT/Al composites. They observed that most of the CNT walls fractured during tensile test due to the existence of bridging walls which were helpful to improve inter-wall bonding, leading to enhanced of strength compared with pure Al. Their study might be provided a new understanding of the strengthening effect of CNT reinforcements in MMCs for designing high-performance next-generation strong and light MMCs. Yamamoto et al. [134] investigated the failure

mechanism of the MWCNTs during crack opening in MWCNT/Al_2O_3 composites and suggested that the use of MWCNTs with much higher load carrying capacity might lead to composite with higher fracture toughness.

A comprehensive review on the progressive failure analysis of conventional composite materials has been presented by Tay et al. [135]. In order to determine the strain energy release rate (SERR), a pre-existing crack or delamination must be present. The virtual crack closure integral (VCCI) technique for calculation of SERR in conventional fiber-reinforced composites has been reported in some earlier literatures [136-138]. Irwin's [136] used crack closure integral (CCI) to obtain the SERR by considering an incremental crack extension and to evaluate the work done to close the crack to the original configuration. Xie and Biggers [137] proposed a simple and efficient algorithm to trace a moving delamination front with an arbitrary and changing shape therefore delamination growth can be analyzed by using stationary meshes. This approach avoids adaptive re-meshing techniques therefore it reduce computational burden in delamination growth analysis. This approach is useful for analysis of complex delamination shapes. Venkatesha et al. [138] proposed a generalized modified crack closure integral algorithm for four and eight-noded quadrilateral elements to estimate the SERR components for several sizes of virtual crack extension through a single FE analysis. The same has been achieved through a numerical integration of the crack closure integral and for various sizes of virtual crack extension covering a large number of equal and unequal size elements ahead and behind the crack tip. Brewer and Lagace [139] investigated the initiation of delamination of graphite/epoxy composites using a strength-based failure criterion such as the quadratic stress criterion. This quadratic stress criterion is useful for preliminary design of composite to investigate the propensity of delamination initiation.

Faulkner et al. [140] experimentally observed a significant improvement of mode-II critical energy release rate due to CNT reinforcement in carbon fiber/vinylester composite with a pre-existing crack. They fabricated three sample with the CNT concentration of 5 g/m^2, 7 g/m^2 and 10 g/m^2 to determine the effect of the surface concentration of CNTs (i.e. the mass of CNT per unit of CNT reinforced surface area of interface) and reported that 7 g/m^2 of CNT was the best concentration among the three samples. They reported that critical energy release rate could be increased 19% due to CNT reinforcement with 7.5 g/m^2 CNT

concentration. They also reported that interface toughness with the CNT concentration of 5 g/m^2 was even lower than that of non CNT reinforced specimen.

2.7 Summary of literature review

It could be concluded from literatures review on CNTs that CNTs could be used as a fiber in matrix materials due to their extraordinary mechanical, thermal and electrical properties The literatures available in the broad area of CNT-reinforced composites reported that the load carrying capacity of CNTs in matrix is significant and CNT-reinforced composites have the potential to provide extremely strong lightweight new materials. Therefore, in future the CNT-reinforced may be one of the lighter and tougher new structural advanced nanocomposites. Therefore, in near future CNTs could be used as a reinforcing element for future advanced nanocomposites in all engineering fields. Fracture behavior of isolated CNT has also been reported.

There have been good numbers of works reported in the broad filed of CNT-reinforced composites in recent time. From the exhaustive literature review, the following important observations are listed below.

- Potential use of CNTs as reinforcing members in structural components has been established.
- Most of these literatures have focused on the fabrication, characterization, load carrying capacities and strength of CNT-reinforced composites.
- Good number of works has been reported in the direction of evaluation of thermo-mechanical properties of CNT composites and the advantages of FE simulation for evaluation of such properties have been substantiated.
- In search of better design, there have been a number of works reported in stress analysis in general and failure of CNT composites in particular.
- The stress transfer characteristics in CNT-reinforced composites have been investigated and predicted that a high interfacial shear stress transfer were observed from fiber to matrix
- Fracture behaviors of CNT composites have also been studied by researchers mostly with an aim of improving fracture toughness of components and to study the influence of important parameters.

- Very few works were also performed on failure analysis of CNT-reinforced composites to find the critical strain energy release rate of CNT-reinforced composites.

2.8 Gaps in the existing literatures

Summary of literature review reveals three important aspects where the current research on CNT composites as structural components is focused. These are –

- Evaluation of thermo-mechanical properties of CNT composites,
- Stress analysis in such CNT composite and
- Failure analysis of such CNT composites

While good numbers of works have been reported in determination of thermo-mechanical properties, most of those were based on linear behavior of CNTs. However, it is already established that the stress-strain relation of CNTs are non-linear especially at higher strains. Therefore it is essential to revisit the determination of thermo-mechanical properties of CNT composites considering the non-linear stress-strain relation of CNTs and to study the necessity of such multi-scale modeling.

In the failure analysis side, it is well known that composite have different failure mode like fiber break, delamination, matrix cracking etc. which are their distinct feature and not encountered in components made of conventional metallic materials. It is therefore important to study those aspects of failure. It was observed that even though numbers of works are reported in fiber debonding, pull out etc., no work is still reported on the analysis of a CNT composite with a fiber break. On the other hand, compared to conventional graphite/epoxy composites the volume fraction of CNTs in CNT reinforced composites is low. Again, due to variability of strengths of fibers (i.e. CNTs), it is possible that one or more CNTs may break in the CNT composites during loading. In such a case, the location of fiber break becomes the weakest link of the CNT composites. Once a fiber breaks, stress redistribution occurs in the vicinity of the break and depending upon the magnitude of the stress at the interface, fiber matrix debonding may take place. When one fiber breaks it may lead to breaking of the adjacent intact CNTs, leading to successive failure of CNTs and finally the failure of CNT composites. Therefore, at low volume fraction, even breaking of few CNT fibers will have pronounced effect on the performance of the CNT composites. It is therefore important to

undertake a study to simulate the stress redistribution due to such broken CNT and the chances of failure from such break.

Progress of debonding in the vicinity of broken fiber in CNT-reinforced composites can be predicted knowing the values of the strain energy release rate (SERR) components at the interface. Investigation of the SERR and critical SERR at the interface between CNT and matrix with a small debonding which is considered as a pre-existing crack is also one of the important tasks. These are also few works available on fracture behavior and calculation of SERR of CNT-reinforced composite. But comparatively very few works have focused on failure analysis of CNT-reinforced composites. However, till date there has been no work reported in studying the influence of broken CNT on the adjacent intact CNTs and chances of debonding from such a fiber break in presence of the surrounding matrix and the adjacent intact CNTs. In addition, determination of critical SERR for such composites has not been reported till date.

Based on the literature review and the existing gap in the available works reported in the literatures, the present thesis work aims at the following specific objectives.

- To develop a full 3D FE model for analyzing a CNT-reinforced composites considering a representative volume element (RVE).
- Finite element based estimation of Young's modulus of CNT-reinforced composites and to study the
    - effect of volume fraction
    - effect of matrix materials considering non-linear stress-strain relation of CNT.
- Finite element based estimation of coefficient of thermal expansion (CTE) of CNT-reinforced composites and to study the
    - effect of volume fraction
    - effect of matrix materials considering non-linear stress-strain relation of CNT.
- To develop a FE model for RVE of a CNT composite having a broken CNT fiber to
    (i) study the axial normal stress (ANS) distribution in the broken CNT to assess the ineffective length of CNT and to understand the

- effect of volume fraction
- effect of matrix materials

(ii) study of interfacial normal stress (IFNS) and interfacial shear stress (IFSS) distribution at the interface between the broken CNT and matrix materials to investigate the chances of initiation of debonding at the site of break and to understand the

- effect of volume fraction
- effect of matrix materials

(iii) study of axial normal stress distribution in the adjacent intact CNTs to determine the stress concentration factor (SCF) to assess the chances of failure of adjacent CNTs and to understand the

- effect of volume fraction
- effect of matrix materials

- To develop a FE model of an RVE for a CNT composite with a broken CNT and carry out FE analysis using the concept of linear elastic fracture mechanics (LEFM) for evaluating SERR components to
  - study the propensity of the growth of the debonding at the interface of the broken fiber and the matrix
  - study the effect of important parameters like volume fraction, matrix materials on the components of SERR.
  - propose a model for evaluation of critical SERR components using virtual crack closure integral (VCCI) and quadratic stress criterion (QSC).

2.9 Organization of the thesis

The present thesis has been organized as follows. Chapter 1 presents the overall introduction of the subject of the thesis along with motivation and scope. Chapter 2 provides detail of the review for understanding the state of art and thus deciding the specific objectives of the thesis. Chapter 3 presents the FE based determination of thermoelastic properties of CNT composites using a RVE and to study the influence of important parameters. Chapter 4 presents the FE analysis using RVE of CNT composites having a defect in the form of a

broken CNT with the aim of understanding stress redistribution due to such break. Chapter 5 describes the use of LEFM in conjunction with QSC to compute SERR considering a small debonding ahead of the broken CNT and to study the influence of important parameters on SERR. This chapter also presents a method to numerically determine critical SERR. Chapter 6 lists the important conclusions from the present work and discusses the scope for the future work.

Chapter 3

Thermoelastic Properties of CNT-Reinforced Composites

3.1 Introduction

In this chapter, thermoelastic properties of CNT-reinforced composites have been determined numerically considering a representative volume element (RVE) and using finite element (FE) analysis. Both linear stress-strain relation and non-linear stress-strain relation of CNTs have been considered to study the effect of such modeling on the predicted properties. Different types of CNT-reinforced composites viz. CNT-polymer (CNT/epoxy), CNT-metal (CNT/magnesium, CNT/titanium, CNT/steel) and CNT-ceramic (CNT/alumina) have been considered and the thermoelastic properties are determined. Computed Young's moduli of CNT-reinforced composites are compared with those obtained from simplified rule of mixtures (ROM) to understand the limitations in use of ROM. Predicted coefficient of thermal expansion (CTE) of CNT-reinforced composites are compared with those obtained from thermoelastic extremum principle (TEEP). Effect of important parameters on different properties has also been investigated.

3.2 Square representative volume element and FE modeling

3.2.1 Square representative volume element with a central CNT

In the present work, RVE with a single-CNT has been considered to determine the thermoelastic properties of CNT-reinforced composites using FE method. The CNT is considered to be placed at the center of the RVE which is surrounded by the matrix materials. The RVE has been modeled for different volume fractions of CNT in the matrix

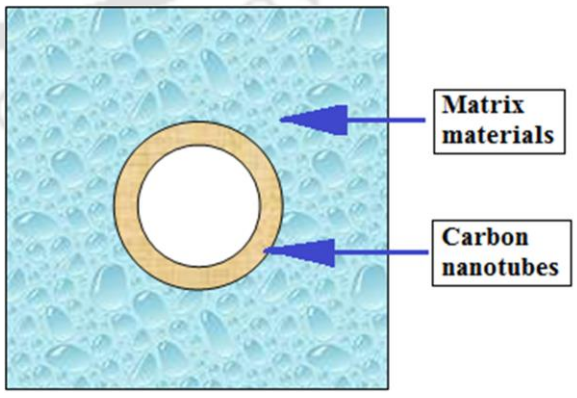

Figure 3.1 Front view of square RVE with a central CNT.

with volume fraction ranging from 0.5% to 15.77%. Dimensions of square RVE relative to the CNT are chosen so as to conform to the volume fraction. Figure 3.1 shows the front view of square RVE.

In this present work, the matrix in a RVE is considered linear elastic, isotropic and homogeneous materials. It has also been assumed that the CNTs and matrix are perfectively bonded with no slip at the interface between the CNT and the matrix.

3.2.2 Finite element modeling

Figures 3.2(a) and 3.2(b) show the front view and pictorial view of a typical 3D FE mesh of the square RVE of CNT-reinforced composites. In the present model, the *x*-*y* plane is the transverse plane and the *z*-axis is the axial direction of the CNT. It has been assumed that the orientation of the CNT in the matrix is aligned. Single-walled CNT (SWCNT) is considered in the present work. The thickness (*t*) of CNT is considered 0.34 nm [6-7]. Since the curvature effect of the CNT in the range of diameter ≥ 1.88 nm are negligible [13], therefore in the present thesis work, the diameter of CNT is always considered to be equal to 1.88 nm, which is equal to the diameter of zigzag (24, 0) CNT. In

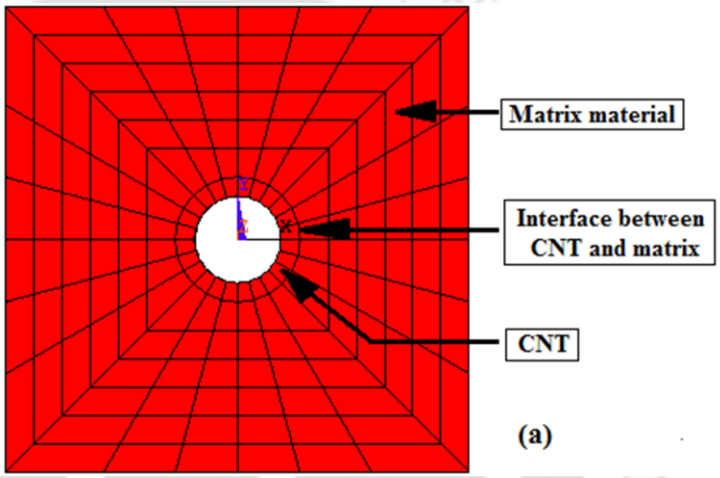

Figure 3.2(a) Front view of square RVE with FE mesh.

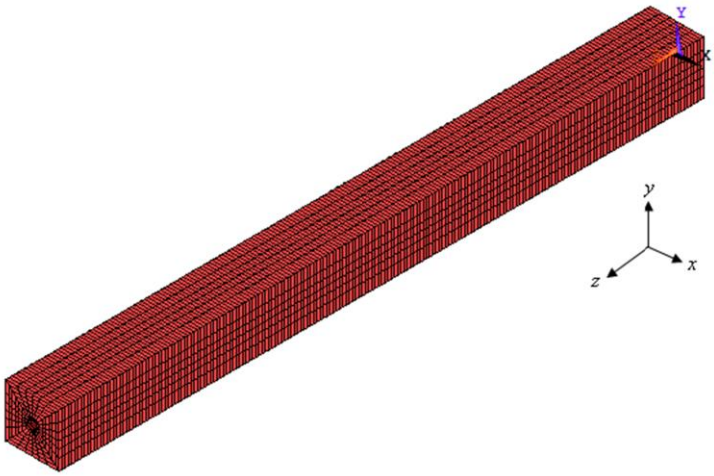

Figure 3.2(b) 3D FE mesh of square RVE.

the present analysis a 200 nm length of CNT is considered however, any other length of the CNT could also be used in the FE model. The number of nodes and elements used in the present FE model are 76992 and 67200, respectively as shown in Fig. 3.2(b).

3.2.2.1 Characteristics of SOLID45 element

SOLID45 element embodied in ANSYS has been used for modeling the square RVE. The element SOLID45 is a 3D brick element and the element is defined by eight nodes having three degrees of freedom at each node: translations in the nodal *x*, *y* and *z* directions. The geometry, node locations, and the coordinate system of the element are shown in Fig. 3.3.

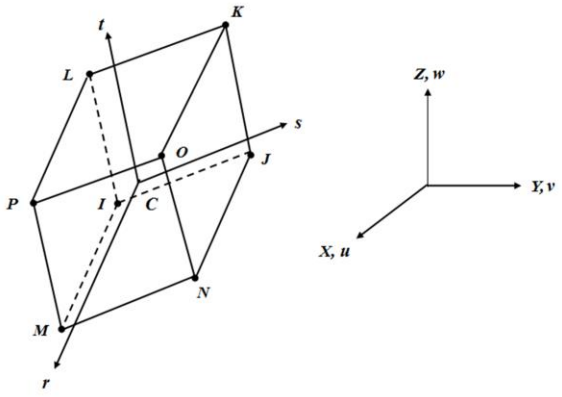

Figure 3.3 Geometry and the coordinate system of SOLID45

The element SOLID45 is used for the 3D modeling of solid structures and it has plasticity, creep, swelling, stress stiffening, large deflection and large strain capabilities. Shape functions of the SOLID45 element are listed Table 3.1.

Table 3.1 Shape functions of SOLID45

Node	Shape functions
I	$N_I = \frac{1}{8}\{(1-s)(1-t)(1-r)\}$
J	$N_J = \frac{1}{8}\{(1+s)(1-t)(1-r)\}$
K	$N_K = \frac{1}{8}\{(1+s)(1+t)(1-r)\}$
L	$N_L = \frac{1}{8}\{(1-s)(1+t)(1-r)\}$
M	$N_M = \frac{1}{8}\{(1-s)(1-t)(1+r)\}$
N	$N_N = \frac{1}{8}\{(1+s)(1-t)(1+r)\}$
O	$N_O = \frac{1}{8}\{(1+s)(1+t)(1+r)\}$
P	$N_P = \frac{1}{8}\{(1-s)(1+t)(1+r)\}$

3.3 Determination of thermoelastic properties

3.3.1 Effective Young's modulus

Figure 3.4 shows a simple strength of materials model of a square RVE for calculating the effective axial Young's modulus with a long CNT reinforced inside the matrix. The boundary conditions of the model are - one end is fully restrained and the other end is

subjected to uniform axial tensile load. The axial Young's modulus (E_1) of the RVE is calculated using the following relation –

$$E_1 = \frac{F_a / A_c}{\Delta L_a / L_a} \tag{3.1}$$

where, F_a is the total axial force acting at one end, A_c is the cross sectional area, L_a is the initial axial length, and ΔL_a is elongation of the composites in axial direction. The transverse Young's modulus is calculated using the same principle as in case of axial Young's modulus calculation keeping at one end is fully restrained but the other end is subjected to uniform surface loads (or constant pressure load). The transverse Young's modulus (E_2) is calculated using the following relation –

$$E_2 = \frac{F_y}{\Delta L_t / L_t} \tag{3.2}$$

where, F_y is the constant pressure load applied along y-direction at one end, L_t (i.e. $2a$) is the initial transverse length and ΔL_t is elongation of the composites in transverse direction.

In calculating the cross sectional area of the composites, the thickness of the CNT is considered as 0.34 nm [6-7] which is the interlayer spacing of graphite. The volume fraction of the CNT (V_{nt}) in the square RVE is calculated using the following relation –

$$V_{nt} = \frac{\pi(r_0^2 - r_i^2)}{4a^2 - \pi r_i^2} \tag{3.3}$$

where, r_0 and r_i are the outer and inner radius of the CNT, respectively and $2a$ is the thickness (or width) of the square RVE.

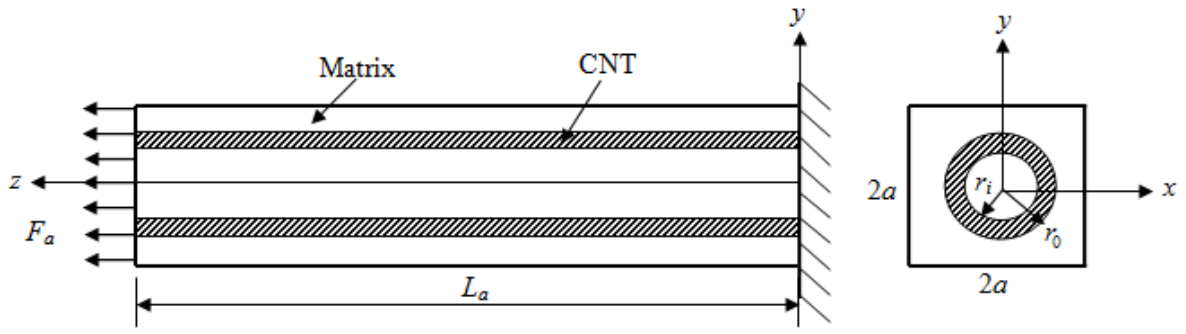

Figure 3.4 A strength of materials model of a square RVE.

For a fiber composite under uniaxial loading, the dependence of the effective Young's modulus in terms of the modulus and the volume fraction of each constituent can be estimated by using the rule of mixture (ROM) [141]. The same equations of the ROM are used to predict the effective Young's modulus of the CNT-reinforced composites. The longitudinal effective Young's modulus of the nanocomposites with long CNT is calculated using the following relation –

$$E_1 = E_{nt}V_{nt} + E_mV_m \tag{3.4}$$

where E_{nt} and E_m are the elastic modulus of the CNT and matrix, respectively, and V_{nt} and V_m are the volume fractions of the CNT and matrix, respectively in the nanocomposites. The effective transverse Young's modulus of the nanocomposites with long CNT is calculated using the following relation –

$$\frac{1}{E_2} = \frac{V_{nt}}{E_{nt}} + \frac{V_m}{E_m} \tag{3.5}$$

where,

$$V_{nt} + V_m = 1 \tag{3.6}$$

These ROM formulae are used to compare the Young's modulus obtained in the present FE analysis of the CNT-reinforced nanocomposites.

3.3.2 Effective coefficient of thermal expansion

The thermal expansion of a solid can be anisotropic if the coefficients of thermal expansion (CTE) are direction dependent. This situation occurs in composite or nanocomposites materials with a directional reinforcement. In the present study, the axial and transverse linear CTE of the nanocomposites have been evaluated using FE method. The uniform temperature is applied on each node by fixing all the nodes at one end (zero displacement). The axial CTE (α_1) of the nanocomposites in the axial direction is given by

$$\alpha_1 = \frac{1}{L_a}\frac{\Delta L_a}{\Delta T} \tag{3.7}$$

where, ΔT is the change in temperature. Similarly, the transverse CTE (α_2) of the nanocomposites in the transverse direction is given by

$$\alpha_2 = \frac{1}{L_t}\frac{\Delta L_t}{\Delta T} \tag{3.8}$$

To compare the computed CTE of the CNT-reinforced composite materials, following are the expressions developed for the two thermal expansion coefficients using the thermoelastic extremum principle (TEEP) by Schepery [142].

$$\alpha_1 = \frac{\alpha_{nt}V_{nt}E_{nt} + \alpha_m V_m E_m}{E_{nt}V_{nt} + E_m V_m} \tag{3.9}$$

$$\alpha_2 = (1+\nu_{nt})\alpha_{nt}V_{nt} + (1+\nu_m)\alpha_m V_m - \alpha_1 \nu_{12} \tag{3.10}$$

where, α_{nt} and α_m are the CTE of the CNT and the matrix, ν_{nt} and ν_m are the Poisson's ratio for the CNT and the matrix, respectively. The effective Poisson's ratio (ν_{12}) is

$$\nu_{12} = \nu_{nt}V_{nt} + \nu_m V_m \tag{3.11}$$

which is approximated by the ROM expression [141], as in axial effective Young's modulus of the nanocomposites.

3.4 Boundary conditions

Figure 3.5 shows the 3D view along with the applied boundary conditions of the FE model. All the nodes at $z = 0$ are fully restrained and the nodes at $z = L_a$ are subjected to uniform tensile load. In the case of transverse effective Young's modulus, all the nodes at $y = -L_t/2$ are fully restrained and the nodes at $y = +L_t/2$ are subjected to a constant pressure load (refer Fig. 3.4).

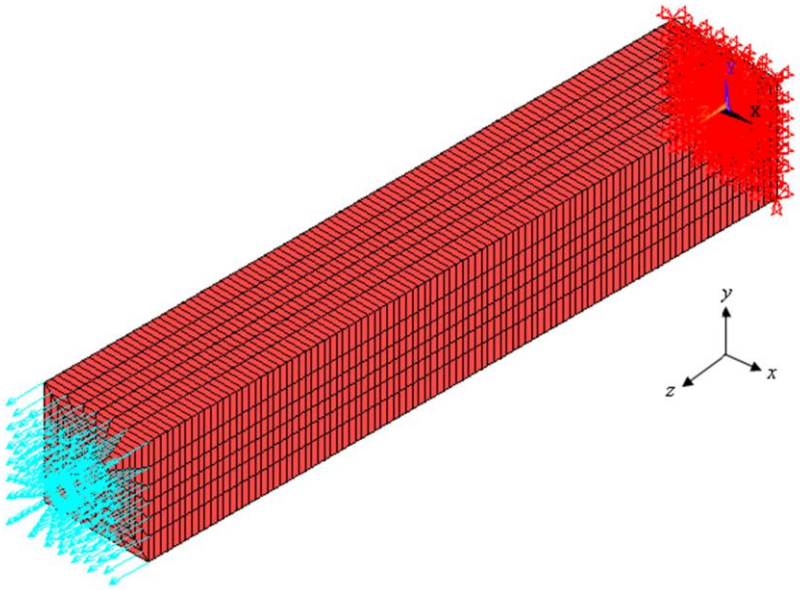

Figure 3.5 3D FE mesh for the RVE with boundary conditions.

The same 3D FE model is used for the calculation of the effective CTE of CNT-reinforced composites as described in section 3.2.2. In this case, all the nodes at $z = 0$ are fully restrained and a uniform temperature, $\Delta T = 10^0$C is applied on all nodes of the FE model.

3.5 Results and discussion

The effective Young's modulus and the coefficient of thermal expansion (CTE) of the CNT-reinforced composite has been evaluated considering a square RVE using the FE method as discussed in the previous section. The computed Young' modulus and CTE so obtained are compared with the Young's modulus and CTE of the matrix, respectively. To get a clear idea on the variation of the Young's modulus and CTE of the different types of nanocomposites, five types of matrix materials have been chosen. The matrix materials are epoxy, magnesium (Mg), titanium (Ti), steel and alumina (Al_2O_3) i.e. from low strength to high strength those are polymeric (epoxy), metallic (Mg and Ti) and ceramic (Al_2O_3) materials. Properties of matrix materials and CNT are listed in Table 3.2.

Table 3.2 Properties of epoxy and single-walled CNT

Materials	Young's modulus (GPa)	Poisson's ratio	Coefficient of thermal expansion ($\times 10^{-6}$ K^{-1})	Density (kg/m^3)
SWCNT	1000	0.28	-1.5	1300
Epoxy	3.89	0.37	58	1380
Magnesium	45	0.29	24.8	1740
Titanium	116	0.32	8.6	4500
Steel	210	0.29	12	7800
Alumina	375	0.22	8.1	3950

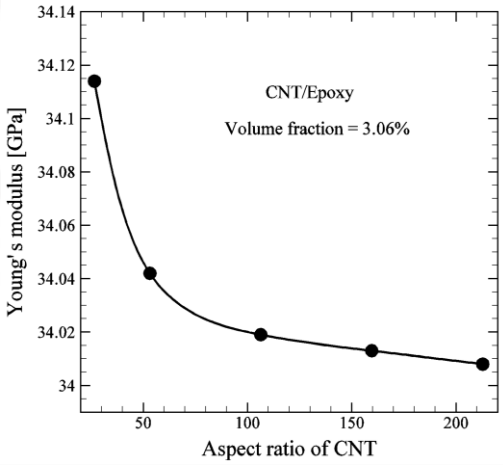

Figure 3.6(a) Young's modulus of CNT/epoxy composite with aspect ratio.

Effect of volume fraction on the Young's modulus and on the CTE of the nanocomposites has also been studied. Properties of epoxy and SWCNT are chosen from published literatures [7, 13, 17, 143-145] and listed in Table 3.2. Figure 3.6(a) shows

variation of axial Young's modulus of CNT/epoxy with aspect ratio (length/diameter) of CNT for a constant volume fraction 3.06%. It can be seen from this Fig. 3.6(a) that after an aspect ratio of 106, change in axial Young's modulus is insignificant. Therefore, in the present analysis, the diameter of CNT is taken as 1.88 nm keeping the aspect ratio of CNT as 106. Lusti and Gusev [83] reported that the elastic modulus of CNT/polymer composite does not change beyond an aspect ratio of 300. Dong [87] also reported that the changes in stiffness and CTE of CNT/epoxy composite become negligible when the aspect ratio is greater than 100.

3.5.1 Thermoelastic properties considering linear stress-strain relation of CNT

3.5.1.1 Convergence study

Before using the FE model for determination of thermoelastic properties, convergence of results with mesh refinement has been studied. Figure 3.6(b) shows for a typical CNT composites (CNT/epoxy), how the Young's modulus values vary with the mesh refinement. It is clearly seen from this figure that after 67200 number of elements, there is no further variation and hence the convergence. Thus in all the analysis this FE mesh is used. It can also be seen that the variation of Young's modulus for the elements range from 8400 to 67200 are not significant.

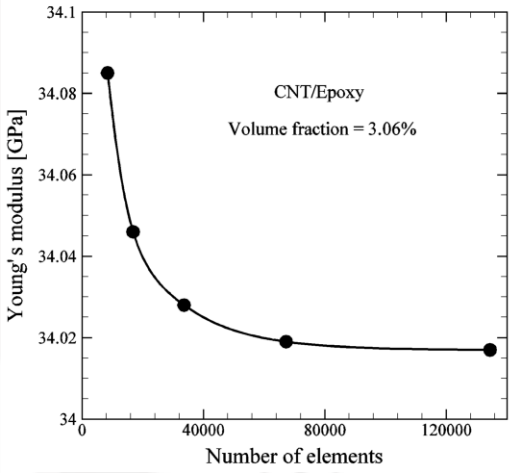

Figure 3.6(b) Young's modulus of CNT/epoxy composite with number of elements.

3.5.1.2 Effective axial Young's modulus

Referring to the Fig. 3.4, subject to an axial loading, displacement along the *z*-direction has been calculated from the FE analysis and longitudinal (or axial) Young's modulus is computed using Eq. (3.1). Table 3.3(a) shows the axial Young's modulus of the CNT/epoxy composites for a constant volume fraction 3.06% and for different matrix materials. For

CNT/epoxy composite 3.06 vol% of CNT is equivalent to 2.89 wt% of CNT. To compare the computed results, theoretical values of E_1 has also been determined using Eq. (3.4) based on rule of mixture (ROM) and also listed in Table 3.3(a).

Results in Table 3.3(a) shows that by adding 3.06 vol% CNT in a matrix, the axial Young's modulus of CNT/epoxy composites (34.02 GPa) could be increased about nine times compared to that of the pure epoxy (3.89 GPa). It could be observed from Table 3.3(a) that the axial Young's modulus of CNT/epoxy and CNT/steel composites could be increased by 774.55% and 11.75 % compared to the Young's modulus of the pure epoxy and steel, respectively.

Table 3.3(a) Effective axial Young's modulus of CNT-reinforced composites for V_{nt} = 3.06%.

Types of nanocomposites	Axial Young's modulus (GPa)		% increase of E_1 compared to pure matrix	
	Computational (FEM)	Theoretical (ROM)	Computational (FEM)	Theoretical (ROM)
CNT/epoxy	34.02	34.33	774.55	782.52
CNT/Magnesium	74.11	74.22	64.89	64.93
CNT/Titanium	143.23	143.02	23.47	23.29
CNT/Steel	234.64	234.15	11.75	11.49

For comparison of axial Young's modulus obtained from the present study, elastic properties of CNT and matrix materials are considered as E_{nt} = 1000 GPa, E_m = 100 GPa, ν_{nt} = 0.3 and ν_m = 0.3 following Chen and Liu [77]. Axial Young's modulus of CNT-reinforced composites is listed in Table 3.3(b) for a constant volume fraction of 3.617%. It could be observed from Table 3.3(b) that the axial Young's modulus obtained from the present study is in good agreement with that reported by Chen and Liu [77] in their FE analysis and that obtained from ROM thus validating the present FE model.

Table 3.3(b) Comparison of axial Young's modulus for V_{nt} = 3.617%.

Axial Young's modulus [GPa]		
Theoretical (ROM)	Chen and Liu [77]	Present study
132.55	132.55	132.74

Figure 3.7 shows the percentage increase of effective axial Young's modulus for different types of nanocomposites at a constant volume fraction of 3.06%. It can be concluded from

Fig. 3.7 that the axial Young's modulus obtained from the present FE analysis are in good agreement with theoretical axial Young's modulus obtained based on ROM.

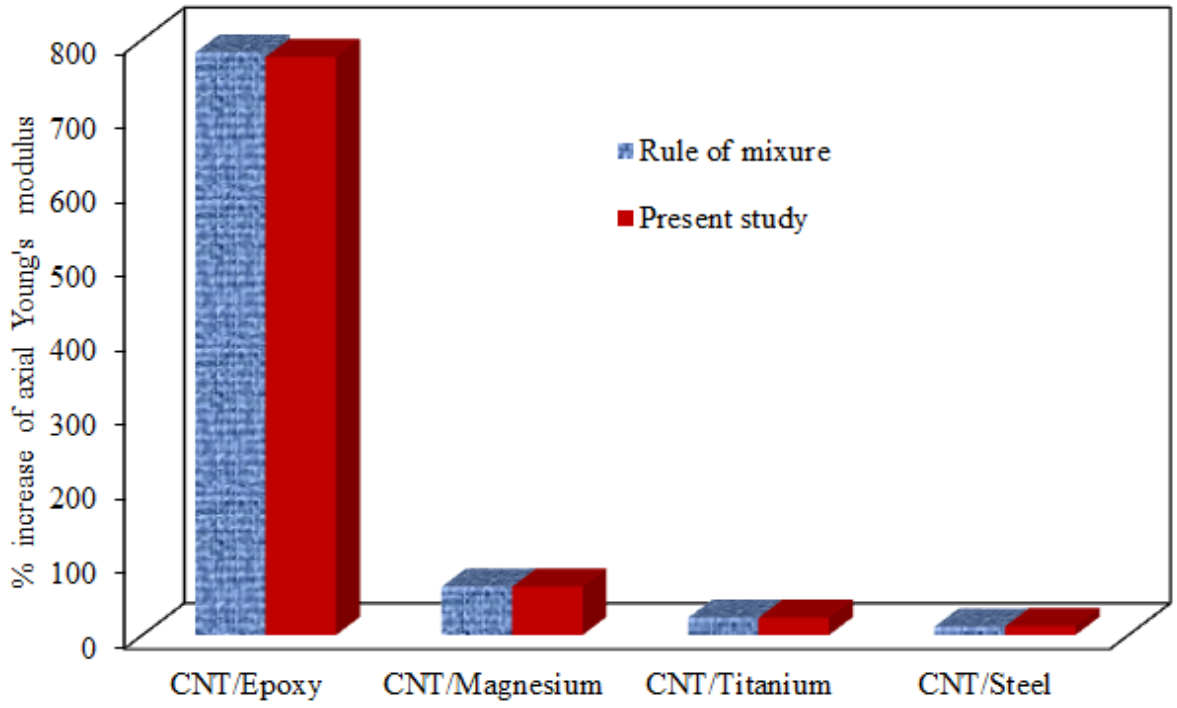

Figure 3.7 Percentage increases of effective axial Young's modulus over matrix.

3.5.1.3 Effective transverse Young's modulus

Referring to the Fig. 3.4, subject to constant pressure load, displacement along the *y*-direction has been calculated from the FE analysis and transverse Young's modulus is computed using Eq. (3.2). Table 3.4 shows the transverse Young's modulus of the CNT-reinforced composites for a constant volume fraction 3.06%. To verify the computed results, theoretical values of E_2 has also been determined using Eq. (3.5) based on ROM and also listed in Table 3.4.

Figure 3.8 shows the percentage increase in effective transverse Young's modulus for different types of nanocomposites at a constant volume fraction of 3.06%. It can be seen from Fig. 3.8 that the present FE model overestimates the E_2 compared to that obtained by ROM. In the present work diameter of CNT is considered as 1.88 nm. For lager diameter of CNT (9.6 nm), it underestimates, which was reported by Chen and Liu [77]. In the present analysis, the same has also been checked considering larger diameter of CNT (9.6 nm). It has

also been found that the computational values of E_2 are much closer to theoretical value for the diameter of CNT is equal to 4.4 nm. Discrepancy may be attributed to the fact that the CNTs are hollow tube which gets more pronounced in the FE results corresponding to larger diameter.

Table 3.4 Effective transverse Young's modulus of the CNT-reinforced composites for V_{nt} = 3.06%.

Types of nanocomposites	Transverse Young's modulus (GPa)		% increase of E_2	
	Computational (FEM)	Theoretical (ROM)	Computational (FEM)	Theoretical (ROM)
CNT/epoxy	4.99	4.01	28.28	3.08
CNT/Magnesium	52.25	46.35	16.11	3.00
CNT/Titanium	133.95	119.22	15.47	2.78
CNT/steel	231.89	215.19	10.42	2.47

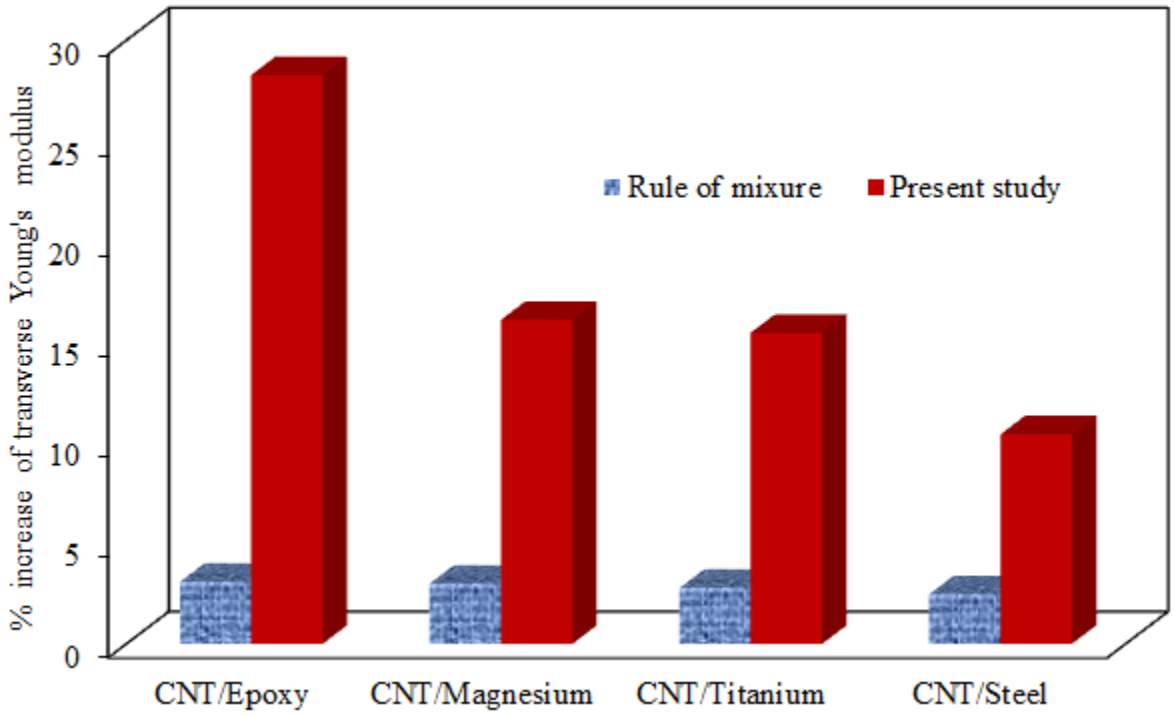

Figure 3.8. Percentage increase of effective transverse Young's modulus over matrix.

3.5.1.4 Effective axial coefficient of thermal expansion

Referring to the Fig. 3.4, subject to uniform temperature, displacement along the *z*-direction has been calculated from the FE analysis and axial CTE is computed using Eq.

(3.7). Table 3.5 shows the axial CTE of the CNT-reinforced composites at a constant volume fraction 3.06%. To compare the computed results, theoretical values of α_1 has also been determined using Eq. (3.9) and also listed in Table 3.5.

Results in Table 3.5 shows that the axial CTE of all types of CNT-reinforced composites decreased by adding 3.06 vol% CNT in a matrix. It could be observed from Table 3.5 that the percentages of reduction of axial CTE of nanocomposites are maximum for CNT/epoxy (~91%) and minimum for CNT/steel (~15%) compared to the CTE of the pure epoxy and steel, respectively.

Table 3.5 Effective axial CTE of the CNT-reinforced composites for V_{nt} = 3.06%.

Types of nanocomposites	Axial CTE ($\times 10^{-6}$ K^{-1})		% decrease of α_1 compared to matrix	
	Computational (FEM)	Theoretical (TEEP)	Computational (FEM)	Theoretical (TEEP)
CNT/epoxy	5.09	5.03	-91.2	-91.32
CNT/Magnesium	13.92	13.96	-43.87	-43.71
CNT/Titanium	6.42	6.44	-25.22	-25.1
CNT/steel	10.19	10.23	-15.08	-14.69

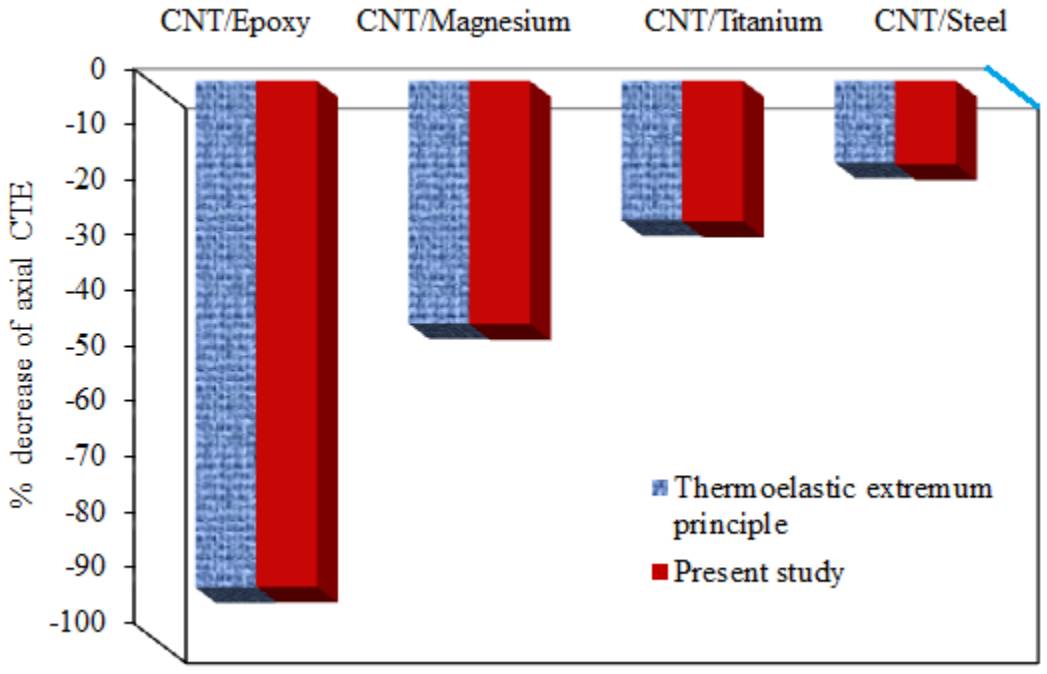

Figure 3.9 Percentage decrease of axial CTE over matrix.

Figure 3.9 shows that the percentage reduction of effective axial CTE of different types of nanocomposites at a constant volume fraction of 3.06%. It can be concluded from Fig. 3.9 that the present computational axial CTE obtained from FE analysis are in good agreement with theoretical axial CTE calculated based on thermoelastic extremum principle [142].

3.5.1.5 Effective transverse coefficient of thermal expansion

Referring to the Fig. 3.4, subject to uniform temperature, displacement along the *y*-direction has been calculated from the FE analysis and transverse CTE is computed using Eq. (3.8). The calculated effective transverse CTE of the CNT-reinforced composites are listed in Table 3.6 for a constant volume fraction of 3.06%. To compare the computed results, theoretical values of transverse CTE of CNT-reinforced composites have also been determined using Eq. (3.10) based on thermoelastic extremum principle [142] and also listed in Table 3.6.

Table 3.6 Effective transverse CTE of CNT-reinforced composites (V_{nt} = 3.06%).

Types of nanocomposites	Transverse CTE ($\times 10^{-6}$ K^{-1})		% increase/decrease of α_2 compared to matrix	
	Computational (FEM)	Theoretical (TEEP)	Computational (FEM)	Theoretical (TEEP)
CNT/epoxy	74.71	75.12	28.82	29.52
CNT/Magnesium	26.28	26.91	5.97	8.51
CNT/Titanium	8.72	8.89	1.4	3.4
CNT/Steel	11.79	11.98	-1.75	-0.15

Figure 3.10 shows the percentage increase or decrease of transverse CTE of CNT-reinforced composites for a constant volume fraction of 3.06%. It could be observed form Fig. 3.10 that percentage of the transverse CTE of CNT/steel composite decreased compared to the CTE of pure steel. But in the case of CNT/epoxy, CNT/Mg and CNT/Ti composites transverse CTE of the CNT composite increased compared to pure matrix materials (epoxy, Mg, Ti). The difference in result is due the fact that the stiffness of epoxy, Mg and Ti are lower than that of steel and therefore CNT/epoxy, CNT/Mg and CNT/Ti composites have lower relative stiffness than the CNT/steel composite. It could be concluded from Fig. 3.10 that the transverse CTE obtained from the present FE analysis are in good agreement with

theoretical transverse CTE calculated based on thermoelastic extremum principle [142]. It could be observed from Fig. 3.10 that the transverse CTE compared to the CTE of the matrices increased upto 28.28% for CNT/epoxy composites but decreased upto 1.75% for CNT/steel composites.

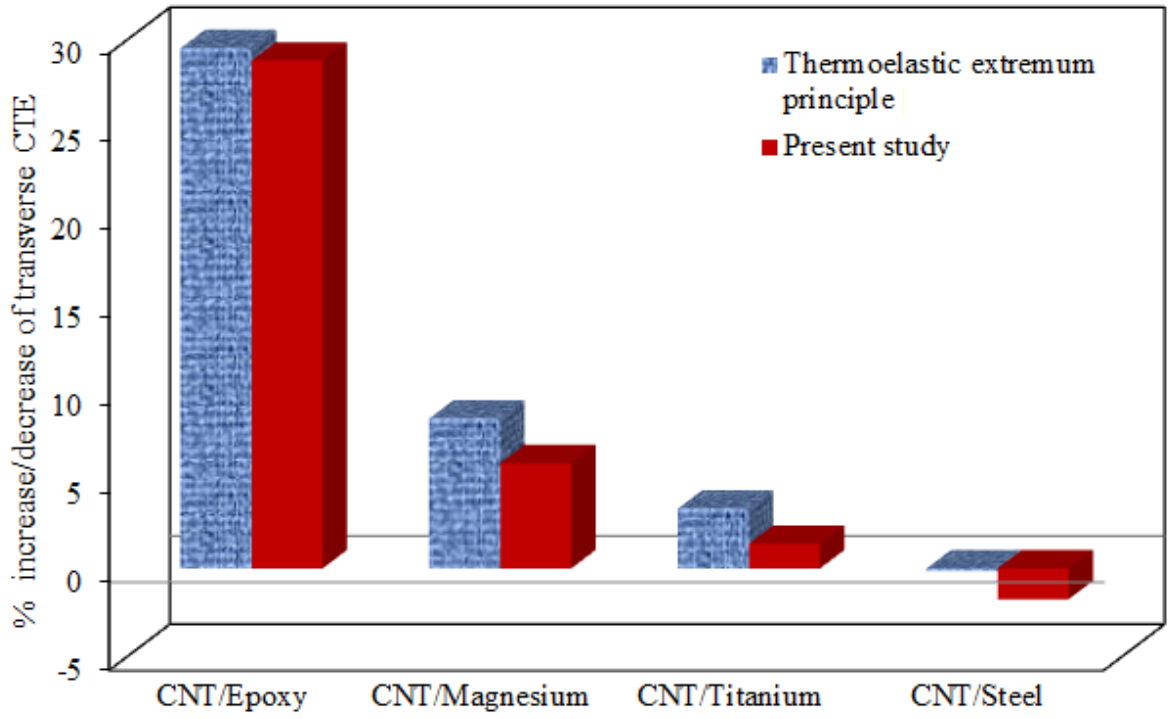

Figure 3.10 Percentage increase/decrease of transverse CTE over matrix.

3.5.2 Thermoelastic properties of CNT/epoxy composites considering linear and non-linear stress-strain relation of CNT

Most of the earlier literatures have considered the linear stress-strain relation of CNTs for analysis of CNT-reinforced composites. But in reality CNTs behave nonlinearly especially at higher strain and the nonlinear behavior of CNT needs to be considered for the analysis. The stress-strain curves of the armchair and zigzag CNTs were found experimentally by Tserpes et al. [117] and by fitting the data of the curves using third order polynomials, they obtained the following relations between the stress and strain

$$\sigma_n = 2909.8\varepsilon_n^3 - 4995.6\varepsilon_n^2 + 1364.9\varepsilon_n \quad \text{(for zigzag CNT)} \tag{3.12}$$

$$\sigma_n = 5958.5\varepsilon_n^3 - 4769.4\varepsilon_n^2 + 1334.7\varepsilon_n \quad \text{(for armchair CNT)} \tag{3.13}$$

Equation (3.12) has been used in the present FE analysis considering zigzag CNT. From Eqs. (3.12) and (3.13) the stiffness of nanotube could be also derived as a function of strain also [117].

The same 3D FE model and boundary conditions have been used for calculation of thermoelastic properties of CNT/epoxy composites as described in sections 3.2.2 and 3.4, respectively. However, the non-linear stress-strain relation for CNT (Eq. (3.12)) has been input for the FE modeling. But in case of linear stress-strain relation, the Young' modulus of CNT is take as 1.364 TPa [117]. The effective Young's modulus and CTE of the CNT/epoxy composite has been evaluated considering linear and non-linear stress-strain relation of CNT at a constant volume fraction of 3.06% as well as for different volume fraction.

3.5.2.1 For a constant volume fraction

3.5.2.1.1 Axial and transverse Young's modulus

The effective axial and transverse Young's moduli of the CNT/epoxy composites have been computed using the results from FE analysis and using Eqs. (3.1 - 3.2) for a constant volume fraction of 3.06% and listed Table 3.7. Theoretical values of effective axial and transverse Young's modulus of the CNT/epoxy composites have also been calculated using Eqs. (3.4 - 3.5) based on ROM and listed in Table 3.7.

Table 3.7 Effective axial and transverse Young's modulus of the CNT/epoxy composites for V_{nt} = 3.06%.

Young,s modulus (GPa)	Theoretical (ROM)	Computational (linear)	Computational (non-linear)
Axial (E_1)	45.51	45.11	39.36
Transverse (E_2)	4.01	5	4.99

It could be observed from Table 3.7 that the computed axial Young's modulus of CNT/epoxy composite considering linear stress-strain relation of CNT shows little deviation compared to theoretical values calculated based on ROM but there is considerable deviation when the same has been computed considering non-linear stress-strain relation of CNT. It could also be observed from Table 3.7 that the difference of estimated longitudinal Young's

modulus by considering linear and non-linear model is almost 15% and the linear model overestimates the longitudinal stiffness.

3.5.2.1.2 Axial and transverse coefficient of thermal expansion

The effective axial and transverse CTE of CNT/epoxy composites have been computed using the result from FE analysis and using Eqs. (3.7) and (3.8) for a constant volume fraction of 3.06% and listed in Table 3.8. Theoretical values of effective axial and transverse CTE of the CNT/epoxy composites have also been determined using Eqs. (3.9 - 3.10) based on thermoelastic extremum principle and listed in Table 3.8.

Table 3.8 Effective axial and transverse CTE of the CNT/epoxy composites for V_{nt} = 3.06%.

Coefficient of Thermal Expansion ($\times 10^{-6}$ K^{-1})	Theoretical (TEEP)	Computational (linear)	Computational (non-linear)
Axial (α_1)	3.43	3.48	4.95
Transverse (α_2)	75.71	75.34	74.87

It has been observed from Table 3.8 that the computed axial CTEs of CNT/epoxy composite have a difference of almost 42% between the linear and non-linear model of CNT and the non-linear model estimates a higher value of longitudinal CTE.

3.5.2.2 Effect of volume fraction

3.5.2.2.1 Axial and transverse Young's modulus

In order to understand the effect of volume fraction, range of the volume fraction is taken from 0.5% to 15.77% for calculation of Young's modulus and CTE of CNT/epoxy composites. Figures 3.11(a) and 3.11(b) show the variation of axial and transverse Young's modulus, respectively of CNT/epoxy composites with volume fraction.

It could be observed from Fig. 3.11 that the Young's modulus of CNT/epoxy composites increased with increase in volume fraction. It could be observed from Fig. 3.11(a) that the computed values of E_1 matches exactly with that obtained from rule of mixture (ROM) in the case of linear stress-strain relation of CNT. However, while non-linear stress-strain relation is considered, there has been considerable difference of E_1 obtained from the present

FE analysis compared to that obtained from ROM and the difference increases as volume fraction increases. At 15.77% volume fraction, the difference of axial Young's modulus is as high as almost 7%. In the case of transverse Young's modulus, it could be observed from Fig. 3.11(b) that there has been considerable difference of E_2 obtained from the present FE analysis for both the linear and non-linear stress-strain relation of CNT compared to those obtained from ROM. The reason of the same has already been discussed in section 3.5.1.3.

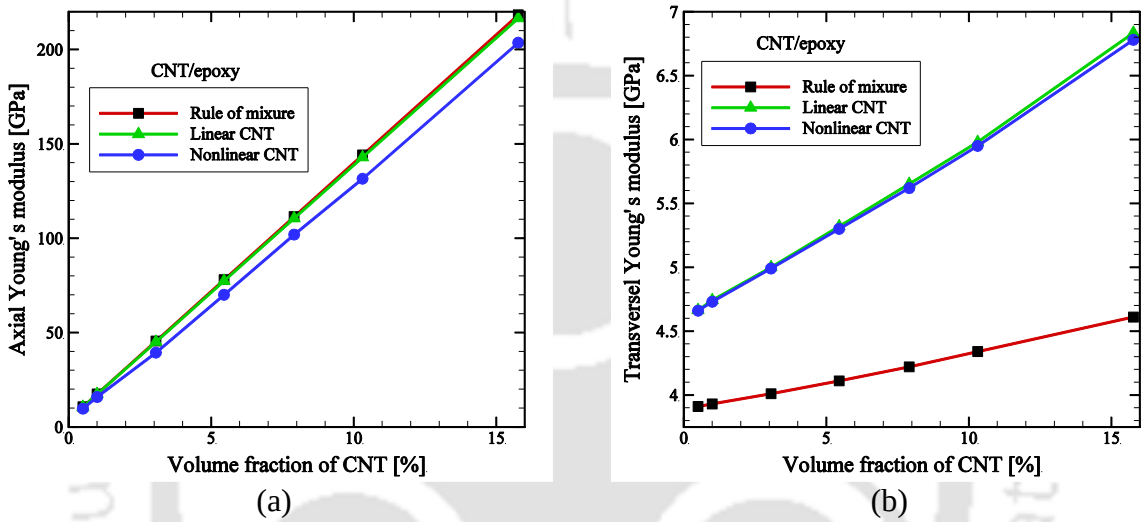

Figure 3.11 Variation of (a) axial and (b) transverse Young's modulus of CNT/epoxy composite with volume fraction.

3.5.2.2.2 Axial and transverse coefficient of thermal expansion

Figures 3.12(a) and 3.12(b) show the variation of effective axial and transverse CTE, respectively of the CNT/epoxy composites with volume fractions. It can be seen from Fig. 3.12(a) that the axial CTE of the CNT/epoxy composites are $20.04\times10^{-6}\,\mathrm{K}^{-1}$ and $-0.61\times10^{-6}\,\mathrm{K}^{-1}$ corresponding to volume fractions of 0.5% and 15.77%, respectively. It could be concluded that the axial CTE of CNT/epoxy composites decreases with the increase in volume fraction. Another important observation from Fig. 3.12(a) is that the axial CTE of the CNT composites is zero at a volume fraction ~10%. It is important to note that the volume fraction of CNT at which the longitudinal CTE = 0 is estimated to be higher compared to that estimated by thermoelastic extremum principle (TEEP) or linear model and hence in designing components from the view point of thermal stability, it is important to use the non-linear model. It could be concluded from Fig. 3.12(a) that the computed effective

axial CTE of CNT/epoxy composite considering linear and nonlinear stress-strain relation of CNT are in good agreement at lower volume fraction with the theoretical results based on TEEP [142]. But it is also observed from Fig. 3.12(a) that at higher volume fraction the computed longitudinal CTE obtained from present FE analysis considering non-linear stress-strain relation of CNT shows deviation when compared to both the theoretical results obtained based on thermoelastic extremum principle and computational result obtained considering linear relation of CNT.

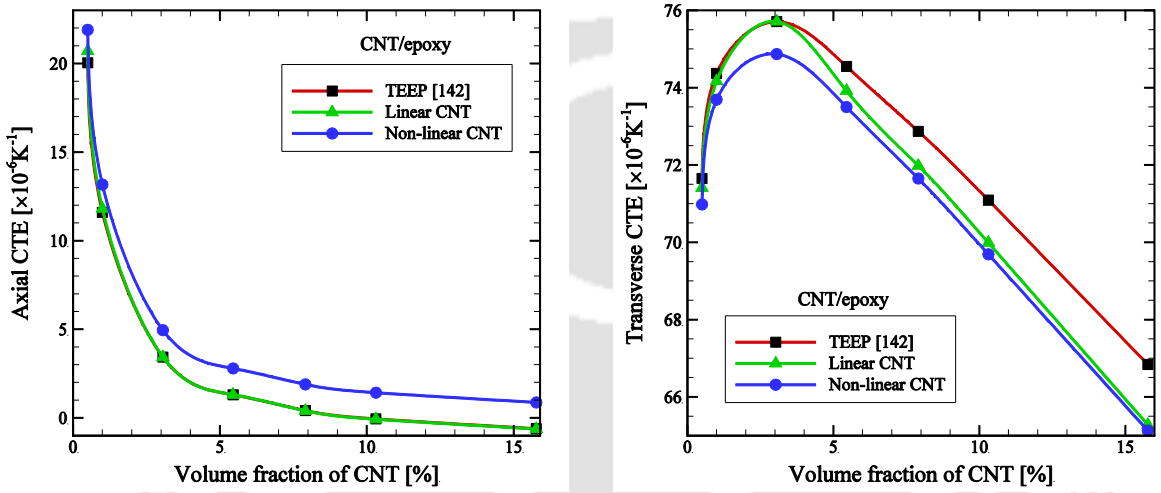

(a) (b)

Figure 3.12 Variation of (a) axial and (b) transverse CTE of CNT/epoxy composite with volume fraction.

It can be seen from Fig. 3.12(b) that the transverse CTE of CNT/epoxy initially increases with increase in volume fraction, attains the maximum value at a particular volume fraction and then decreases with further increase in volume fraction. It could be concluded that the computed transverse CTE considering both the linear and nonlinear stress-strain behavior of CNT are in good agreement at lower volume fraction compared to the theoretical results obtained based on thermoelastic extremum principle. It is also observed from Fig. 3.12(b) that at higher volume fraction the computed transverse CTE shows deviation when compared to the theoretical results obtained based on thermoelastic extremum principle.

It could also be observed from Figs. 3.11 and 3.12 that there has been deviation of thermoelastic properties of CNT/epoxy composites which obtained considering non-linear stress-strain relation of CNT compared to the values obtained by not considering non-linear

stress-strain relation of CNT and the difference increases as volume fraction increases. Since non-linear relation of CNT is actual as reported by Tserpes et al. [117] therefore in the next section for calculation of thermoelastic properties of different CNT-reinforced composite the non-linear stress-strain relation of CNT has been input in the analysis.

3.5.3 Young's modulus of CNT-reinforced metal matrix composites (CNT/Mg, CNT/Ti and CNT/steel) considering non-linear stress-strain relation of CNT

The same 3D FE model and boundary conditions have been used for calculation of Young's modulus of CNT-reinforced composites as described in section 3.2.2 and section 3.4, respectively. The effective Young's modulus of CNT-reinforced composites have been evaluated considering linear and non-linear stress-strain relation of CNT at a constant volume fraction of 3.06% as well as for different volume fraction. The computed Young's modulus of the CNT-reinforced composites are also compared with theoretical values obtained using ROM. Effect of volume fraction on the Young's modulus of the CNT-reinforced composites have also been studied. The Young's modulus of CNT is considered as 1.364 TPa [117] for linear stress-strain relation of CNT.

3.5.3.1 Axial and transverse Young's modulus for V_{nt} = 3.06%

Based on the average displacement obtained from FE analysis as described in sections 3.3.1 and 3.4, the effective Young's modulus of CNT-reinforced composites is calculated using Eqs. (3.1 -3.2). The computed values of Young's modulus are listed in Table 3.9. For comparison of the results obtained using the present multi-scale FE analysis, the theoretical values of Young's modulus based on ROM (Eqs. (3.4 - 3.5)) are also listed in Table 3.9.

It could be observed from the result listed in Table 3.9 that the computed axial Young's modulus of CNT-reinforced metal matrix composites (MMCs) shows little deviation when compared to the theoretical results based ROM. But in case of transverse Young's modulus of CNT-reinforced MMCs there are considerable difference when compared to the theoretical results based ROM.

Table 3.9 Effective axial and transverse Young's modulus of CNT-reinforced composites for V_{nt} = 3.06%

CNT-reinforced composites	Young,s modulus (GPa)	Theoretical (ROM)	Computational (Non-linear)
CNT/Mg	Axial (E_1)	85.36	82.47
	Transverse (E_2)	46.37	52.59
CNT/Ti	Axial (E_1)	154.18	149.96
	Transverse (E_2)	119.34	135.24
CNT/Steel	Axial (E_1)	245.31	242.16
	Transverse (E_2)	215.58	234.68

3.5.3.2 Axial and transverse Young's modulus for different volume fractions

Range of the volume fraction is taken from 0.5% to 15.77% for calculation of effective Young's modulus of CNT-reinforced composites. Figures 3.13(a) and 3.13(b) show the variation of axial and transverse Young's modulus, respectively of CNT/Mg composites with volume fraction.

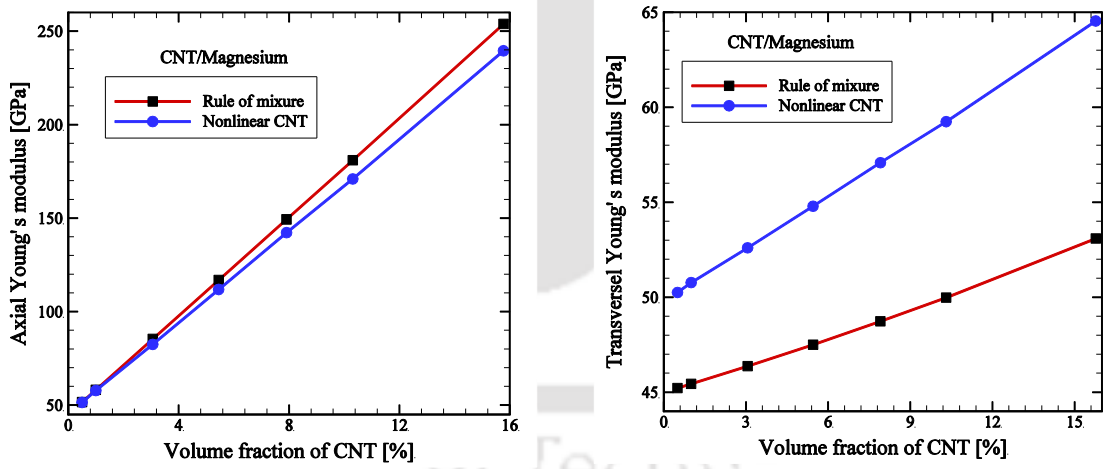

(a) (b)

Figure 3.13 Variation of (a) axial and (b) transverse Young's modulus of CNT/Mg composite with volume fraction.

It can be seen form Fig. 3.13(a) that axial Young's modulus of CNT/Mg composite increased with the increase in volume fraction. It could be observed from Fig. 3.13(a) that there has been considerable difference of E_1 obtained from the present FE analysis

considering non-linear stress-strain relation of CNT compared to that E_1 obtained from ROM and the difference increases as volume fraction increases. It could also be observed from Fig. 3.13(a) that the difference of estimated longitudinal Young's modulus by considering ROM and non-linear stress-strain relation of CNT is almost 6% and the ROM model overestimates the longitudinal stiffness.

It can be seen in Fig. 3.13(b) that the computed value of E_2 of CNT/Ti composite increased with increase in volume fraction. It could be observed from Fig. 3.13(b) that there has been considerable difference of the computed values of E_2 obtained from present FE analysis compared to the values of E_2 computed based on ROM and the difference increases as volume fraction increases.

Figures 3.14(a) and 3.14(b) show the variation of axial and transverse Young's modulus, respectively of CNT/Ti composites with volume fraction. It can be seen form Fig. 3.14(a) that axial Young's modulus of CNT/Ti composite increased with the increase in volume fraction.

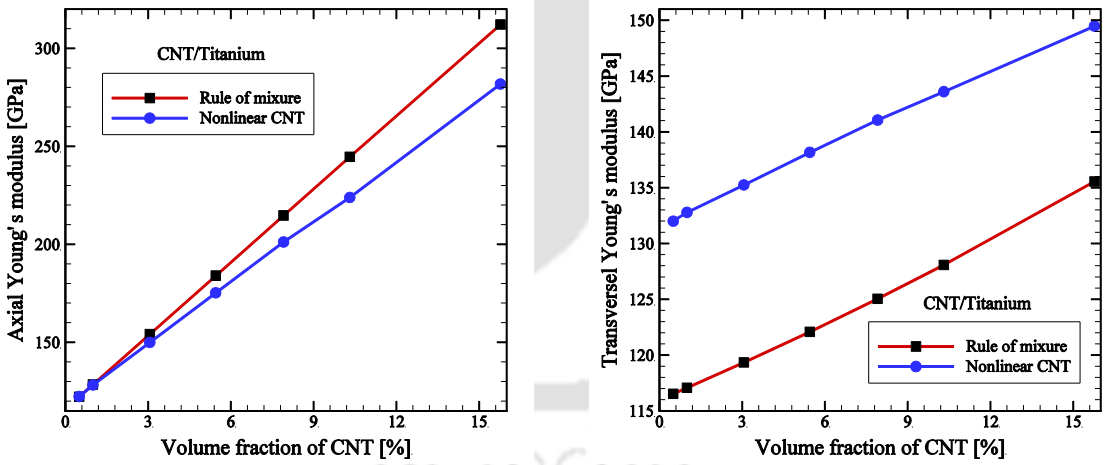

(a) (b)

Figure 3.14 Variation of (a) axial and (b) transverse Young's modulus of CNT/Ti composite with volume fraction.

It could be observed from Fig. 3.14(a) that there has been considerable difference of E_1 obtained from the present FE analysis considering non-linear stress-strain relation of CNT compared to that E_1 obtained from ROM and the difference increases as volume fraction

increases. It could also be observed from Fig. 3.14(a) that the difference of estimated longitudinal Young's modulus by considering ROM and non-linear stress-strain relation of CNT is almost 11% and the ROM model overestimates the longitudinal stiffness.

It can be seen in Fig. 3.14(b) that the computed value of E_2 of CNT/Ti composite increased with increase in volume fraction. It could be observed from Fig. 3.14(b) that there has been considerable difference of the computed values of E_2 obtained from present FE analysis considering non-linear stress-strain relation of CNT compared to the values of E_2 computed based on ROM.

Figures 3.15(a) and 3.15(b) show the variation of axial and transverse Young's modulus, respectively of CNT/steel composites with volume fraction. It can be seen form Fig. 3.15(a) that axial Young's modulus of CNT/steel composite increased with the increase in volume fraction.

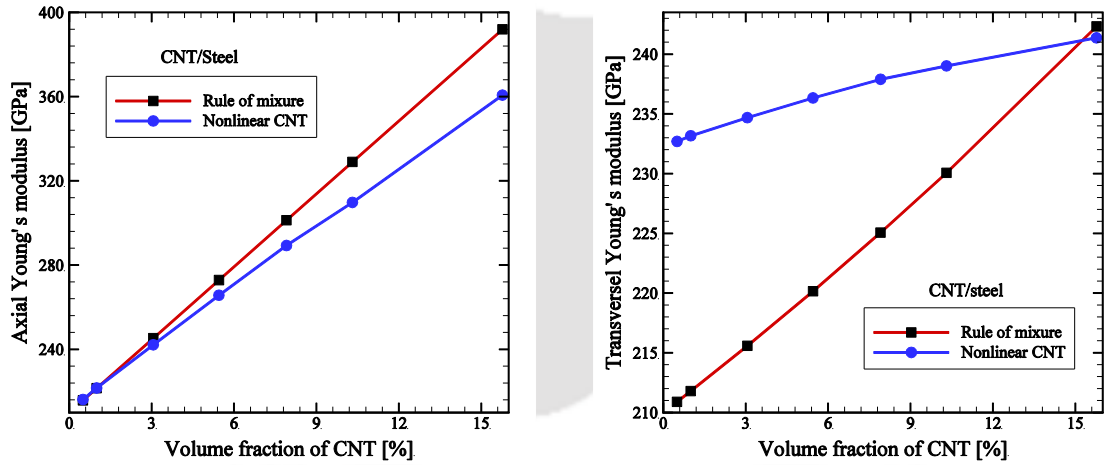

(a) (b)

Figure 3.15 Variation of (a) axial and (b) transverse Young's modulus of CNT/steel composite with volume fraction.

It could be observed from Fig. 3.15(a) that there has been considerable difference of E_1 obtained from the present FE analysis considering non-linear stress-strain relation of CNT compared to that E_1 obtained from ROM and the difference increases as volume fraction increases. It could also be observed from Fig. 3.15(a) that the difference of estimated

longitudinal Young's modulus by considering ROM and non-linear stress-strain relation of CNT is almost 9% and the ROM model overestimates the longitudinal stiffness.

It can be seen in Fig. 3.15(b) that the computed value of E_2 of CNT/steel composite increased with increase in volume fraction when computed based on ROM and from present FE analysis while considering non-linear stress-strain behavior of CNT. It could also be observed from Fig. 3.15(b) that there has been considerable difference of E_2 values those obtained considering non-linear stress-strain behavior of CNT compared to the values obtained from ROM and the difference decreases as volume fraction increases. It could also be observed from Fig. 3.15(b) that at higher volume fraction of ~ 15.77% the values of E_2 is almost same.

3.5.4 Young's modulus of CNT-reinforced ceramic matrix composite (CNT/Al_2O_3) considering non-linear stress-strain relation of CNT

Ceramics have many advantages over polymer and metals. Therefore, in this section, the Young's modulus of CNT/Al_2O_3 composite will be evaluated. The same 3D FE model and boundary conditions have been used for calculation of Young's modulus of CNT/Al_2O_3 as described in section 3.2.2 and section 3.4. The effective Young's modulus of CNT/Al_2O_3 composites have been evaluated considering non-linear behavior of CNT at a constant volume fraction of 3.06% as well as for different volume fraction. The computed Young's modulus of CNT/Al_2O_3 composites are also compared with theoretical values obtained using ROM. Effect of volume fraction on the Young's modulus of CNT/Al_2O_3 composites have also been studied. The Young's modulus of CNT is considered as 1.364 TPa [117] for linear stress-strain relation of CNT.

3.5.4.1 Axial and transverse Young's modulus for V_{nt} = 3.06%

Based on the average displacement obtained from FE analysis as described in sections 3.3.1 and 3.4, the effective Young's modulus of CNT/Al_2O_3 composites is calculated using Eqs. (3.1 - 3.2). The computed values of Young's modulus are listed in Table 3.10. For comparison of the results obtained using the present multi-scale FE analysis, the theoretical values of Young's modulus based on ROM (Eqs. (3.4 - 3.5)) are also listed in Table 3.10.

Table 3.10 Axial and transverse Young's modulus of CNT/Al_2O_3 composites for V_{nt} = 3.06%.

CNT-reinforced composites	Young,s modulus (GPa)	Theoretical (ROM)	Computational (Non-linear)
CNT/Al_2O_3	Axial (E_1)	405.26	402.97
	Transverse (E_2)	383.51	392.67

It could be observed from the result listed in Table 3.10 that there has been considerable difference of computed effective Young's modulus of CNT/Al_2O_3 composites obtained from present FE analysis by considering non-linear stress-strain behavior of CNT when compared to the theoretical values results obtained based on ROM.

3.5.4.2 Axial and transverse Young's modulus for different volume fractions

Figures 3.16(a) and 3.16(b) show the variation of axial and transverse Young's modulus, respectively of CNT/Al_2O_3 composites with volume fraction. It can be seen form Fig. 3.16(a) that the axial Young's modulus of CNT/Al_2O_3 composite increased with the increase in volume fraction.

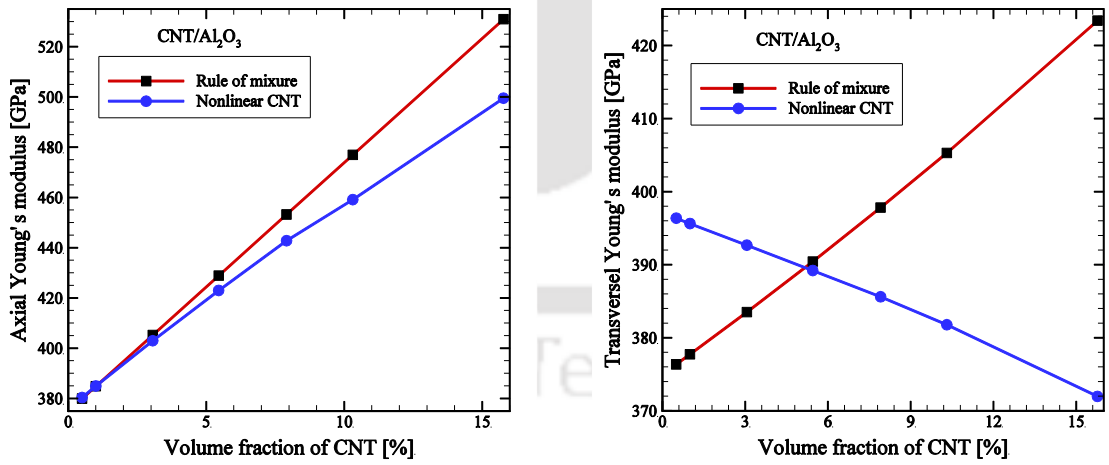

(a) (b)

Figure 3.16 Variation of (a) axial and (b) transverse Young's modulus of CNT/Al_2O_3 composite with volume fraction.

It could be observed from Fig. 3.16(a) that there has been considerable difference of E_1 obtained from the present FE analysis considering non-linear stress-strain relation of CNT

compared to that E_1 obtained from ROM and the difference increases as volume fraction increases. It could also be observed from Fig. 3.16(a) that the difference of estimated longitudinal Young's modulus by considering ROM and non-linear stress-strain relation of CNT is almost 6.3% and the ROM model overestimates the longitudinal stiffness.

It can be seen in Fig. 3.16(b) that the computed value of E_2 of CNT/Al_2O_3 composite increased with increase in volume fraction when computed based on ROM. But the computed value of E_2 of CNT/Al_2O_3 composite decreased with increase in volume fraction when computed from present FE analysis considering non-linear stress-strain behavior of CNT. It could also be observed from Fig. 3.16(b) that there has been considerable difference of E_2 values those obtained considering non-linear stress-strain behavior of CNT compared to the theoretical values obtained from ROM. It could also be observed from Fig. 3.16(b) that at a volume fraction of ~ 5 both the values of E_2 are same.

In the present work, it has also been found that the computed values of E_2 for CNT/Al_2O_3 composite are much closer to theoretical values when a solid CNT has been consider in place of a hollow CNT.

3.5.5 Comparison of Young's modulus considering linear and non-linear stress-strain relation of CNT

It can be seen form Figs. 3.11(a) and 3.13(a) to 3.16(a) that axial Young's modulus of CNT-reinforced composite increased with the increase in volume fraction. It could be observed from Fig. 3.11 that the computed values of E_1 match exactly with those obtained from rule of mixture (ROM) in the case of linear behavior of CNT. However, while non-linear stress-strain relation of CNT is considered, there has been considerable difference of E_1 obtained from the present FE analysis compared to that obtained from ROM and the difference increases as volume fraction increases. It can be seen in Figs. 3.11(b) and 3.13(b) to 3.16(b) that the computed value of E_2 of CNT-reinforced composite increased with increase in volume fraction for CNT/epoxy composite but in the case of CNT/Al_2O_3 the computed value of E_2 decreased with increase in volume fraction.

Some important conclusions can be drawn from the above results on Young's modulus of CNT-reinforced composites. The increase in effective Young's modulus in transverse direction is very less compared to the effective Young's modulus in axial direction. The computed effective Young's modulus using FE method may be compared with earlier experimental [45, 75] and computational [77, 83] published results. The computed effective CTE using FE method may be compared with the computational results as reported by Lusti and Gusev [83] and with the experimental results as reported by Dong C [87] and Guo et al. [88].

Since in actual case the stress-strain relation of CNTs are nonlinear as observed experimentally [117] and since not considering that in FE analysis make a difference in thermoelastic properties of CNT-reinforced composites, therefore non-linear stress-strain relation should be considered for reliable computation of properties of CNT-reinforced composites.

3.6 Summary

Thermo-mechanical properties of CNT composites have been determined considering a RVE and FE analysis and effect of volume fraction of those properties have been studied. It is observed that when linear behavior of CNT is considered, the results match with the well-known ROM but considering non-linear stress-strain relation of CNT, result deviate and the deviation is much pronounced at higher volume fraction. This has been observed for all the three types of CNT-reinforced composites considered viz. CNT/PMCs, CNT/MMCs and CNT/CMCs. Thus in view of the established fact that stress-strain relation of CNT is non-linear and the present observation, it is recommended that for accurate results, non-linear stress-strain relation of CNT needs to be incorporate in the FE analysis especially at higher strain. Some of the important observations are

- Even a small volume fraction of CNT sufficiently increases the Young's modulus of CNT composites compared to the matrix. This however depends upon type of matrix materials. For a volume fraction of 3.06% the axial Young's modulus of CNT/epoxy and CNT/steel composites could be increased 8.76 times and 1.11 times compared to the Young's modulus of pure epoxy and steel, respectively.

- The axial Young's modulus of CNT composite increases with the increase in volume fraction for all the CNT-reinforced composites.
- The increase in effective Young's modulus in transverse direction is very less compared to the effective Young's modulus in axial direction.
- The computed transverse Young's modulus of CNT composite increases with the increase in volume fraction for CNT/epoxy composite but decreases with the increase in volume fraction for CNT/A_2O_2 composite. Therefore transverse Young's modulus of CNT-reinforced composites depends on the relative stiffness of the matrix materials.
- Estimate of longitudinal Young's modulus using non-linear stress-strain relation of CNT is less than that obtained using linear stress-strain relation of CNT and the differences are more at higher volume fraction of CNT. It is observed that the linear model estimates a higher value of longitudinal Young's modulus and hence using non-linear model will provide a conservative design approach.
- The computed axial transverse Young's modulus of CNT composite considering non-linear stress-strain relation of CNT show significant deviation at higher volume fraction when compared to the theoretical results obtained from ROM and computational results obtained by considering linear stress-strain relation of CNT.
- It could also be observed for CNT/epoxy composite that the difference of estimated longitudinal Young's modulus by considering linear and non-linear model is almost 15% and the linear model overestimates the longitudinal stiffness.
- For a volume fraction of 3.06% the axial CTE of CNT/epoxy and CNT/steel composites could be decreased by 91.2% and 15.08% compared to the CTE of the pure epoxy and steel, respectively. In the same line for a volume fraction of 3.06% the transverse CTE of CNT/epoxy and CNT/steel could be increased and decreased by 28.28% and 1.75% compared to the CTE of pure epoxy and steel, respectively.
- Increase in volume fractions of CNT in CNT-reinforced composites leads to decrease in CTE. Therefore, it is possible to decide on volume fraction of CNT to achieve the desired CTE. For example the axial CTE of the CNT/epoxy could be

reduced to zero corresponding to a volume fraction of ~10%. Non-linear model overestimate the volume fraction at which axial CTE become zero.

- It is important to note that the volume fraction of CNT at which the longitudinal CTE is zero is estimated to be higher compared to that estimated by TEEP or linear model and hence in designing components from the view point of thermal stability, it is important to use the non-linear model.
- It has been observed that the computed longitudinal CTEs of CNT/epoxy composite have a difference of almost 42% between the linear and non-linear model of CNT and the non-linear model estimates a higher value of longitudinal CTE.
- The transverse CTE of CNT/epoxy composite shows deviation when compared to the theoretical results obtained from thermoelastic extremum principle at higher volume fraction.

Chapter 4

Stress Analysis of CNT-Reinforced Composites with a Broken CNT using Finite Element Method

4.1 Introduction

In the previous chapter, it was concluded that even a very small volume fraction of CNT (V_{nt}) leads to a very high value of stiffness of the CNT composites. Generally, therefore, the volume fraction of CNT in CNT-reinforced composite is less compared to that in conventional glass or carbon fiber composites. Thus defect in CNT will have more impact on the strength and stiffness of such composites. However due to statistical distribution of strength of CNTs, it is possible that one or more CNT breaks during loading. This chapter presents finite element (FE) analysis of different types of CNT-reinforced composites viz. CNT-polymer (CNT/epoxy), CNT-metal (CNT/aluminum, CNT/titanium, CNT/copper) and CNT-ceramic (CNT/alumina) having a broken fiber (CNT) to study the stress redistribution in the vicinity of the break and the chances of failure due to such redistribution. Two types of representative volume element (RVE) have been considered for FE modeling viz. a single-CNT RVE and a nine-CNT RVE to understand the limitations and advantages of such modeling. In addition, analysis has been performed considering both linear and nonlinear stress-strain relations of CNTs to study the importance of considering or not considering non-linear stress-strain relation. Finite element analysis has been carried out and axial normal stresses (ANS) in the broken CNT, interfacial stresses at the interface of the broken CNT and the matrix, and ANS in the adjacent intact CNTs have been computed. Effect of important parameters such as volume fraction, matrix materials on the stress distribution around the broken CNT has also been investigated.

4.2 Finite element modeling of CNT-reinforced composites

Representative volume element model of CNT-reinforced composites with interface and its surrounding matrix is constructed on the basis of multi-scale approach. The same has been

shown in Fig. 1.6 in Chapter 1 (Section 1.4.3.1) and successive development of a square RVE with nine CNTs model from a C-C bond via continuum model of SWCNT from the geometry of a zigzag SWCNT has been described in Chapter 1 (section 1.4.3.1).

4.3. Stress redistribution around a broken CNT by considering linear stress-strain relation of CNT

4.3.1 Single-CNT square RVE model

4.3.1.1 Geometry, material properties and volume fraction

A square RVE with single-CNT surrounded by matrix materials has been considered in the present analysis. It has been assumed that the CNTs and matrix in a RVE are linearly elastic, isotropic, and homogeneous materials. It has also been assumed that the CNTs and matrix are perfectively bonded with no slip at the interface in the RVE to be studied. In order to study the effect of a broken CNT on the distribution of ANS in the broken CNT and interfacial stresses at the interface between the broken CNT and the matrix, a 1-CNT RVE of CNT-reinforced composite has been considered. The CNT is considered to be placed at the center of the RVE which is surrounded by the matrix materials. Figure 4.1(a) shows the front view of 1-CNT RVE model along with broken CNT, and interface between broken CNT and matrix materials. The linear stress-strain relation of SWCNT is considered in the present work. The diameter of CNT has been taken as 1.88 nm (which is equal to the diameter of zigzag (24, 0) CNTs), and the thickness (t) of CNT layer is considered 0.34 nm [6-7]. In case of polar coordinate system, the r-θ plane is the transverse plane and the z-axis is the axial direction of the square RVE as shown in Fig. 4.1(a). Properties of CNT and matrix materials are listed in Chapter 3 (section 3.5).

In practice the weight fraction of CNT in CNT-based composites is limited to 10 wt% which has been reported by Meyyappan [144] in 2005. For CNT/epoxy composite 10 wt% of CNT is equivalent to 10.55 vol% of CNT. This limitation may be due to high cost of CNT and hence in the present analysis the range of the volume fraction is taken from 1% - 10.3%. But with improved manufacturing process the cost of CNTs is getting reduced which is also reported by Wardle et al. [63] in 2008, where they fabricated aligned CNT/polymer composites with a volume fraction of 20%. Bradford et al. [64] also fabricated CNT/epoxy composites with long aligned CNTs up to 27 vol% of CNT in 2010. From these two

literatures it could be concluded that volume fraction of CNT could be considered more that 10% also. From the present analysis it could be observed from Fig. 3.12(a) in Chapter 3 (section 3.5.2.2.2) that the axial CTE of CNT/epoxy composites is zero at a volume fraction ~10% for the chosen epoxy and hence keeping volume fraction in and around 10% may also be important from thermal response view point.

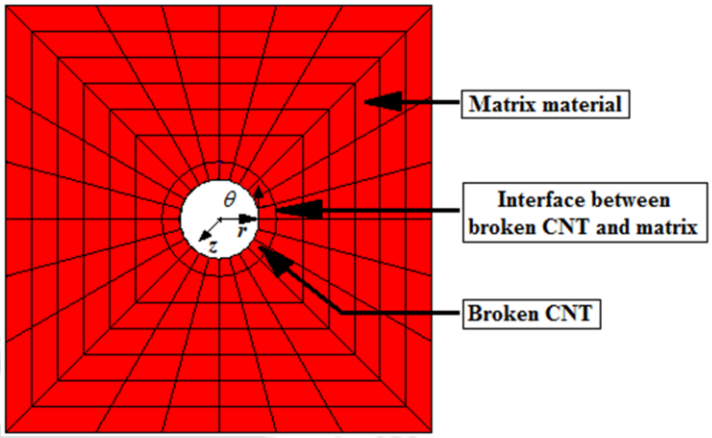

Figure 4.1(a) Front view of FE mesh of single-CNT RVE model along with broken CNT.

4.3.1.2 Finite element modeling

Figure 4.1(b) shows the pictorial view of 3D FE model of single-CNT RVE composites at a constant volume fraction of 3.06% corresponding to weight fraction of 2.89% for CNT/epoxy composite. In the present work, it has been assumed that the orientation of the broken CNTs in the matrix is aligned and the corresponding RVE is used for the analysis. In the present analysis, a 100 nm length of CNT is considered.

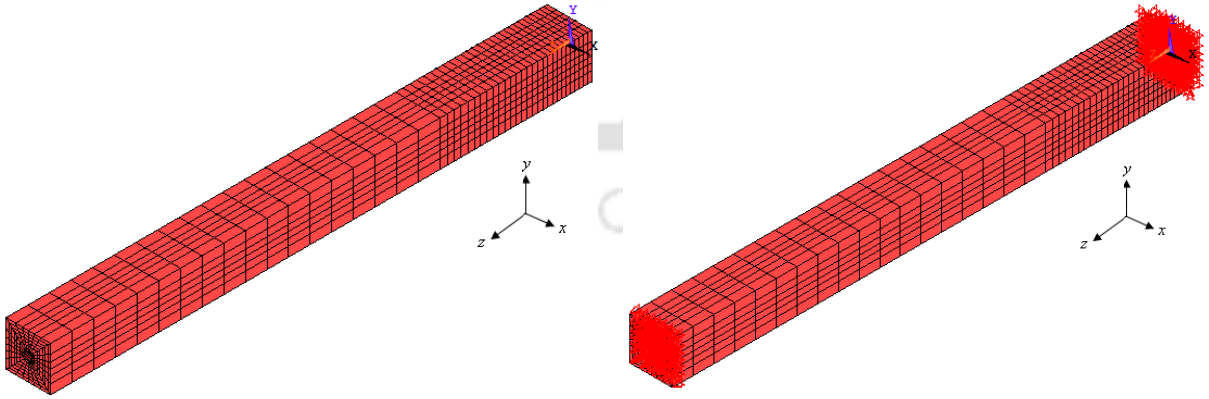

(b) (c)

Figure 4.1 3D FE model of single-CNT RVE (b) without and (c) with boundary conditions.

Convergence of mesh refinement has been performed before using the FE model for stress analysis of CNT-reinforced composites. In the present analysis, the number of nodes and elements of the 1-CNT RVE model are 9024 and 7728, respectively for a constant volume fraction of 3.06% as shown in Fig. 4.1(b).

SOLID45 elements embodied in ANSYS have been used for modeling the square RVE. Details of SOLID45 element are presented in Chapter 3 (section 3.2.2.1). Mesh refinement has been done to capture the expected high stress gradient in the vicinity of the broken CNT. So a fine mesh has been used near the broken CNT and away from the break along the length, coarse meshes were used for the FE analysis.

In the present analysis, a RVE with 1-CNT has been considered with the central CNT broken at the mid span of its length. Therefore, in the FE analysis only half of the length has been modeled and the boundary conditions are put accordingly.

A 3D FE model of the 1-CNT RVE of the composites is shown in Fig. 4.1(c) along with applied boundary conditions, where the *x*-*y* plane is the transverse plane and the *z*-axis is the axial direction. All the nodes at $z = 0$ are fully restrained except the nodes belonging to the broken fiber. The axial mechanical loading is applied by a uniform displacement in the axial direction at the far end of the model i.e. at nodes at $z = L_a$, where L_a is the axial length of the model. Applied displacement is such that the total strain in the axial direction is 1.5%.

4.3.1.3 Results and discussion

A Full 3D finite element analysis has been performed to compute the stress distributions in the broken CNT and at the interface of broken CNT and matrix reinforced on a square 1-CNT-RVE. In the present study, the axial normal stress in the broken CNT and interfacial stresses at the interface of the broken CNT and matrix has been determined at a constant volume fraction of 3.06%.

Two different types of matrix materials (epoxy and titanium) have been chosen to study the effect of matrix materials on the stress redistribution due to broken CNT in CNT-reinforced composites. Properties of epoxy (E_e = 3.89 GPa and ν_e = 0.37) and the SWCNT (E_{nt} = 1000 GPa and ν_{nt} = 0.28) have already been presented in Chapter 3 (section 3.5). The

Young's modulus and Poisson's ratio of titanium are considered as 116 GPa and 0.32, respectively

4.3.1.3.1 Axial normal stresses in the broken CNT

Figure 4.2 shows the variation of the axial normal stress (ANS) in the broken CNT along the fiber (i.e. CNT) length for CNT/epoxy and CNT/Ti composites at a constant volume fraction of 3.06%. It could be observed from Fig. 4.2 that the broken fiber regains 95% of the nominal stress value at a distance of 13 nm ahead of the break for CNT/epoxy and at a distance of 6 nm ahead of the break for CNT/Ti composites. Therefore, it could be concluded that the ineffective length (where 95% of the strength is regained) of the fiber in CNT/epoxy composites is 13% but for CNT/Ti composites it is 6% i.e. the ineffective length of the CNT/Ti composites is about 2 times less than the ineffective length of the CNT/epoxy composites. It could also be observed from Fig. 4.2 that the magnitude of ANS is higher in the case of CNT/Ti composites compared to that in CNT/epoxy composites. The magnitude of ANS of CNT/epoxy and CNT/Ti composites are 11.27 GPa and 14.89 GPa, respectively. The reason for this variation is the stiffness difference of the matrix materials. Even though the length of the CNT is 100 nm, for better clarity near the CNT break, stress variation is shown only up to 50 nm and beyond this there is no change in ANS along the length.

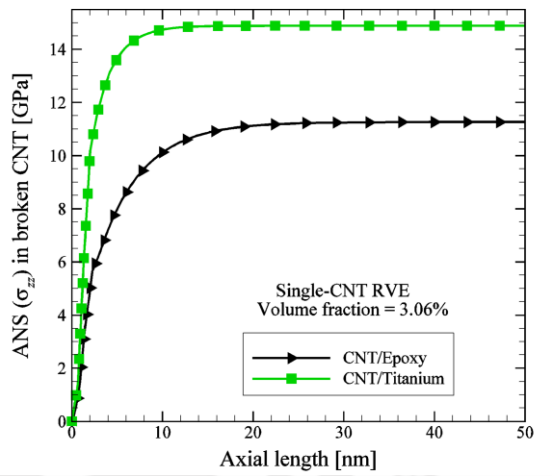

Figure 4.2 Axial normal stress in the broken CNT for 1-CNT RVE model.

4.3.1.3.2 Interfacial stresses at the interface of broken CNT and matrix

Debonding is caused by the interfacial shear and normal stresses. Since near the broken CNT there has been an interfacial shear stress (IFSS), therefore debonding may take place depending upon the magnitude of the IFSS and the corresponding strength. Since, interfacial normal stress (σ_{rr}) and interfacial shear stresses ($\tau_{r\theta}$ and τ_{rz}) are responsible for debonding

of the CNT from the matrix, therefore determination of these stresses in the vicinity of the broken CNT is important. Figures 4.3(a) and 4.3(b) show the distribution of interfacial stresses ($\sigma_{rr}, \tau_{r\theta}$ and τ_{rz}) at the interface of the broken fiber and matrix along the fiber length of 1-CNT RVE in CNT/epoxy and CNT/Ti composites, respectively at a constant volume fraction of 3.06%. It can be seen from Fig. 4.3 that the magnitude of τ_{rz} is maximum near the vicinity of broken fiber and the magnitude of $\tau_{r\theta}$ is zero along the length of fiber. It can be seen from Fig. 4.3(a) that the value of σ_{rr} is negative at z = 0, a positive value slightly away from broken point and a zero value along the fiber away from the fiber break in CNT/epoxy composite. It could be concluded that τ_{rz} is responsible for debonding, σ_{rr} has little effect on debonding and $\tau_{r\theta}$ has no effect on debonding of CNT from the matrix in the case of axial loading.

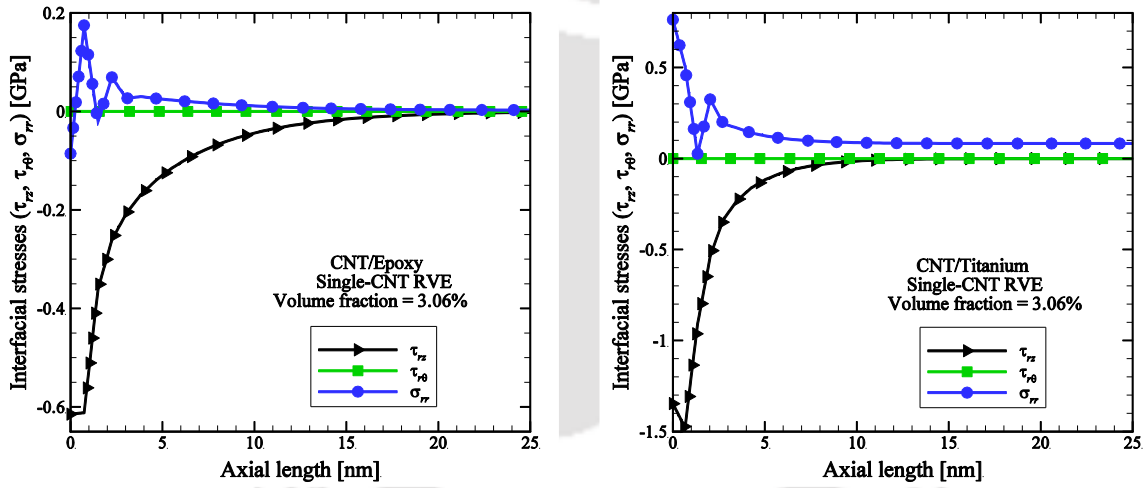

(a) (b)

Figure 4.3 Interfacial stresses at the interface of broken CNT and matrix for 1-CNT RVE model (a) CNT/epoxy and (b) CNT/Ti composites.

It can be seen from Fig. 4.3(b) that the value of σ_{rr} is positive at $z = 0$ and a small positive value along the fiber away from the fiber break in CNT/Ti composites. It could be observed that a high magnitude of τ_{rz} to have developed at the interface and in the vicinity of fiber break, the value of σ_{rr} is less compared to the value of τ_{rz}. Even though the length of

the CNT is 100 nm, for better clarity near the CNT break, stress variation is shown only up to 25 nm and beyond this there is no change in interfacial stresses (IFSs) along the length.

Figure 4.4 shows the distribution of τ_{rz} at the interface of the broken fiber and matrix of 1-CNT RVE in CNT/epoxy and CNT/Ti composites at a constant volume fraction of 3.06%. It can be seen in Fig. 4.4 that the magnitude of τ_{rz} is higher in the case of CNT/Ti composites compared to that in CNT/epoxy composites. Even though the length of the CNT is 100 nm, for better clarity near the CNT break, stress variation is shown only up to 25 nm and beyond this there is no change in interfacial shear stress (IFSS) along the length.

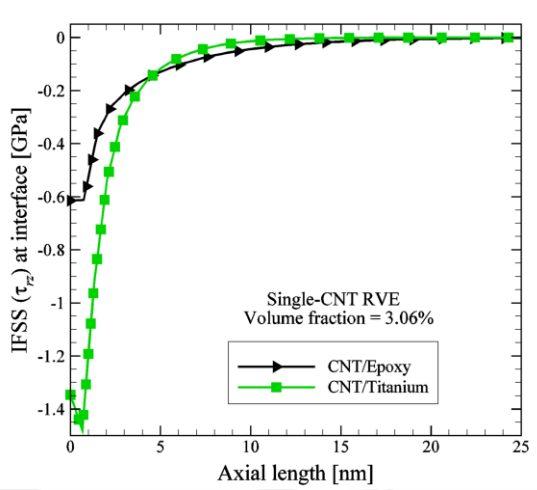

Figure 4.4 Interfacial shear stress at the interface of broken CNT and matrix for 1-CNT RVE model.

It may be mentioned that the 1-CNT model is computationally simpler. However, a single-CNT model will not be appropriate as the stress concentration factor in the adjacent intact fiber cannot be evaluated. Therefore, 9-CNTs RVE needs to be used for analysis of such CNT-reinforced composites with fiber break.

4.3.2 Nine-CNT square RVE model with central CNT broken

In this case, a square RVE having nine uniformly spaced CNT in the matrix have been considered for FE analysis. In addition of axial normal stress in broken CNT and interfacial stresses at the interface of the broken CNT and matrix here axial normal stress at the adjacent intact CNTs has also been determined.

4.3.2.1 Finite element modeling

In order to study the effect of a broken CNT on the adjacent CNTs as well as at the interface of the broken CNT and matrix, a square RVE with nine CNTs have been considered. The broken fiber is also considered to be placed at the center of the RVE and it has been assumed that the orientation of the broken CNTs in the matrix is aligned in the 9-

CNTs RVE. Since the RVE is modeled with 9-CNTs, so the broken fiber is surrounded by eight neighboring fibers and matrix.

Figure 4.5(a) shows the FE mesh of the front view of 9-CNT RVE along with broken CNT and interface between broken CNT and matrix material. In the present analysis a 100 nm length of CNT is considered. Since the thickness of CNT is constant so the volume of the CNT is also constant but to get different volume fraction, the volume of the matrix materials surrounding the CNT has been varied. The same pattern of mesh refinement has been done as like 1-CNT RVE as described earlier. Figure 4.5(b) shows the pictorial view of 3D FE model for square RVE with 9-CNTs.

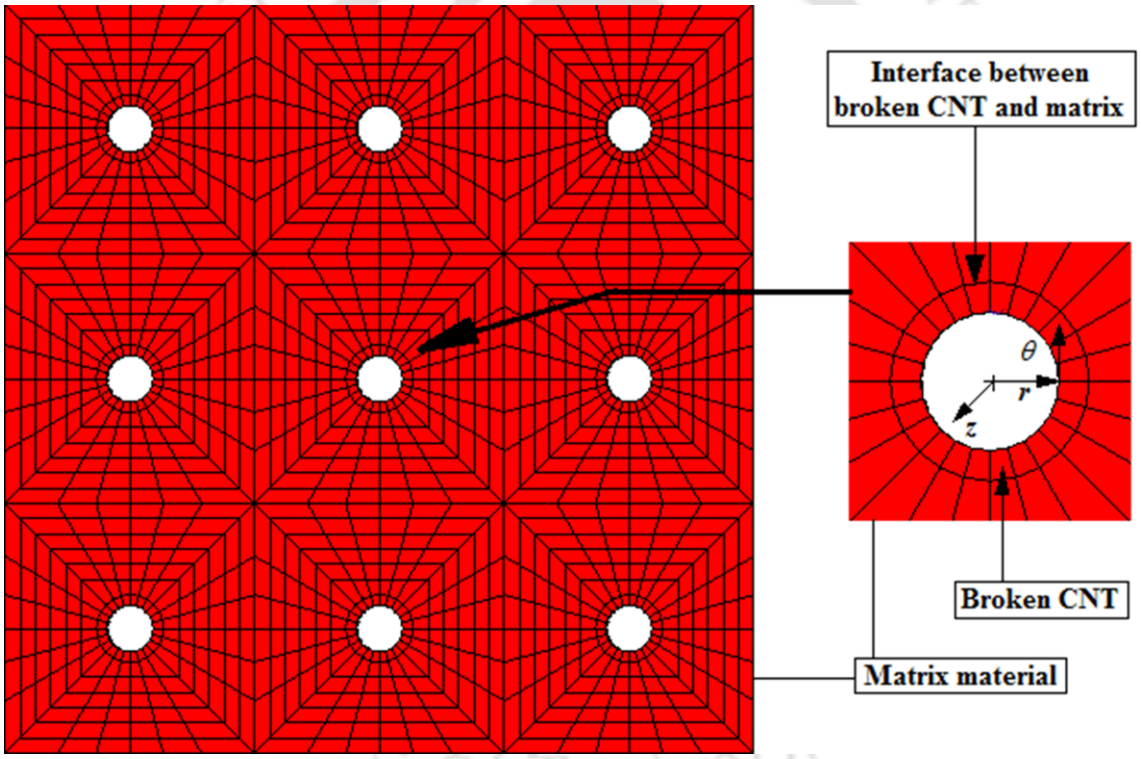

Figure 4.5(a) Front view of FE mesh of the 9-CNT RVE model along with broken CNT.

The same types of boundary conditions have also been used for 9-CNT RVE as like 1-CNT RVE and the same has been described in previous section 4.3.1.2. Here, the total applied strain in the axial direction is also considered equal to 1.5%.

4.3.2.2 Results and discussion

A full 3D finite element analysis has been performed to obtain the stress distributions in 9-CNTs RVE composite with a broken CNT. In the present study, the axial normal stress in the broken CNT, interfacial shear stress at the interface of the broken CNT and matrix, and axial normal stress in the adjacent intact CNTs of a square RVE with nine CNTs have been evaluated for a constant volume fraction. The effect of volume fraction on the stress distribution has also been investigated. In the present analysis, stresses are calculated corresponding to volume fractions of 1%, 3.06%, and 10.31% of CNT in CNT-reinforced composites. Properties of CNT and matrix materials have been considered as listed Table 3.2 in earlier Chapter 3 (section 3.5).

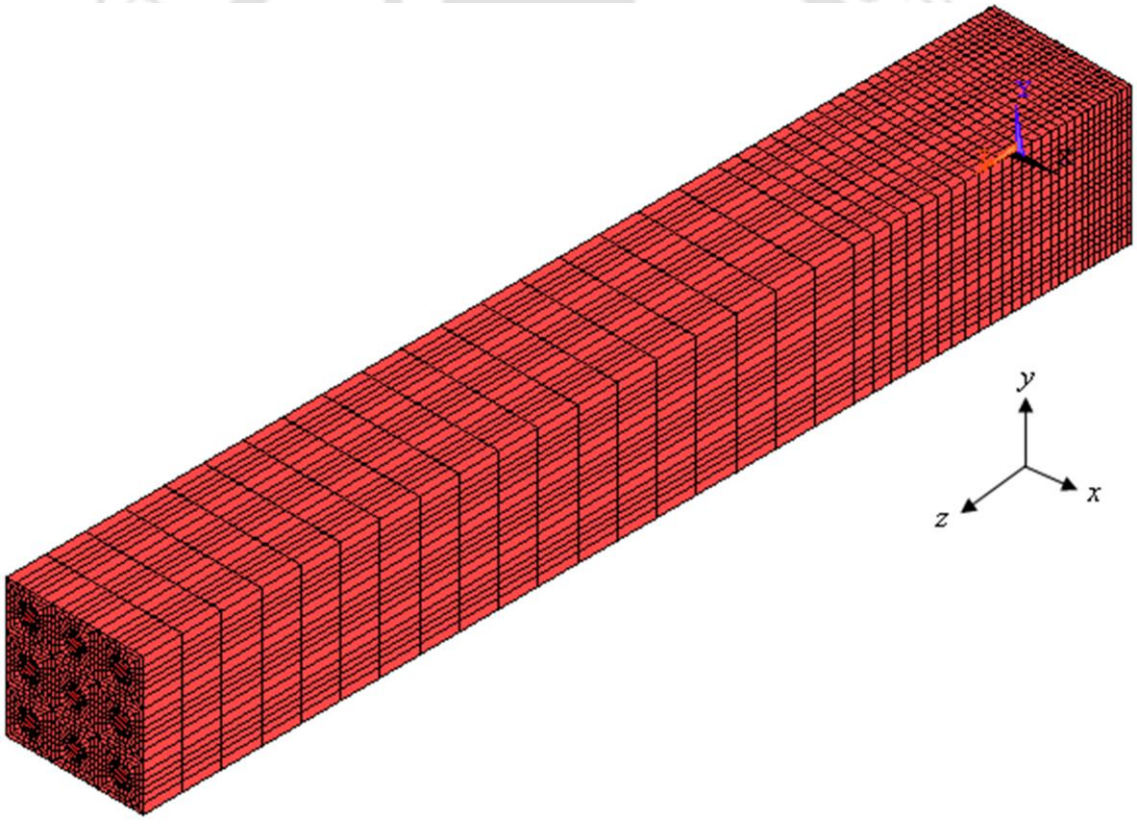

Figure 4.5(b) Pictorial view of 3D FE mesh of the 9-CNTs RVE.

4.3.2.2.1 For a constant volume fraction of 3.06%

4.3.2.2.1.1 Axial normal stress in the broken CNT

Figure 4.6 shows the variation of the axial normal stress along the length of the broken fiber in the CNT-reinforced composites at a constant volume fraction of 3.06%. It could be observed from Fig. 4.6 that the broken fiber regains the nominal stress value at a distance of 7 nm ahead of break for CNT/Ti and at a distance of 53 nm ahead of break for CNT/epoxy composites. Therefore, it could be concluded that the ineffective length of the broken fiber in CNT/Ti composites is 7% but for CNT/epoxy composites it is 53% i.e. the ineffective length of the CNT/Ti composites is about 8 times less than the ineffective length of the CNT/epoxy composites.

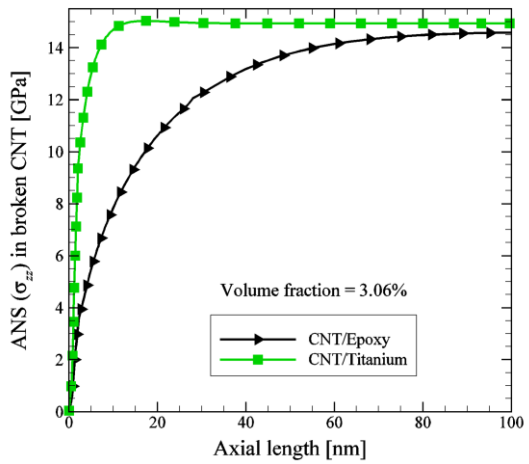

Figure 4.6 Axial normal stress in the broken CNT.

This shows that a broken CNT in CNT/epoxy composite has more effect on the load bearing compared to that in CNT/Ti composite. This means that the stiffness degradation due to such break is more in the case of CNT/epoxy composites compared to that in CNT/Ti composite. The reason for this variation is the mismatch of the mechanical properties between the fiber and matrix. In addition, the ineffective length estimated using the 9-CNT model is more compared to that is observed using 1-CNT model.

Comparing these results with 1-CNT model, it could be observed that ineffective lengths estimated by the 9-CNT and 1-CNT RVE model are very close for CNT/Ti composite. However in the case of CNT/epoxy composite, the difference in the estimate of ineffective length by 1-CNT (13%) and 9-CNT (53%) RVE model are more. This means that the use of 9-CNT RVE is more so important for CNT-reinforced polymeric composites where the relative stiffness of the matrix material is much lower.

4.3.2.2.1.2 Interfacial stresses at the interface of broken CNT and matrix

Figures 4.7(a) and 4.7(b) show the distribution of interfacial stresses (σ_{rr}, $\tau_{r\theta}$ and τ_{rz}) at the interface of the broken fiber (i.e. CNT) and matrix along the fiber length of 9-CNTs RVE in CNT/epoxy and CNT/Ti composites, respectively at a constant volume fraction of 3.06%. It can be seen in Figs. 4.7 that the magnitude of τ_{rz} is maximum near the vicinity of broken fiber and the magnitude of $\tau_{r\theta}$ is zero along the length of fiber for both the CNT-reinforced composites.

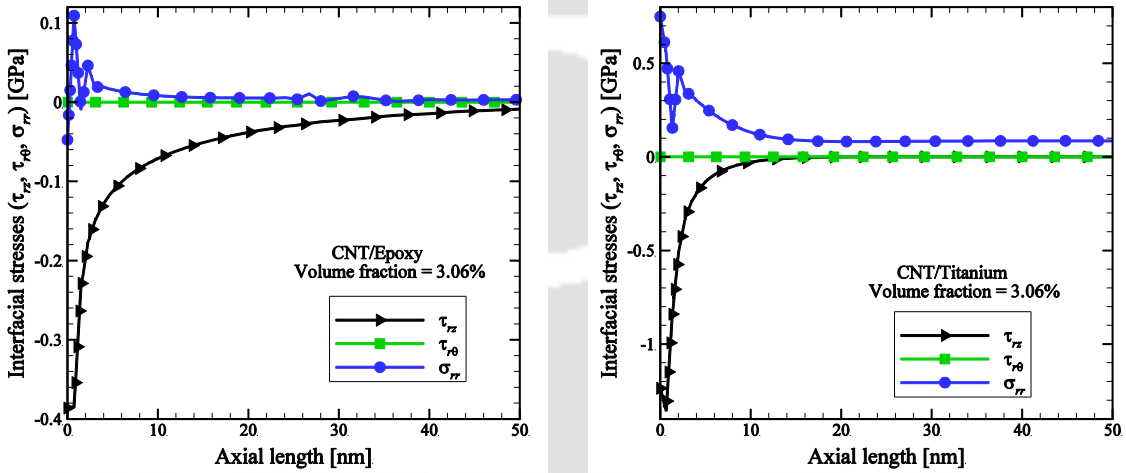

(a) (b)

Figure 4.7 Interfacial stresses at the interface of broken CNT and matrix (a) CNT/epoxy and (b) CNT/Ti composites.

It can be seen in Fig. 4.7(a) that the value of σ_{rr} is negative at z = 0, a positive value slightly away from broken point and a zero value along the fiber away from the fiber break in CNT/epoxy composite. It can be seen in Fig. 4.7(b) that the value of σ_{rr} is positive at z = 0 and a small positive value along the fiber away from the fiber break in CNT/Ti composites. It could be observed that a high magnitude of τ_{rz} to have developed at the interface and in the vicinity of fiber break, the value of σ_{rr} is less compared to the value of τ_{rz}. Even though the length of the model is 100 nm, for better clarity near the CNT break, stress variation is shown only up to 50 nm and beyond this there is no change in interfacial stresses (IFSs) along the length.

Magnitude of interfacial stresses depends upon the relative stiffness of the CNT and matrix material. It this case it could be clearly seen that in case of CNT/epoxy composite interfacial normal stress σ_{rr} is negative near the break and then attains a positive value over a small region and becomes zero. However, in the case of CNT/Ti composite the interfacial normal stress is always positive and it extend over a considerable length of the interface. Therefore, it could be concluded that τ_{rz} is responsible for debonding and $\tau_{r\theta}$ has no effect on debonding of CNT from both the epoxy and titanium matrices in the case of axial loading. It could also be concluded that σ_{rr} has no effect on debonding of CNT from epoxy matrix but σ_{rr} has some effect on debonding of CNT from titanium matrix in the case of axial loading.

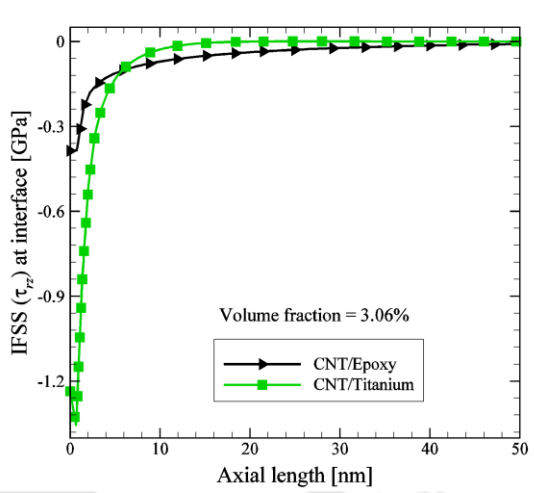

Figure 4.8 Interfacial shear stress at the interface of broken CNT and matrix.

Comparing these results with 1-CNT model, it could be observed that interfacial stress distribution estimated by the 9-CNT and 1-CNT RVE model are very close for CNT/Ti composite. However, in the case of CNT/epoxy composite, the difference in the estimate of interfacial stresses by 1-CNT and 9-CNT RVE model are more. Hence, once again it could be observed that the use of 9-CNT RVE is more so important for CNT-reinforced polymeric composites.

Figure 4.8 shows the IFSS (τ_{rz}) distribution at the interface of the broken fiber and matrix in CNT-reinforced composites at a constant volume fraction of 3.06%. It can be seen in Fig. 4.8 that the magnitude of IFSS is higher in the case of CNT/Ti composites compared to that in CNT/epoxy composites. The magnitude of IFSS of CNT/epoxy and CNT/Ti composites are 0.4 GPa and 1.37 GPa, respectively. It could be concluded that the IFSS of CNT/epoxy composites is about 3.5 times less than the IFSS of CNT/Ti composites. However, it should be noted that in spite of lower magnitude of IFSS in case of CNT/epoxy composite, non-zero value of IFSS is spread over a larger length ahead of the break

compared to that in case of CNT/Ti composites. The reason for this variation is the mismatch of the mechanical properties between the fiber and matrix.

4.3.2.2.1.3 Axial normal stress in the adjacent intact CNTs

Figure 4.9 shows the variation of axial normal stress in the adjacent intact CNTs of CNT-reinforced composites for a constant volume fraction of 3.06%. It could be observed that due to the presence of a broken CNT, the adjacent CNTs experience a stress concentration in the vicinity of the break. So, it could be concluded that there is a possibility that the adjacent CNTs may break as a consequence of over loading. It could be calculated from Fig. 4.9 that the stress concentration factor (maximum stress/nominal stress) in the CNT/epoxy is 1.1 and that in CNT/Ti is 1.01. It could be concluded that the stress concentration factor (SCF) of CNT/epoxy composite is higher compared to that of CNT/Ti composite for a constant volume fraction. Higher stress concentration factor (SCF) in CNT/epoxy composite is expected in view of the larger ineffective length and the higher stress reaches normal value over a longer length compared to CNT/Ti composite.

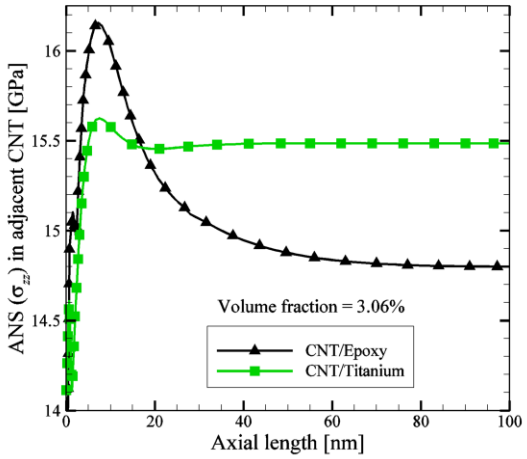

Figure 4.9 Axial normal stress in the adjacent intact CNT.

4.3.2.2.2 Effect of volume fraction

4.3.2.2.2.1. Axial normal stresses in the broken CNT

Figures 4.10(a) and 4.10(b) show the variation of the axial normal stress along the length of the broken fiber with volume fractions for CNT/epoxy and CNT/Ti composites, respectively. It could be observed that the ineffective lengths of the broken CNT in CNT/Ti composites is 7 nm for the volume fraction of 3.06% but 11 nm for the volume fraction of 1%. It has also been observed that there is not much difference in ineffective lengths in CNT/Ti composite for the volume fraction of 3.06% and 10.31%. It could also be concluded

that there is not much difference in ineffective length for the volume fractions of 1% and 10.31% of the CNT/Ti composites.

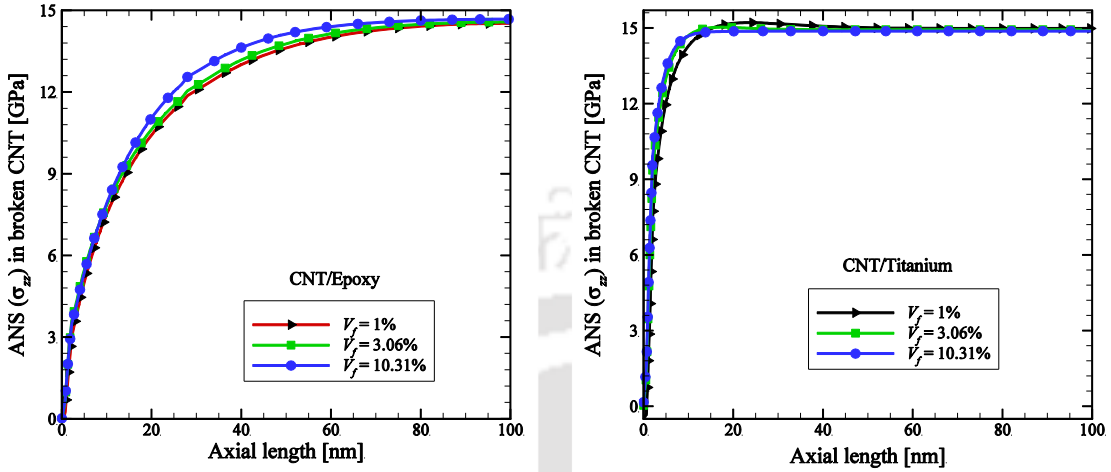

(a) (b)

Figure 4.10 Axial normal stress in the broken CNT with volume fraction (a) CNT/epoxy and (b) CNT/Ti composites.

But in the case of CNT/epoxy composites the ineffective lengths are 45 nm and 55 nm for the volume fraction of 10.31% and 1%, respectively. It has also been observed that there is not much difference in ineffective lengths in CNT/epoxy composite for the volume fraction of 1% and 3.06%. It could also be concluded that there is a difference in ineffective length for the volume fractions of 1% and 10.31% for the CNT/epoxy composites.

Therefore, in the case of CNT/epoxy composites, for all the range of volume fractions, the broken CNT is ineffective and does not contribute to the load bearing of the composite. However, in the case of CNT/Ti composites, a major length of the broken CNT contributes to the load bearing. The ineffective length of the broken CNT decreases with the increase in volume fraction for both the CNT-reinforced composites.

4.3.2.2.2.2 Interfacial shear stress at the interface of broken CNT and matrix

Figures 4.11(a) and 4.11(b) show the variation of interfacial shear stress with volume fraction at the interface of the broken CNT and matrix for CNT/epoxy and CNT/Ti composites, respectively. It could be observed from Fig. 4.11(a) that the magnitudes of IFSS are 0.275 GPa and 0.424 GPa corresponding to volume fractions of 1% and 10.31%,

respectively for CNT/epoxy composites. Therefore, it could be concluded that the magnitude of IFSS increases nearly 1.5 times with the increase in volume fraction of CNT from 1% to 10.31% for CNT/epoxy composites. But in case of CNT/Ti composite, it could be observed from Fig. 4.11(b) that the magnitudes of IFSS are 1 GPa and 1.5 GPa corresponding to volume fractions of 1% and 10.31%, respectively. Therefore, it could be concluded that the magnitude of IFSS increases 1.5 times with increase in volume fraction of CNT from 1% to 10.31% for CNT/Ti composites.

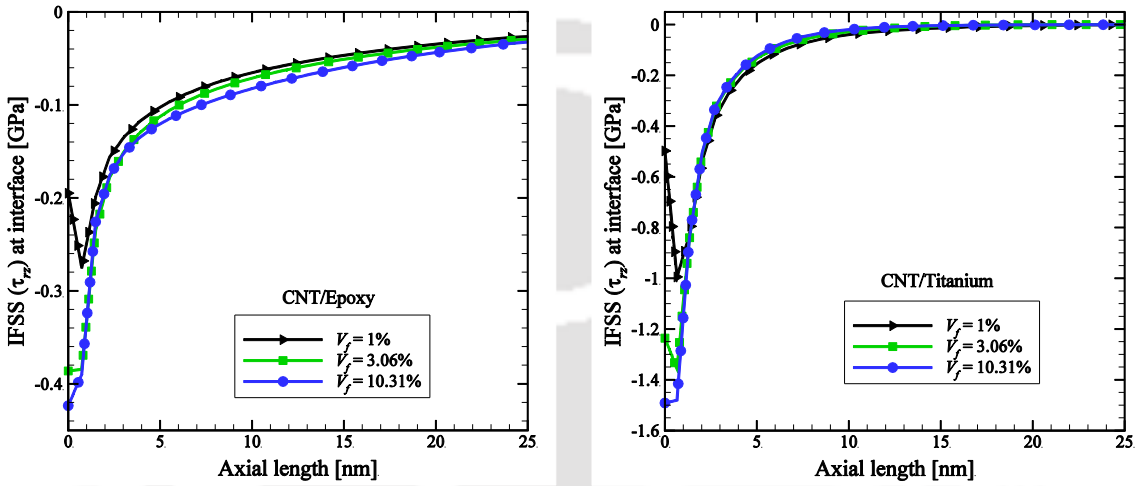

(a) (b)

Figure 4.11 Interfacial shear stress at the interface of broken CNT and matrix with volume fraction (a) CNT/epoxy and (b) CNT/Ti composites.

It could also be concluded that the magnitude of the IFSS increases with the increase in volume fraction for both the CNT-reinforced composites. Therefore, even though the axial strength and stiffness of CNT-reinforced composites increase with the increase in volume fraction, in the event of a fiber break, the interfacial shear stress developed at the interface of the broken fiber and the matrix actually increases with the increase in volume fraction thereby enhancing the chances of debonding initiation at such interface. Even though the length of the model is 100 nm, for better clarity near the CNT break, stress variation is shown only up to 25 nm and beyond this there is no change in interfacial shear stress (IFSS) along the length.

4.3.2.2.2.3 Axial normal stresses in the adjacent intact CNTs

Figures 4.12(a) and 4.12(b) show the variation of axial normal stress with volume fractions in the adjacent intact CNTs for CNT/epoxy and CNT/Ti composites, respectively.

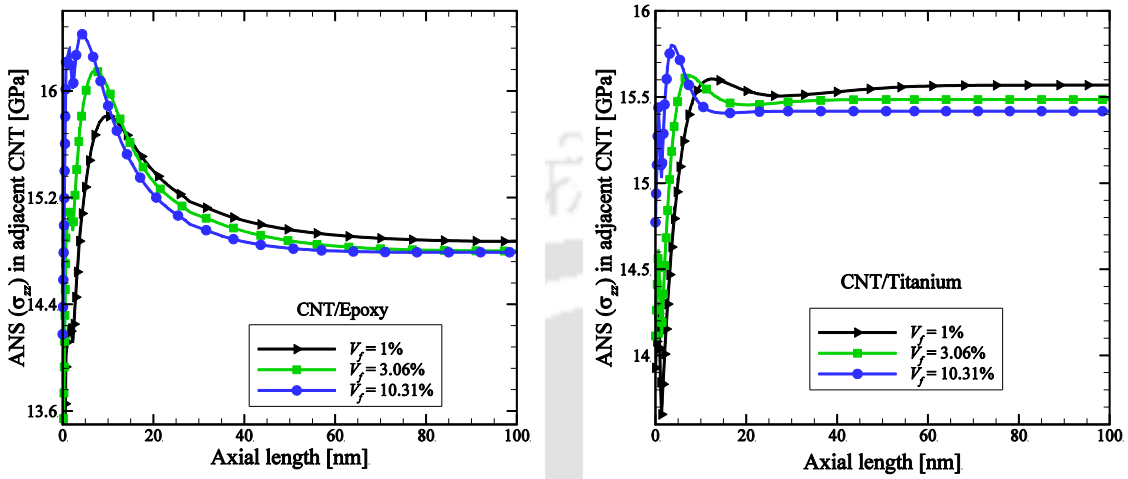

(a) (b)

Figure 4.12 Axial normal stress in the adjacent intact CNT with volume fraction (a) CNT/epoxy and (b) CNT/Ti composites.

It could be observed from Fig. 4.12 that the magnitudes of axial normal stresses are different for different volume fractions. For CNT/epoxy composites corresponding to the volume fractions of 1%, 3.06%, and 10.31% the magnitudes of SCFs are 1.04, 1.09, and 1.11 respectively. But for CNT/Ti composites corresponding to the volume fractions of 1%, 3.06%, and 10.31% the magnitude of SCFs are 1.00, 1.01, and 1.03 respectively. Above results conclude that the SCF increases with the increase in volume fraction for both the CNT-reinforced composites, however the increase in stress concentration factor with volume fraction is more sensitive in the case of CNT/epoxy composite.

4.3.3 Comparison between 1-CNT RVE and 9-CNT RVE model

4.3.3.1 Axial normal stress in the broken CNT

Figures 4.13 show the variation of the axial normal stress (ANS) in the broken CNT along the CNT length of 1-CNT model and 9-CNT model for CNT/epoxy composites for a constant volume fraction of 3.06%. Ineffective lengths using 1-CNT model and 9-CNs model in CNT/epoxy composites have already been investigated in the previous section. It could be

observed from Fig. 4.13(a) that the ineffective length of 1-CNT model and 9-CNTs model in CNT/epoxy composites are 13 nm and 53 nm, respectively. It could be concluded that the estimated ineffective length using 9-CNT model is more than that estimated using 1-CNT model of CNT/epoxy composites. It could be observed from Fig. 4.13(a) that the nominal stress of 1-CNT model and 9-CNTs model are 11.3 GPa and 14.5 GPa, respectively in CNT/epoxy composites. It could be concluded that the estimated magnitude of nominal stress is higher for 9-CNTs model than that of 1-CNT model in CNT/epoxy composites for a constant volume fraction of 3.06%.

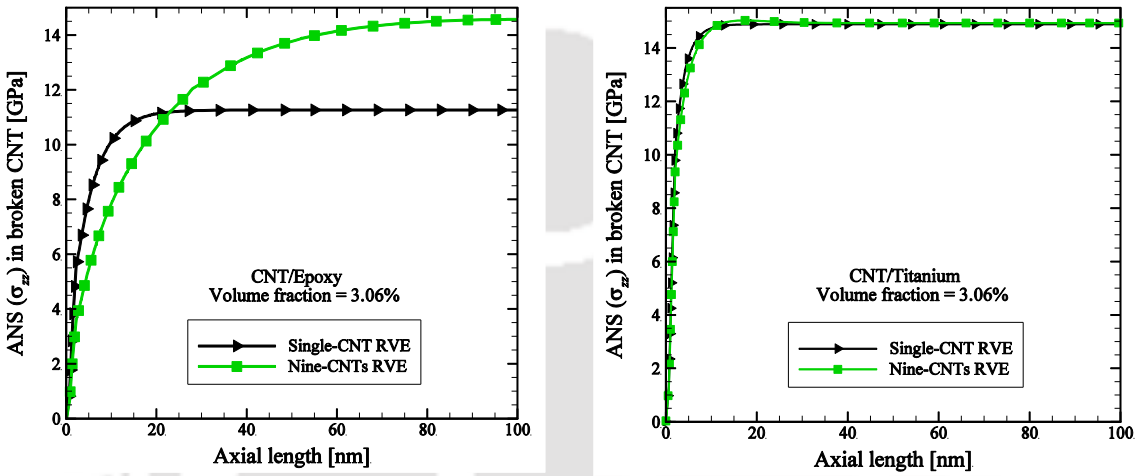

(a) (b)

Figure 4.13 Axial normal stress in the broken CNT (a) CNT/epoxy and (b) CNT/Ti composites.

Figure 4.13(b**)** shows the variation of the ANS in the broken fiber along the fiber length between 1-CNT model and 9-CNTs model in CNT/Ti composites for a constant volume fraction of 3.06%. Ineffective lengths using 1-CNT model and 9-CNTs model in CNT/Ti composites have already been observed as 6 nm and 7 nm, respectively in earlier sections 4.3.1.3.1 and 4.3.2.2.1.1. It could be concluded that the difference in ineffective length of 1-CNT model and 9-CNTs model are not significant in the case of CNT/Ti composite.

Comparing these results with 1-CNT model, it could be observed that ineffective lengths estimated by the 9-CNT and 1-CNT RVE model are very close for CNT/Ti composite. However in the case of CNT/epoxy composite, the differences in the estimate of ineffective length by 1-CNT (13%) and 9-CNT (53%) RVE model are more. This means that the use of

9-CNT RVE is more so important for CNT-reinforced polymeric composites where the relative stiffness of the matrix material is much lower

There is a significant difference between the magnitudes of nominal stress of 1-CNT model and 9-CNTs model in CNT/epoxy composites. But in case of CNT/Ti composite those differences are less. This is due to fact that the ratio of Young's modulus of CNT (1TPa) to epoxy (3.89 GPa) is 30 times higher compared to the ratio of Young's modulus of CNT to titanium (116 GPa), since, the ratios of Young's modulus of CNT to epoxy and CNT to titanium are 257.07 and 8.62, respectively. It could be concluded that the difference in magnitude of the nominal stress between 1-CNT model and 9-CNTs model depends upon the relative stiffness of the CNT and matrix materials. In addition, the ineffective length estimated using the 9-CNT model is more compared to that is observed using 1-CNT model.

4.3.3.2 Interfacial shear stress at the interface of broken CNT and matrix

Figure 4.14(a) shows the variation of the IFSS at the interface of the broken fiber and matrix between 1-CNT model and 9-CNTs model of CNT/epoxy composites for a constant volume fraction of 3.06%.

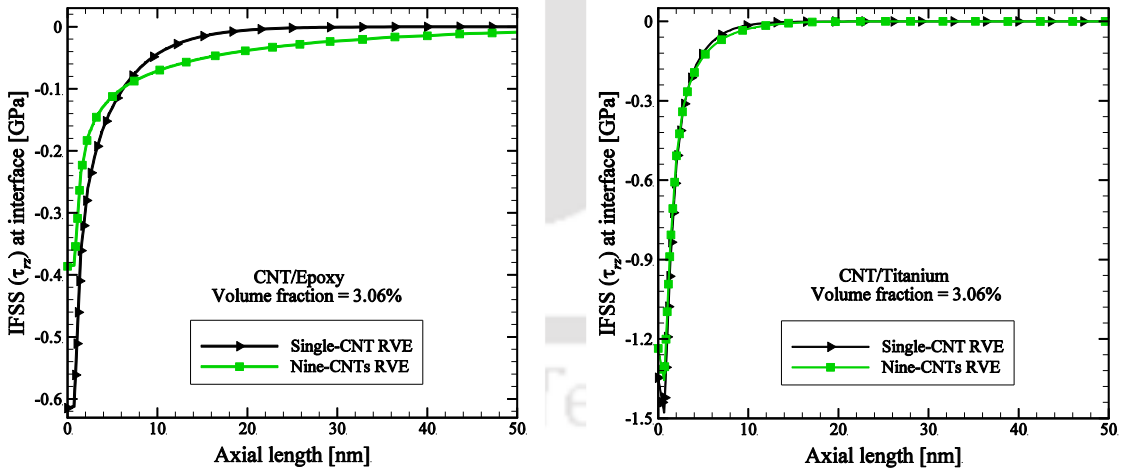

(a) (b)

Figure 4.14 Interfacial shear stress at the interface of broken CNT and matrix (a) CNT/epoxy and (b) CNT/Ti composites.

It could be observed from Fig. 4.14(a) that the estimated magnitude of IFSS is higher in the case of 1-CNT model compared to that of 9-CNT model in CNT/epoxy composites. The

magnitudes of IFSS of 1-CNT model and 9-CNT model are 0.61 GPa and 0.37 GPa, respectively in CNT/epoxy composites. Figure 4.14(b) shows the variation of the IFSS at the interface of the broken fiber and matrix between 1-CNT model and 9-CNTs model in CNT/Ti composites for a constant volume fraction of 3.06%. It could be observed from Fig. 4.14(b) that the magnitudes of IFSS is higher in the case of 1-CNT/Ti composite compared to that of 9-CNT/Ti composites but differences are not much. Reason behind this is that there is huge difference between Young's modulus of epoxy and titanium. Even though the length of the model is 100 nm, for better clarity near the CNT break, stress variation is shown only up to 50 nm and beyond this there is no change in interfacial shear stress (IFSS) along the length.

Comparing these results with 1-CNT model, it could be observed that interfacial stress distribution estimated by the 9-CNT and 1-CNT RVE model are very close for CNT/Ti composite. However in the case of CNT/epoxy composite, the differences in the estimate of interfacial stresses by 1-CNT and 9-CNT RVE model are more. Therefore, once again it could be observed that the use of 9-CNT RVE is more so important for CNT-reinforced polymeric composites. Thus it could be observed that 9-CNTs model gives a more realistic magnitudes of interfacial shear stress (IFSS) compared to 1-CNT model, even though the differences of nominal stress is more pronounced in the case CNT/epoxy composite where the relative stiffness of CNT to epoxy is very high.

4.4. Stress redistribution around a broken CNT by considering non-linear stress-strain relation of CNT

It chapter 3, it was clearly observed that for correct estimation of Young's modulus and coefficient of thermal expansion (CTE), non-linear stress-strain relation of CNT needs to be incorporated even though linear model is much simpler in terms of computation. Here in the same 3D FE model, non-linear stress-strain relation of CNT has been input in the analysis which resulted in non-linear solution of the equation. Even though incorporation of non-linear stress-strain relation leads to larger computational time, it is important to understand the effect of this on the modeling especially at higher strain. In the present study a strain of 14% is considered.

4.4.1 Finite Element modeling

In order to simulate the broken CNT, a square RVE having nine uniformly spaced CNTs in the matrix has been considered. SOLID45 element has also been used for multi-scale FE modeling of the square RVE with 9-CNTs. The front view of RVE along with broken CNT and interface between broken CNT and matrix, and pictorial views of the 3D finite element model of square has been shown in Fig. 4.5. The length of the RVE with a continuous CNT has been taken as 100 nm.

The same boundary conditions and loading have also been used as described in previous section 4.3.2.1. The central CNT is considered broken at $z = 0$. This has been simulated by restraining all the nodes at $z = 0$ except the nodes belonging to the broken CNT. A uniformed displacement is applied in 14 steps to simulate 14% axial strains at the other end of the model. The displacement increment was chosen equal to 1% of the length of the model; therefore the total applied strain in the axial direction is 14% of the total axial length of the model. To study the stress distribution around the broken CNT, a full 3D FE analysis has been performed where the stress-strain relation of CNT as described in Eq. (3.12) is input to take care of the non-linear relation of the zigzag CNTs. The Eq. (3.12) is given below.

$$\sigma_n = 2909.8\varepsilon_n^3 - 4995.6\varepsilon_n^2 + 1364.9\varepsilon_n \quad \text{(for zigzag CNT)} \tag{3.12}$$

4.4.2 Results and discussion for CNT/epoxy and CNT/Ti composites

In the present study, a square RVE with nine uniformly spaced CNTs has been considered for analysis. The square 9-CNTs RVE with the central CNT broken has been considered to study the effect of broken CNT on the stress redistribution around the broken CNT in CNT-reinforced composites. Axial normal stress in the broken CNT, interfacial normal and shear stresses at the interface of the broken CNT and the matrix, and axial normal stress in the adjacent intact CNTs have been evaluated. Two different types of matrix materials viz. epoxy and titanium have been chosen to study the effect of matrix materials on the stress distribution in the CNT-reinforced composites. Effect of volume fraction on the distribution has also been studied. Properties of SWCNT, epoxy and titanium have been listed in previous section 4.3.1.3.

4.4.2.1 For a constant volume fraction of 3.06%

4.4.2.1.1 Axial normal stress in the broken CNT

Figure 4.15 shows the distribution of the axial normal stress (ANS) along the length of the broken fiber in CNT/epoxy and CNT/Ti composites for a constant volume fraction of 3.06%. It could be observed that the broken fiber regained the nominal stress value after a length of 3 nm for CNT/Ti and 28 nm for CNT/epoxy composites, respectively. Therefore, it could be concluded that the ineffective length of the broken CNT in CNT/Ti composites is 3% but for CNT/epoxy composites it is 28%. It could also be concluded that the ineffective length of the CNT/Ti composites is about 9 times less than that of the CNT/epoxy composites. This shows that a broken CNT in CNT/epoxy composite has more effect on the load bearing compared to that in CNT/Ti composite. This means that the stiffness degradation due to such break is more in the case of CNT/epoxy composites compared to that in CNT/Ti composite. The reason for this difference is the mismatch of the mechanical properties between the CNT and matrix. Even though the length of the model is 100 nm, for better clarity near the CNT break, stress variation is shown only up to 50 nm and beyond this there is no change in ANS along the length.

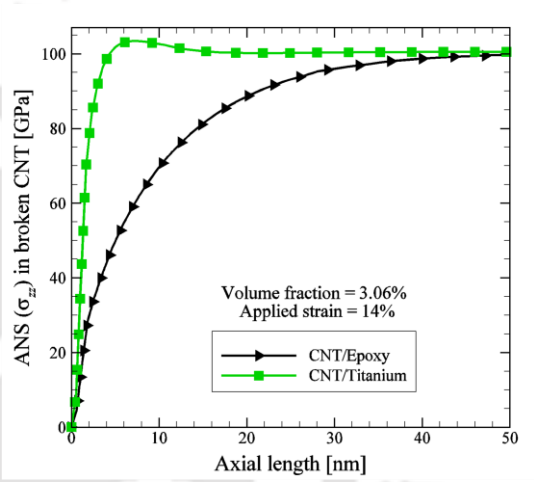

Figure 4.15 Axial normal stress in the broken CNT.

4.4.2.1.2 Interfacial stresses at the interface of broken CNT and matrix

Since, the interfacial shear stresses (τ_{rz} and $\tau_{r\theta}$) and interfacial normal stress (σ_{rr}) are responsible for debonding of the CNT from the matrix, therefore the distribution of these three stresses near the vicinity of the broken CNT is important. Figures 4.16 show the distribution of interfacial stresses τ_{rz}, $\tau_{r\theta}$ and σ_{rr} along the length of fiber in CNT-reinforced composites for a constant volume fraction of 3.06%.

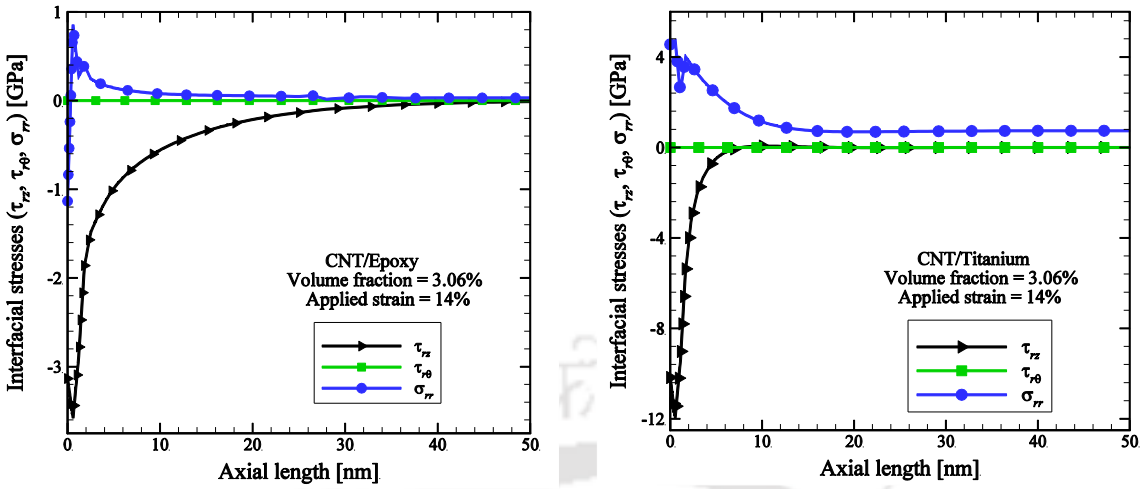

(a) (b)

Figure 4.16 Interfacial stresses at the interface of broken CNT and matrix (a) CNT/epoxy and (b) CNT/Titanium composites.

Magnitude of interfacial stresses depends upon the relative stiffness of the CNT and matrix material. It this case, it could be clearly seen that in case of CNT/epoxy composite interfacial normal stress σ_{rr} is negative near the break and then attains a positive value over a small region and becomes zero. However, in the case of CNT/Ti composite the interfacial normal stress is always positive and it extend over a considerable length of the interface. It could be concluded that the fiber debonding may take place at the interface near the vicinity of the break mainly due to the high value of τ_{rz} at that location and $\tau_{r\theta}$ has no effect on debonding of CNT from both the epoxy and titanium matrices in the case of axial loading. It could also be concluded that σ_{rr} has no effect on debonding of CNT from epoxy matrix but σ_{rr} has some effect on debonding of CNT from titanium matrix in the case of axial loading. Even though the length of the model

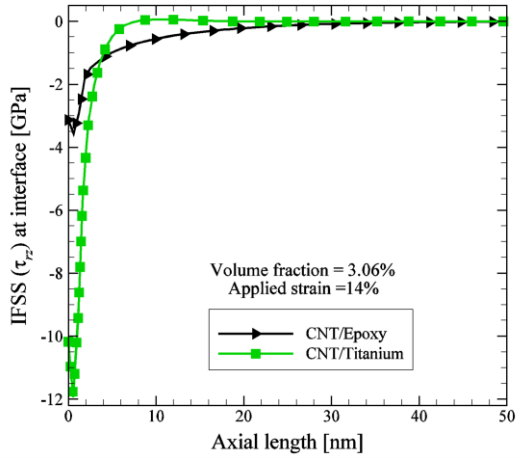

Figure 4.17 Interfacial shear stress at the interface of broken CNT and matrix.

is 100 nm, for better clarity near the CNT break, stress variation is shown only up to 50 nm and beyond this there is no change in interfacial stress (IFSs) along the length.

Figure 4.17 shows the interfacial shear stress (τ_{rz}) distribution at the interface of the broken CNT and matrix in CNT/epoxy and CNT/Ti composites for a constant volume fraction of 3.06%. It could be observed that at the interface near the vicinity of the break, a high value of shear stress occurs indicating that the fiber debonding may take place at that location. The magnitude of IFSS (τ_{rz}) of CNT/epoxy and CNT/Ti composites are 3.58 GPa and 11.94 GPa, respectively. It could be concluded that the IFSS of CNT/epoxy composites is about 3.5 times less than the IFSS of CNT/Ti composites. It could also been concluded that for the same volume fraction, the magnitude of IFSS for CNT/Ti composites is higher than that of the CNT/epoxy composites. Higher magnitude of interfacial shear stress in case of CNT/Ti composite is expected in view ineffective length of the broken fiber. However, it should be noted that in spite of lower magnitude of IFSS in case of CNT/epoxy composite, non-zero value of IFSS is actively spread over a larger length ahead of the break compared to that in case of CNT/Ti composites.

4.4.2.1.3 Axial normal stress in the adjacent intact CNTs

Figure 4.18 shows the distribution of axial normal stress in the adjacent intact CNTs of CNT-reinforced composites for a constant volume fraction of 3.06%. It could be observed that due to the presence of a broken CNT, the adjacent CNTs experience a stress concentration in the vicinity of the break. So, it could also be concluded that there is a possibility that the adjacent CNT may break as a consequence of over loading. It could be calculated from Fig. 4.18 that the stress concentration factor for CNT/epoxy and CNT/Ti composites are 1.02 and 1.07, respectively for a constant volume fraction of 3.06%. It could be concluded that for the same volume fraction, the SCF for

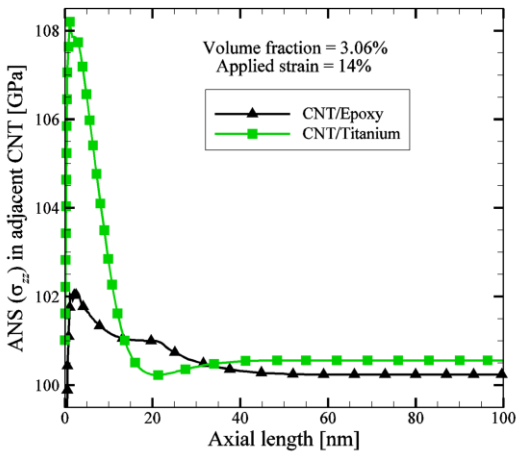

Figure 4.18 Axial normal stress in the adjacent intact CNT.

CNT/Ti composites is higher than that of the SCF of the CNT/epoxy composites. It could be noticed that even though the adjacent fiber in case of CNT/Ti composite experiences a higher SCF, but the length over which the SCF normalizes to one is more in case of CNT/epoxy composite.

4.4.2.2 Effect of volume fraction

4.4.2.2.1 Axial normal stresses in the broken CNT

Figures 4.19(a) and 4.19(b) show the variation of the axial normal stresses with volume fraction along the length of the broken fiber in CNT/epoxy and CNT/Ti composites, respectively.

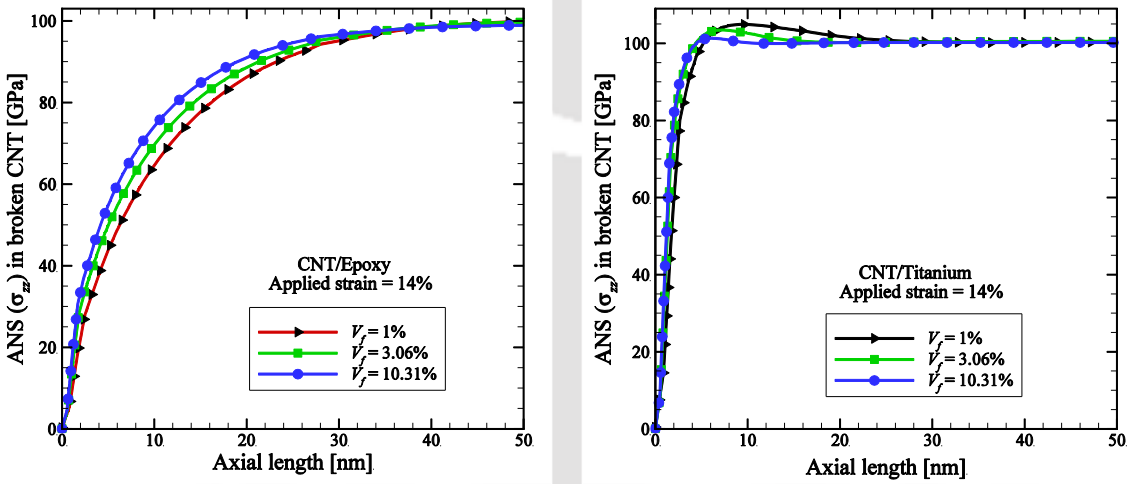

(a) (b)

Figure 4.19 Axial normal stress in the broken CNT with volume fraction (a) CNT/epoxy and (b) CNT/Ti composites.

It could be observed that the ineffective length of the broken CNT in CNT/Ti composites is 3 nm for the volume fraction of 10.31% and 3.06% but 4 nm corresponding to volume fraction of 1%. However, there is not much difference in ineffective length for the volume fractions of 1% to 10.31% in the case of CNT/Ti composites. But in the case of CNT/epoxy composites the ineffective length are 27 nm, 28 nm, and 30 nm corresponding to volume fraction of 10.31%, 3.06% and 1%, respectively. Therefore, in the case of CNT/epoxy composites, for all the range of volume fractions, the broken CNT is ineffective up to 30% of the length and hence it contributes very less to the load bearing of the composite. However,

in the case of CNT/Ti composites, a major length of the broken CNT contributes to the load bearing of the composite.

In could be concluded that the ineffective length of the broken CNT decreases with the increase in volume fraction for both the CNT-reinforced composites. Even though the length of the model is 100 nm, for better clarity near the CNT break, stress variation is shown only up to 50 nm and beyond this there is no change in ANS along the length.

4.4.2.2.2 Interfacial shear stress at the interface of broken CNT and matrix

Figures 4.20(a) and 4.20(b) show the variation of IFSS (τ_{rz}) with volume fraction at the interface of the broken CNT and matrix for CNT/epoxy and CNT/Ti composites, respectively.

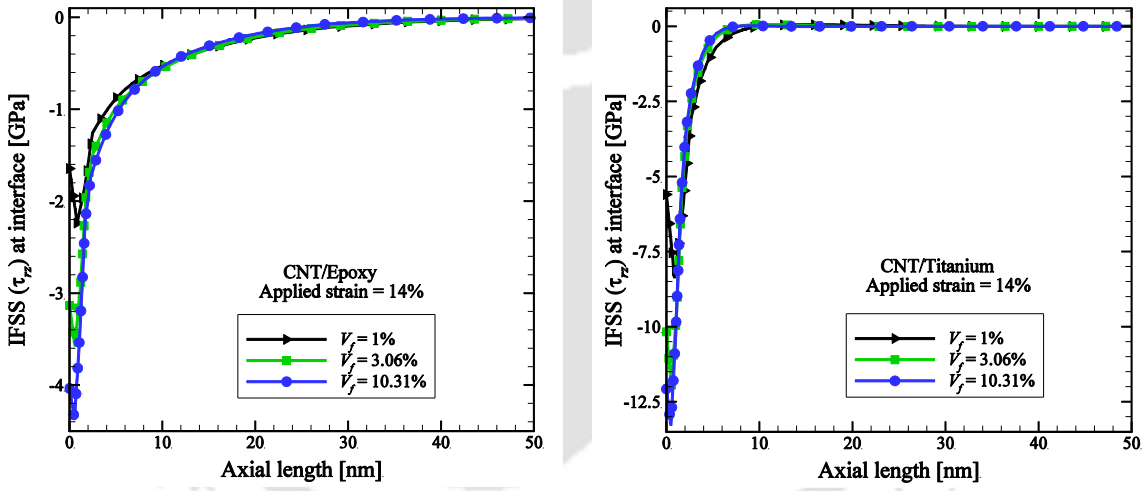

(a) (b)

Figure 4.20 Interfacial shear stress at the interface of broken CNT and matrix with volume fraction (a) CNT/epoxy and (b) CNT/Ti composites.

It could be observed that the magnitude of the IFSS increases with the increase in volume fraction of CNT. The magnitudes of IFSS are 2.24 GPa and 4.34 GPa corresponding to volume fractions of 1% and 10.31%, respectively for CNT/epoxy composites. It could be concluded that the magnitude of IFSS increases 2 times with increase in volume fraction of CNT from 1% to 10.31% for CNT/epoxy composites. But the magnitudes of IFSS are 8.37 GPa and 13.28 GPa corresponding to volume fractions of 1% and 10.31%, respectively for

CNT/Ti composites. It could be concluded that the magnitude of IFSS increases 1.5 times with increase in volume fraction of CNT from 1% to 10.31% for CNT/Ti composites.

Therefore, even though the axial strength and stiffness of CNT-reinforced composites increase with the increase in volume fraction, in the event of a fiber break, the interfacial shear stress developed at the interface of the broken fiber and the matrix actually increases with the increase in volume fraction thereby enhancing the chances of debonding initiation at such interface. Even though the length of the model is 100 nm, for better clarity near the CNT break, stress variation is shown only up to 50 nm and beyond this there is no change in interfacial shear stress (IFSS) along the length.

4.4.2.2.3 Axial normal stresses in adjacent intact CNTs

Figures 4.21(a) and 4.21(b) show the variation of axial normal stress with volume fractions in the adjacent intact CNTs for CNT/epoxy and CNT/Ti composites, respectively.

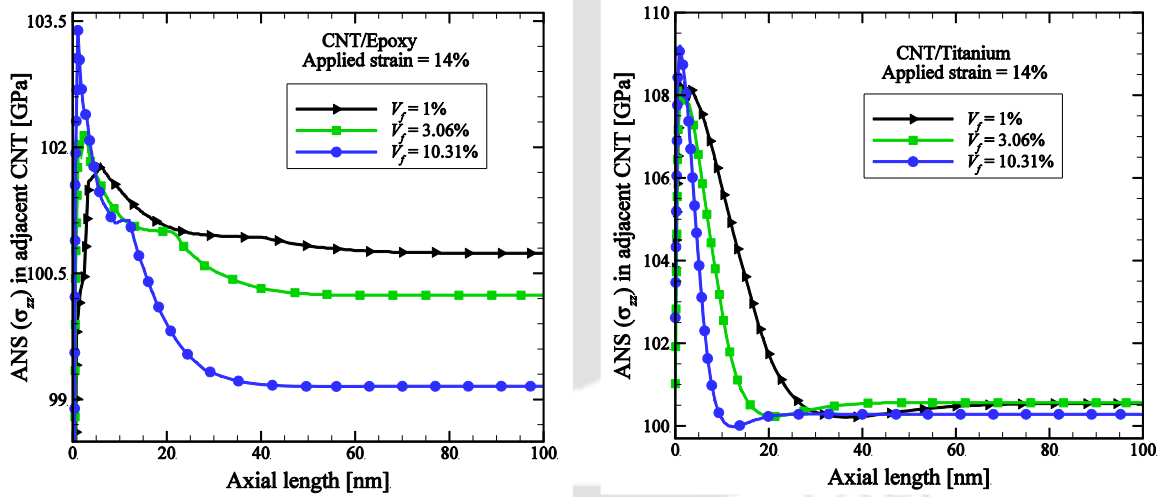

(a) (b)

Figure 4.21 Axial normal stress in the adjacent intact CNTs with volume fraction (a) CNT/epoxy and (b) CNT/Ti composites.

It could be observed from Fig. 4.21 that for CNT/epoxy composites corresponding to the volume fractions of 1%, 3.06%, and 10.31% the magnitudes of SCFs are 1.01, 1.02, and 1.04 respectively. But for CNT/Ti composites corresponding to volume fractions of 1%, 3.06%, and 10.31% the magnitude of SCFs are 1.08, 1.08, and 1.09 respectively. Above results conclude that the SCF increases with increase in volume fraction for both the CNT-

reinforced composites. But for CNT/Ti composite the SCFs for the volume fractions of 1% and 3.06% are not significant. Distributions of stresses are different corresponding to volume fraction of 1% and 3.06% as could be clearly seen in Fig. 4.21 for both the CNT-reinforced composites.

4.5 Comparison of stress distribution considering linear and non-linear stress-strain relation of CNT

It has already been mentioned that the stress-strain relation of CNT is non-linear especially at higher strain, and non-linear stress-strain relation should be considered in the analysis. It order to understand the importance of such incorporation of non-linear stress-strain relation, a comparison has been made by carrying out analysis of broken CNT composite considering both linear and non-linear stress-strain relation of CNT. For the purpose of comparison applied strain of 14% is considered for both the linear and non-linear cases.

For stress analysis of CNT-reinforced composites considering linear behavior of CNT the Young' modulus of CNT is taken as 1 TPa [4-5]. However the non-linear stress-strain relation for CNT (Eq. (3.12)) has been input for the FE modeling. Therefore, when we compared the result of CNT-reinforced composites considering linear and non-linear stress-strain relation of CNT the Young' modulus of CNT is taken as 1.364 TPa [117].

4.5.1 Axial normal stress in the broken CNT

Figures 4.22 show the variation of the ANS in the broken fiber (i.e. CNT) along the fiber length of CNT/epoxy and CNT/titanium composites for a constant volume fraction of 3.06% considering linear and non-linear stress-strain relation of CNT. It could be observed from Fig. 4.22(a) that the ineffective lengths of CNT/epoxy for linear and non-linear stress-strain relation of CNT are 56% and 28%, respectively. It can be seen in Fig. 4.22(a) that the magnitudes of nominal stress of CNT/epoxy for linear behavior and non-linear stress-strain behavior of CNT are 182.53 GPa and 100.22 GPa, respectively. It could be observed from Fig. 4.22(b) that the ineffective lengths of CNT/Ti composite for linear and non-linear stress-strain relation of CNT are 8% and 3%, respectively. It can be seen in Fig. 4.22(b) that the

magnitudes of nominal stress of CNT/Ti for linear and non-linear stress-strain behavior of CNT are 190.05 GPa and 100.51 GPa, respectively.

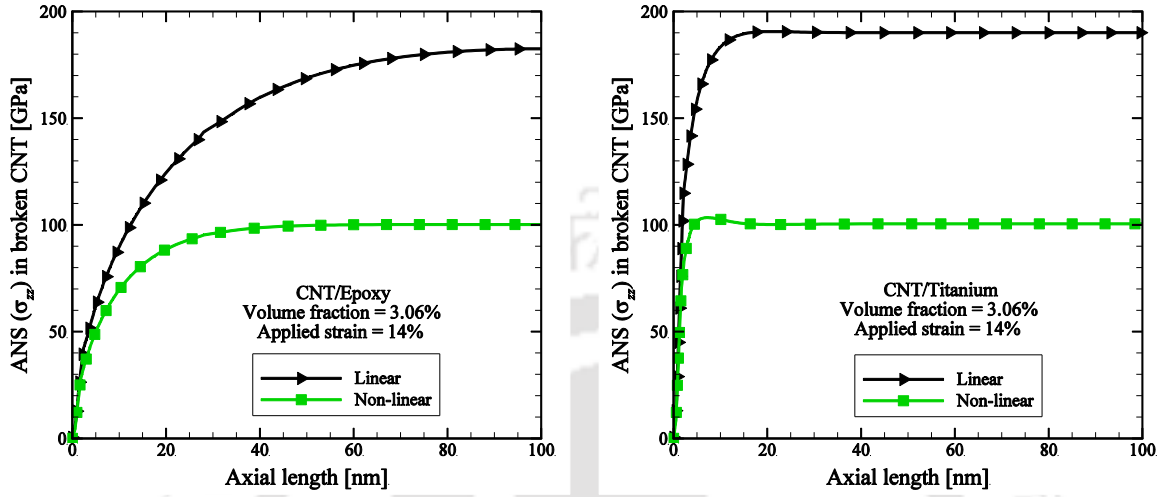

Figure 4.22 Axial normal stress in the broken CNT (a) CNT/epoxy and (b) CNT/Ti composites.

Therefore, it could be seen that incorporating non-linear stress-strain relation of CNT not only estimates normal stress much less than that from linear model but also estimates lower ineffective length for the broken fiber. This is true for both CNT/epoxy and CNT/Ti composites. Thus not incorporating non-linear model actually overestimates both normal stress and ineffective length especially at higher strain.

4.5.2 Interfacial shear stress at the interface of broken CNT and matrix

Figures 4.23 show the variation of the IFSS (τ_{rz}) at the interface of the broken CNT and matrix in CNT-reinforced composites at a constant volume fraction of 3.06% considering linear behavior and non-linear stress-strain relation of CNT. It can be seen in Fig. 4.23(a) that the magnitudes of IFSS of CNT/epoxy for linear behavior and non-linear stress-strain relation of CNT are 4.37 GPa and 3.57 GPa, respectively. It can be seen in Fig. 4.23(b) that the magnitudes of IFSS of CNT/Ti composite for linear behavior and non-linear stress-strain relation of CNT are 15.09 GPa and 11.94 GPa, respectively. It could be concluded from Figs. 4.23 that the magnitude of IFSS for both the CNT-reinforced composites considering linear and non-linear stress-strain relation of CNT are significant.

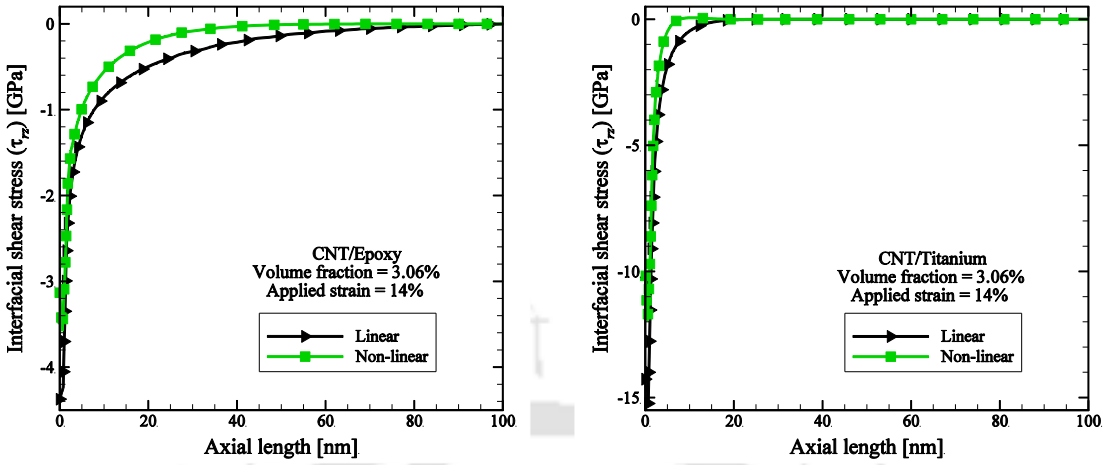

Figure 4.23 Interfacial shear stress at the interface of broken CNT and matrix (a) CNT/epoxy and (b) CNT/Ti composites.

Therefore, not incorporating non-linear stress-strain relation in the model leads to overestimation of interfacial shear stress in both the cases of CNT/epoxy and CNT/Ti composites with a small debonding. Thus once again it could be concluded that to get accurate result the non-linear stress-strain relation of CNT must be incorporated in the CNT-reinforced composites.

4.5.3 Axial normal stress in the adjacent intact CNTs

Figures 4.24 show the variation of axial normal stress in the adjacent intact CNTs of CNT-reinforced composites for a constant volume fraction of 3.06% considering linear and non-linear stress-strain relation of CNT. It could be estimated from Fig. 4.24(a) that the SCF of CNT/epoxy composite considering linear and non-linear stress-strain relation of CNT are 1.1 and 1.02, respectively. It could be estimated from Fig. 4.24(b) that the SCF of CNT/Ti composite for linear and non-linear stress-strain relation of CNT are 1.01 and 1.07, respectively.

It could be concluded that the estimated SCF considering non-linear stress-strain behavior of CNT is lower compared to the estimated SCF considering linear stress-strain relation of CNT for CNT/epoxy composite. But in case of CNT/Ti composite estimated SCF considering non-linear stress-strain behavior of CNT is higher compared to the estimated

SCF considering linear stress-strain relation of CNT. It could also be concluded that the magnitude of axial normal stress in the adjacent intact CNT considering linear stress-strain relation of CNT is higher than that of considering non-linear stress-strain relation of CNT for both the CNT-reinforced composites especially at higher strain.

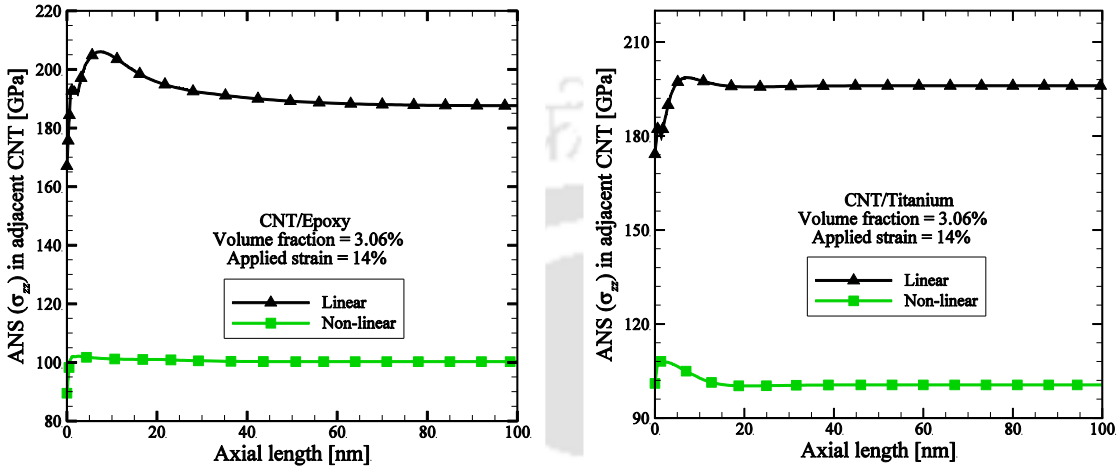

(a) (b)

Figure 4.24 Axial normal stress in the adjacent intact CNTs (a) CNT/epoxy and (b) CNT/Ti composites.

All these comparisons show that even though there is deviation of results between considering linear and non-linear stress-strain relations of CNTs, but the discrepancy is less for lower strain and is much more for higher strain which is expected from the non-linear stress-strain relation of CNT (Eq. 3.12).

4.6 Results and discussion for CNT/Al and CNT/Cu composites

Since CNT/aluminum (Al) and CNT/copper (Cu) are also used in different applications, it was decided to analyze these two CNT-reinforced metal matrix composites (MMCs) with a broken CNT. Since it was seen in previous section that it is essential to use 9-CNT RVE model with non-linear stress-strain relation of CNT, therefore for all these analysis the 9-CNT RVE model with non-linear stress-strain relation is used.

The distribution of stresses in CNT/epoxy and CNT/Ti composites has been studied in the previous section. Majority of the literatures published have focused on CNT-reinforced polymer matrix composites (PMCs). Studies on CNT-reinforced MMCs are few as compared

to those on CNT-reinforced PMCs. But there are also some publications available on CNT/Al and CNT/Cu composites. Therefore, in this section stress analysis of CNT/Al and CNT/Cu composites with a broken CNT considering non-linear behavior of CNT have been studied. In the present study a strain of 14% is considered.

In the present analysis, finite element analysis of CNT/Al and CNT/Cu composites with a broken CNT has been performed to obtain the stress redistribution around the broken CNT. Effect of matrix materials on the stress redistribution around the broken CNT has alo been studied. The effects of volume fraction on the distribution of stress near the vicinity of broken CNT have been investigated. Properties of matrix materials are listed in the follow Table 4.1.

Table 4.1 Elastic properties of aluminium and copper.

Materials	Young's modulus (GPa)	Poisson's ratio
Aluminum	69	0.334
Copper	117	0.355

4.6.1 For a constant volume fraction

4.6.1.1 Axial normal stress in the broken CNT

Figure 4.25 shows the distribution of the axial normal stress (σ_{zz}) along the length of the broken CNT in CNT/Al and CNT/Cu composites for a constant volume fraction of 3.06%.

As expected the ANS at the break of the broken CNT is zero but it could be observed that the broken CNT regained the nominal value after a length of 5 nm for CNT/Al and 3 nm for CNT/Cu composites, respectively. Therefore, it could be concluded that the ineffective length of the broken CNT in CNT/Al composites is 5% but for CNT/Cu composites it is 3%. So,

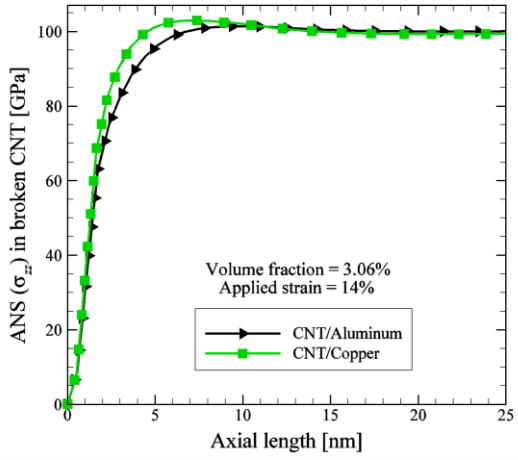

Figure 4.25 Axial normal stress in the broken CNT.

for the same volume fraction the ineffective length of the CNT/Al composites is higher than that of the CNT/Cu composites. Even though the length of the model is 100 nm, for better clarity near the CNT break, stress variation is shown only up to 25 nm and beyond this there is no change in ANS along the length.

4.6.1.2 Interfacial stress at the interface of broken CNT and matrix

Figures 4.26 (a) and 4.26(b) show the distribution of interfacial stresses τ_{rz}, $\tau_{r\theta}$ and σ_{rr} along the length of fiber (i.e. CNT) in CNT/Al and CNT/Cu composites, respectively for a constant volume fraction of 3.06%.

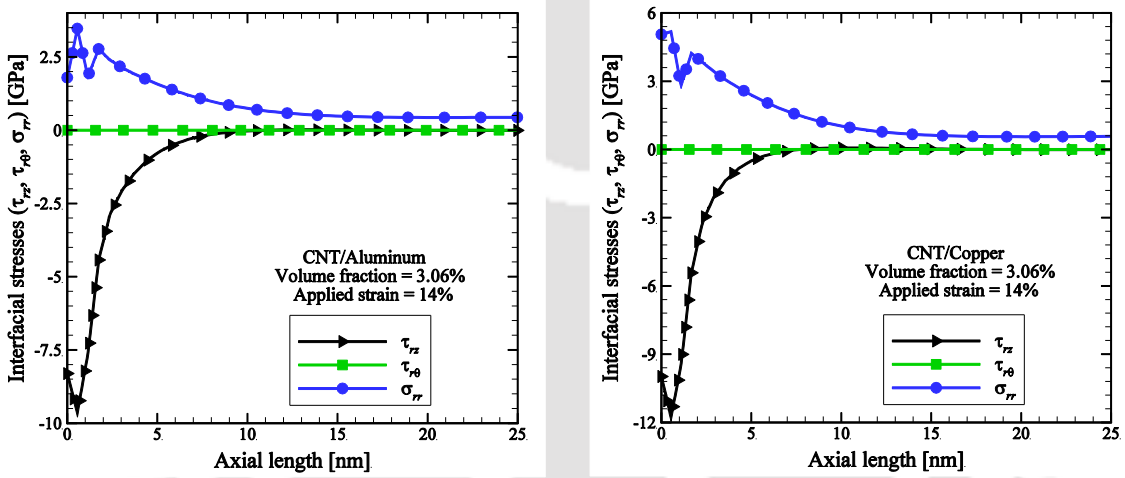

(a) (b)

Figure 4.26 Interfacial stresses at the interface of broken CNT and matrix (a) CNT/Al and (b) CNT/Cu composites.

It can be seen in Fig. 4.26 that a high value of τ_{rz} exists near the vicinity of broken fiber but the magnitude of $\tau_{r\theta}$ is zero along the fiber length for both the CNT-reinforced composites. It could be clearly seen from Figs. 4.26 that the interfacial normal stress (σ_{rr}) is always positive and it extend over a considerable length of the interface for both the CNT/Al and CNT/Cu composites. But the magnitude of σ_{rr} is less than that of the τ_{rz}. It could be concluded that the fiber debonding may take place at the interface near the vicinity of the break due to the high value of τ_{rz} as we as due to σ_{rr}, and $\tau_{r\theta}$ has no effect on debonding of CNT from both the aluminum and copper matrices in the case of axial loading. Even though

the length of the model is 100 nm, for better clarity near the CNT break, stress variation is shown only up to 25 nm and beyond this there is no change in interfacial stresses along the length.

Figure 4.27 shows the distribution of interfacial shear stress (τ_{rz}) at the interface of the broken CNT and matrix in CNT/Al and CNT/Cu composites for a constant volume fraction of 3.06%. It could be observed that at the interface near the vicinity of the break, a high value of IFSS occurs indicating that fiber debonding may take place at that location. In the present case, the magnitudes of IFSS of CNT/Al and CNT/Cu composites are 9.64 GPa and 11.77 GPa respectively. It could be concluded that for the same volume fraction, the magnitude of IFSS for CNT/Cu composites is higher than that of the CNT/Al composites though differences are not much. Higher magnitude of interfacial shear stress in case of CNT/Cu composite is expected in view ineffective length of the broken fiber. The reason for the same is the differences of properties between of matrix materials.

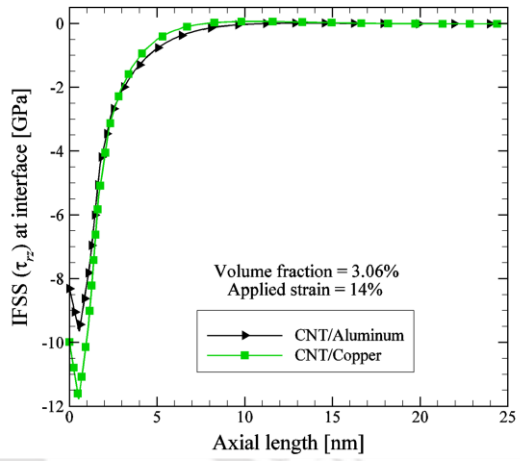

Figure 4.27 Interfacial shear stress at the interface of broken CNT and matrix.

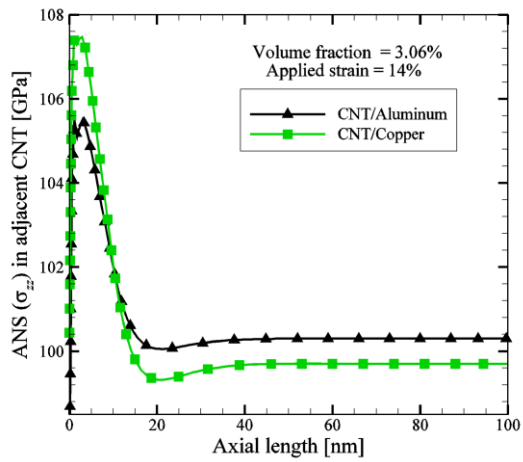

Figure 4.28 Axial normal stress in the adjacent intact CNT.

4.6.1.3 Axial normal stress in the adjacent intact CNTs

Figure 4.28 shows the distribution of axial normal stress (σ_{zz}) in the adjacent intact CNT for CNT/Al and CNT/Cu composites for a constant volume fraction of 3.06%. It could be observed that due to the presence of a broken CNT, the adjacent CNTs experience a stress

concentration in the vicinity of the break. The stress concentration factor for CNT/Al and CNT/Cu composites are 1.05 and 1.08, respectively for a constant volume fraction of 3.06%. So, it could be concluded that there is a possibility that the adjacent CNT may break as a consequence of over loading. It could also be concluded that for the same volume fraction, the SCF for CNT/Cu composite is higher than that of the SCF of CNT/Al composites though differences are not much.

4.6.2 Effect of volume fraction on distribution of stresses

4.6.2.1 Axial normal stresses in the broken CNT

Figures 4.29(a) and 4.29(b) show the variation of the axial normal stress along the length of the broken fiber for different volume fractions in CNT/Al and CNT/Cu composites, respectively. It could be observed from Figs. 4.29 that the ineffective length of the broken CNT remains almost same for all the range of volume fractions of 1% to 10.31% in both the CNT/Al and CNT/Ti composites. Even though the length of the model is 100 nm, for better clarity near the CNT break, stress variation is shown only up to 25 nm and beyond this there is no change in ANS along the length.

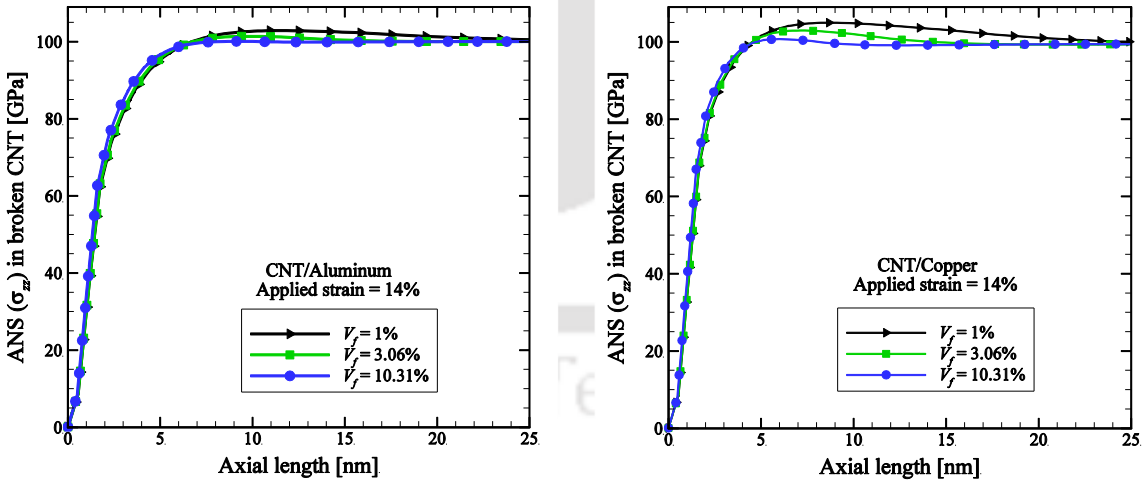

(a) (b)

Figure 4.29 Axial normal stresses in the broken CNT with volume fraction (a) CNT/Al and (b) CNT/Cu composites.

4.6.2.2 Interfacial shear stress at the interface of broken CNT and matrix

Figures 4.30(a) and 4.30(b) show the distribution of interfacial shear stress (τ_{rz}) with volume fraction at the interface of the broken CNT and matrix along the fiber length in CNT/Al and CNT/Cu composites, respectively. It could be observed from Fig. 4.30 that the magnitudes of IFSS are 9.56 GPa and 10.86 GPa corresponding to volume fractions of 1% and 10.31%, respectively for CNT/Al composites. But the magnitudes of IFSS are 11.74 GPa and 13.16 GPa corresponding to volume fractions of 1% and 10.31%, respectively for CNT/Cu composites. Even though the length of the model is 100 nm, for better clarity near the CNT break, stress variation is shown only up to 25 nm and beyond this there is no change in interfacial shear stresses along the length.

It could be concluded that the magnitudes of IFSS increase with the increase in volume fraction for both the CNT/Al and CNT/Ti composites. Therefore, even though the axial strength and stiffness of CNT-reinforced composites increase with the increase in volume fraction, in the event of a fiber break, the interfacial shear stress developed at the interface of the broken fiber and the matrix actually increases with the increase in volume fraction thereby enhancing the chances of debonding initiation at such interface.

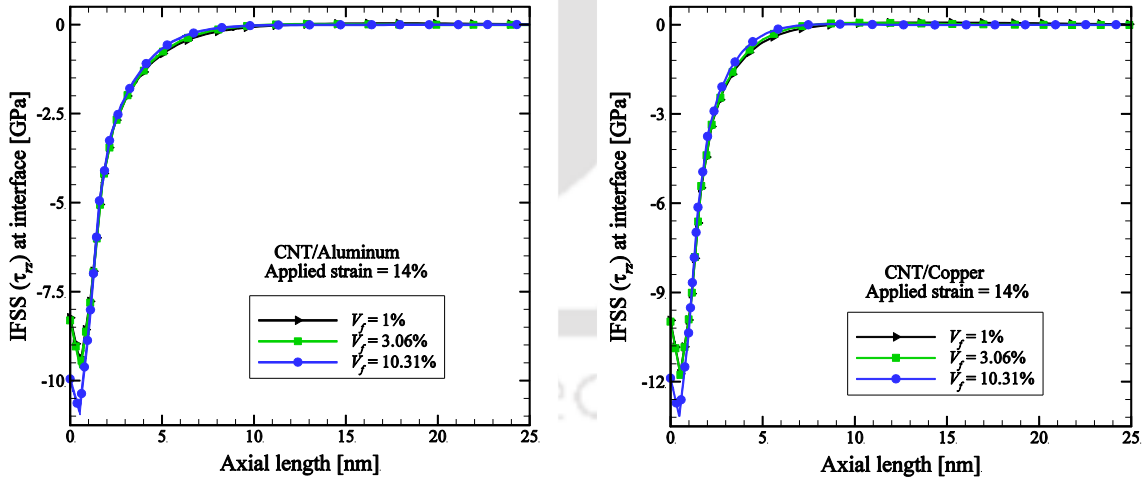

(a) (b)

Figure 4.30 Interfacial shear stresses at the interface of broken CNT and matrix with volume fraction (a) CNT/Al and (b) CNT/Cu composites.

4.6.2.3 Axial normal stresses in the adjacent intact CNTs

Figures 4.31(a) and 4.31(b) show the variation of axial normal stress (σ_{zz}) for different volume fractions in the adjacent intact CNTs in CNT/Al and CNT/Cu composites, respectively.

It could be estimated from Fig. 4.31(a) that for CNT/Al composites corresponding to the volume fractions of 1% and 10.31% the magnitudes of SCFs are 1.04 and 1.07 respectively. But for CNT/Cu composites corresponding to volume fractions of 1% and 10.31% the magnitude of SCFs are 1.08 and 1.1 respectively. Above results conclude that the SCF increases with the increase in volume fraction for both the CNT-reinforced composites. It can be seen clearly in Fig. 4.31 that the distributions of ANS in the adjacent intact CNT are different for different volume fractions.

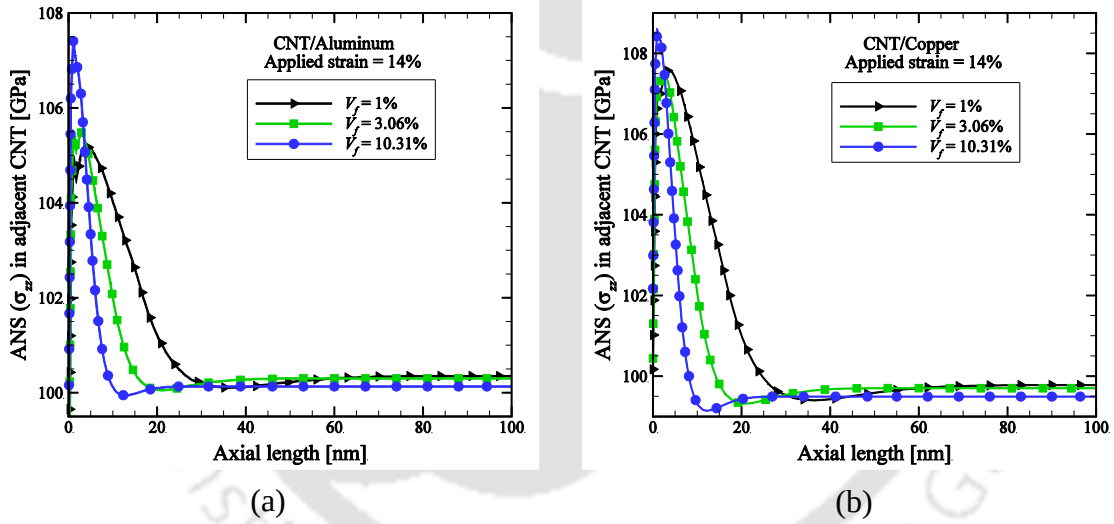

(a) (b)

Figure 4.31 Axial normal stress in the adjacent intact CNTs with volume fraction (a) CNT/Al and (b) CNT/Cu composites.

It could also be noticed that even though SCF increase with the increase in fiber volume fraction, but the increased stress extends over a larger length of the intact fiber for lesser fiber volume fraction for both the CNT/Al and CNT/Cu composites.

4.7 Results and discussion for CNT/Al_2O_3 composites

In the above two sections the distribution of stresses in CNT/epoxy and CNT/metal matrix composites have been studied. Studies on CNT-reinforced ceramic matrix composites (CMCs) are few as compared to those on CNT-reinforced PMCs and MMCs. However, ceramics have many advantages over metals even though it is more brittle than metals. Such as under harsh conditions, the CNT-reinforced metal matrix composites cannot be used effectively. But CNT-reinforced ceramic matrix composites could be potential composite materials for high temperature stability. Mukerji [146] presented a review in detailed on excellent properties of advanced engineering ceramics produced by conventional manufacturing technology and the restriction of ceramics in structural applications due to their extreme brittle nature. The important properties of ceramics are high rigidity and hardness, high-temperature stability, high corrosion resistance, light weight and electrical insulation. So, from structural point of view, ceramics have many advantages over metals even though it is more brittle than metals. The tensile strength of the CNT is around 50 times higher than that of steel and the failure strain of a defect free CNT is 10% - 15%. Thus, CNTs are considered to be the ultimate carbon fiber to incorporate them into ceramics to overcome the intrinsic brittleness property of the ceramic materials. The CNT-reinforced CMCs could be potential composite materials for high temperature stability as well as exceptional toughness and creep resistance. Therefore, in future the CNT-reinforced CMCs may be one of the lighter and tougher structural advanced nanocomposites.

Since CNT/alumina (Al_2O_3) composites are also used in different applications, it was decided to analyze this CNT-reinforced CMCs with a broken CNT. Since it was seen in earlier section that it is essential to use 9-CNT RVE model with non-linear stress-strain relation of CNT, therefore, this section stress analysis of CNT/Al_2O_3 matrix composite with a broken CNT considering non-linear relation of CNT has been carried out.

Based on the FE models described in previous section, multi-scale FE analysis has also been performed to study the stress redistribution around the broken fiber in CNT/Al_2O_3 composites. Where, the non-linear stress-strain relation of CNT in Eq. (3.12) is used. Effect of volume fraction on the redistribution of stress near the vicinity of the broken fiber has also been studied of CNT/Al_2O_3 composites. Boundary conditions of 9-CNT RVE have already been described in earlier section 4.4.1. But here, at $z = L_a$, a uniformed displacement is

applied to simulate 5% axial strains. Young's modulus and Poisson's ratio of alumina are considered as 375 GPa and 0.22, respectively.

4.7.1 For a constant volume fraction

4.7.1.1 Axial normal stress in the broken CNT

Figure 4.32 shows the distribution of the axial normal stress (ANS) in the broken CNT along the length of the broken CNT in CNT/Al_2O_3 nanocomposites for a constant volume fraction of 3.06%. As expected that the ANS at the break of the broken fiber is zero but it could be observed that the broken fiber regained the nominal value of ANS after a length of 4 nm in CNT/Al_2O_3 nanocomposites. Therefore, it could be concluded that the ineffective length of the broken fiber in CNT/Al_2O_3 composites is only 4% for a constant volume fraction of 3.06% in the case of axial loading. Even though the length of the model is 100 nm, for better clarity near the CNT break, stress variation is shown only up to 50 nm and beyond this there is no change in ANS along the length.

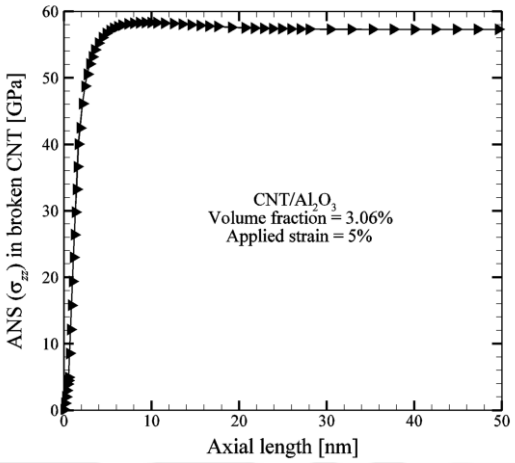

Figure 4.32 Axial normal stress in the broken CNT in CNT/Al_2O_3 composites.

4.7.1.2 Interfacial stresses at the interface of broken CNT and matrix

Distribution of IFSS (τ_{rz} and $\tau_{r\theta}$) and IFNS (σ_{rr}) at the interface of CNT/ Al_2O_3 matrix composite has also been investigated. Figure 4.33 shows the distribution of interfacial stresses along the length of fiber in CNT/Al_2O_3 composites for a constant volume fraction of 3.06%. It could be clearly seen from Fig. 4.33 that a high value of interfacial stress (τ_{rz}) and interfacial normal stress (σ_{rr}) exist near the vicinity of broken fiber but the magnitude of $\tau_{r\theta}$ is zero along the fiber length in CNT/Al_2O_3 composites. It could also be seen from Fig. 4.33 that the σ_{rr} is always positive and it extend over a considerable length at the interface of

CNT/Al_2O_3 composite. It could be concluded that the fiber debonding may take place at the interface near the vicinity of the break due to the high value of τ_{rz} as well as due to σ_{rr} , and $\tau_{r\theta}$ does not contribute to the debonding of CNT from the alumina matrix in the case of axial loading. Even though the length of the model is 100 nm, for better clarity near the CNT break, stress variation is shown only up to 25 nm and beyond this there is no change in interfacial stresses along the length.

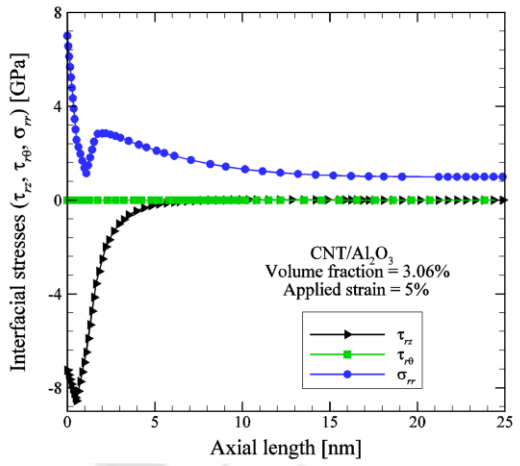

Figure 4.33 Interfacial stress at the interface of broken CNT and matrix in CNT/Al_2O_3 composites.

4.7.1.3 Axial normal stress in the adjacent intact CNTs

Figure 4.34 shows the distribution of axial normal stress in the adjacent intact fibers (CNTs) along the length of CNT in CNT/Al_2O_3 composites for a constant volume fraction of 3.06%. It could be observed from Fig. 4.34 that due to the presence of a broken fiber, the adjacent fibers experienced a stress concentration in the vicinity of the break. It can be seen in Fig. 4.34 that the maximum and nominal (i.e. average) values of axial normal stresses are 59.37 GPa and 57.31 GPa, respectively in CNT/Al_2O_3 composites for a constant volume fraction of 3.06%. This leads to a stress concentration factor equal to 1.04. So, it could be concluded that there is a possibility that the adjacent fiber might break as a consequence of over loading. When one fiber breaks

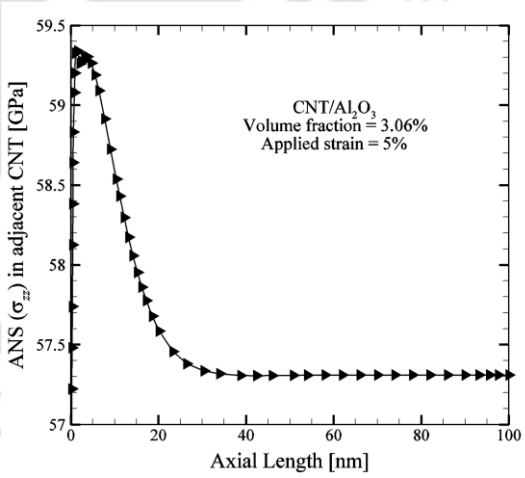

Figure 4.34 Axial normal stress in the adjacent intact CNT in CNT/Al_2O_3 composites.

it may lead to breaking of the adjacent fibers, leading to successive failure of fibers and finally the failure of nanocomposites.

4.7.2 Effect of volume fraction

4.7.2.1 Axial normal stress in the broken CNT

Figure 4.35 shows the distribution of the axial normal stress in the broken CNT along the length of CNT for different volume fractions in CNT/Al_2O_3 composites. It can be seen in Fig. 4.35 that the ineffective length of the broken CNT remains almost same for all the range of volume fractions from 1% - 10.31%. It could be concluded that the ineffective length of the broken fiber does not show significant changes with the change in volume fraction in CNT/Al_2O_3 composites in the rage of volume fraction considered. Even though the length of the model is 100 nm, for better clarity near the CNT break, stress variation is shown only up to 50 nm and beyond this there is no change in ANS along the length.

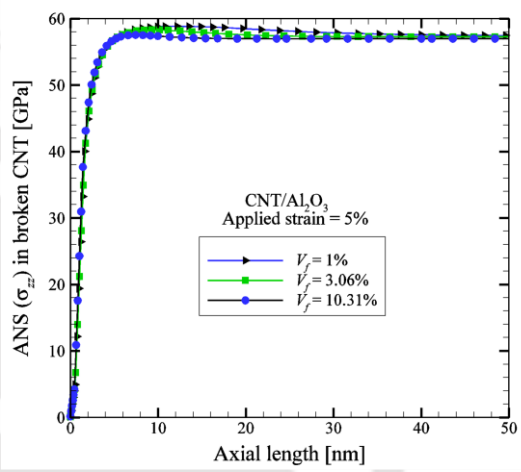

Figure 4.35 Axial normal stress in the broken CNT with volume fraction in CNT/Al_2O_3 composites.

4.7.2.2 Interfacial shear stress at the interface of broken CNT and matrix

Figure 4.36 shows the distribution of interfacial shear stress (τ_{rz}) at the interface between the broken CNT and the matrix along the CNT length for different volume fractions in CNT/Al_2O_3 composites. It can be seen in Fig. 4.36 that the magnitudes of the τ_{rz} in CNT/Al_2O_3 composites are 8.6 GPa and 9.33 GPa corresponding to volume fractions of 1%

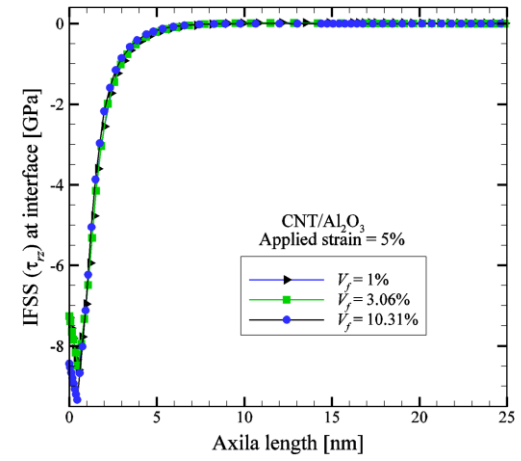

Figure 4.36 Interfacial shear stresses at the interface of broken CNT and matrix with volume fraction in CNT/Al_2O_3 composites.

and 10.31%, respectively. It could also been observed that the magnitudes of the τ_{rz} in CNT/Al_2O_3 composites remain almost same for the volume fractions of 1% and 3.06% but show increment beyond that. It could be concluded that the magnitude of the τ_{rz} increases with increase in volume fraction in the rage of volume fraction considered. Even though the length of the model is 100 nm, for better clarity near the CNT break, stress variation is shown only up to 25 nm and beyond this there is no change in interfacial shear stresses along the length.

4.7.2.3 Axial normal stresses in the adjacent intact CNTs

Figure 4.37 shows the distribution of axial normal stress in the adjacent intact CNTs along the length of CNT for different volume fractions in CNT/Al_2O_3 composites. It can be seen in Fig. 4.37 that the distributions of ANS the adjacent intact fibers near the vicinity of break as well as along the length of fiber are significantly different with different volume fractions. It has been found that the SCFs of CNT/Al_2O_3 composites are 1.03, 1.04 and 1.05 corresponding to the volume fractions of 1%, 3.06% and 10.31%, respectively. So, it could be concluded that the SCFs increase with increase in fiber volume fraction in CNT/Al_2O_3 composites.

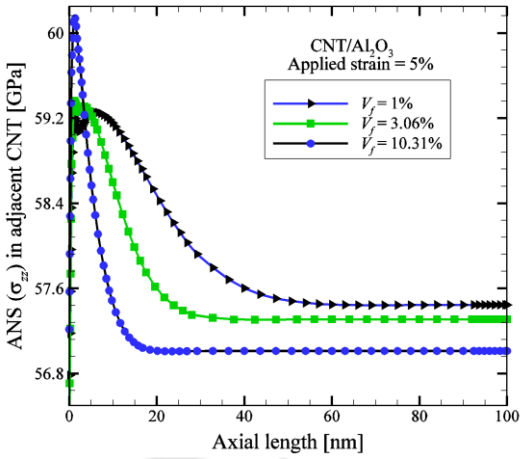

Figure 4.37 Axial normal stress in the adjacent intact CNT with volume fraction in CNT/Al_2O_3 composites.

It could also be noticed that even though SCF increase with increase in fiber volume fraction, but the increased stress extends over a larger length of the intact fiber for lesser fiber volume fraction in CNT/Al_2O_3 composites.

The trend of the distribution of ANS in the broken CNT as well as in the adjacent intact CNT in CNT-reinforced composites studied in the present work are similar to the distribution of ANS in conventional fiber-reinforced composites as reported by Nedele and Wisnom [143].

4.8 Summary

A full 3D multi-scale FE analysis has been performed for CNT-reinforced composites to study the stress redistribution around a broken CNT to assess the chances of fiber fracture or debonding. Distribution of stress around a broken CNT in 1-CNT RVE and 9-CNTs RVE have been carried out by considering both linear as well as non-linear stress-strain relation of CNT. Analysis using 1-CNT RVE model may be computationally simpler than that of 9-CNTs RVE, but a single-CNT model will not be appropriate as the SCF in the adjacent intact fiber cannot be evaluated. Therefore, it could be concluded that for complete understanding of the analysis of CNT-reinforced composites, the use of 9-CNTs RVE is important as 1-CNT RVE neglects the presence of intact fibers surrounding the broken fiber. Therefore, 9-CNTs RVE needs to be used for analysis of such CNT-reinforced composites with fiber break. It is also observed that non-linear stress-strain relation of CNT should be used to get the correct stress distribution especially at higher strain.

In the absence of any published results on the distribution of stress near the vicinity of a broken CNT in CNT-reinforced composites, qualitative trends of the stress distributions around the fiber break have been compared with those for conventional graphite/epoxy composites by Nedele and Wisnom [143] and a good agreement has been observed. Some of the important observations are -

- It has been observed that at interface between the broken CNT and the matrix experience a high value of stress that might lead to debonding of the CNT-reinforced composites.
- In the present case of axial loading of the CNT composites, IFNS (σ_{rr}) and IFSS (τ_{rs}) are negligibly small and only IFSS (τ_{rz}) has a higher magnitude at the interface showing that the debonding of the fiber from the matrix is possible.
- For a CNT composite subjected to axial loading, presence of broken CNT leads to stress concentrations due to axial stress induced in the adjacent fiber.
- Adjacent intact CNTs experience a stress concentration as a consequence of over loading which may lead to breaking of the adjacent intact CNTs, leading to successive failure of CNTs and finally the failure of nanocomposites.

- The estimated stress concentration factor (SCF) considering non-linear stress-strain relation of CNT is lower compared to the estimated SCF considering linear stress-strain relation of CNT for CNT/epoxy composite. But the same has been reverse in case of CNT/Ti composite.
- In general, for all types of CNT composites (polymeric, metallic and ceramic) considered here, the 1-CNT RVE model underestimates ineffective length compared to 9-CNT RVE model. In addition, not incorporating non-linear stress-strain relation of CNT, overestimate both normal stress and ineffective length of broken fiber especially at higher strain.
- Incorporation of non-linear stress-strain relation of CNT not only estimates normal stress much less than that from linear model but also estimates lower ineffective length for the broken fiber. This is true for all the CNT-reinforced composites. Thus not incorporating non-linear model actually overestimates both normal stress and ineffective length especially at higher strain.
- Not incorporating non-linear stress-strain relation in the model leads to overestimation of interfacial shear stress in both the cases of CNT/epoxy and CNT/Ti composites. Thus once again it could be concluded that to get accurate result the non-linear stress-strain relation of CNT must be incorporated in the CNT-reinforced composites.
- The ineffective length of a broken CNT decreases with the increase in stiffness of the matrix materials. In the present work, the ineffective lengths of the broken CNT are 28% and 3% of its original length in CNT/epoxy and CNT/Ti composites, respectively for a volume fraction of 3.06%.
- Ineffective length of a broken CNT decreases with the increase in volume fraction, however the increase is not very significant in the range of volume fraction studied in the present case. Corresponding to applied strain of 14% the ineffective lengths of CNT/epoxy composite are 30% and 27 corresponding to the volume fraction of 1% and 10.31%, respectively.
- For a given load the magnitude of the IFSS depends upon the type of the matrix materials and fiber volume fraction. In the present work, corresponding to an applied strain of 14%, the magnitudes of IFSS (τ_{rz}) for CNT/epoxy and CNT/Ti

composites are 3.58 GPa and 11.94 GPa, respectively for a volume fraction of 3.06%.

- The magnitude of IFSS (τ_{rz}) at the interface increases with the increase in volume fraction for all the CNT-reinforced composites. Corresponding to a volume fraction of 1% and 10.31% the magnitudes of IFSS (τ_{rz}) are 8.37 GPa and 13.28 GPa, respectively for CNT/Ti composites.
- Results for CNT/Al_2O_3 show that the magnitudes of IFSS near the fiber break do not show much variation with the change in volume fractions, even though earlier result (CNT/epoxy**)** showed a significant variation in magnitudes of IFSS with volume fraction.
- For a given load the magnitude of axial normal stress in the adjacent fiber depends upon the type of the matrix materials and fiber volume fraction. The SCFs on the adjacent intact CNTs in CNT/epoxy and CNT/Ti composites are 1.02 abd 1.07, respectively for a volume fraction of 3.06%. In the same line for a volume fraction of 3.06% the SCFs on the adjacent intact CNTs in CNT/Al and CNT/Cu composites are 1.05 and 1.08, respectively.
- The SCFs in the adjacent CNT increases with the increase in volume fraction. Corresponding to a volume fraction of 1% and 10.31% the magnitudes of SCFs are 1.01 and 1.04 respectively, for CNT/epoxy composites.

Chapter 5

Fracture Mechanics Based Analysis of CNT-Reinforced Composites with a Broken CNT

5.1 Introduction

In general, whenever there is a fiber break, it is accompanied by a small fiber matrix debonding at the vicinity of the break. Depending upon the applied load this debonding may grow. In this chapter, stress analysis of two types of CNT-reinforced composites viz. CNT-polymer (CNT/epoxy) and CNT-metal (CNT/aluminum) having a small debonding has been carried out considering a small debonding existing at the interface of broken CNT and matrix. Using the concept of linear elastic fracture mechanics (LEFM), strain energy release rates (SERRs) have been calculated to understand the propensity of growth of such debonding. An attempt has also been made to calculate critical SERRs using LEFM in conjunction with quadratic stress criterion (QSC). Effect of different important parameters on the distribution of stresses and SERR has also been studied.

5.2. Analysis using a single-CNT RVE model

A square representative volume element (RVE) with single-CNT has been considered for the analysis. A three dimensional (3D) finite element (FE) model of CNT, interface and its surrounding matrix is constructed on the basis of multi-scale approach. It has been assumed that the orientation of the broken CNT in the RVE is aligned. It has also been assumed that the CNT and matrix are perfectly bonded with no slip at the interface.

The ‘generalized’ stress-strain curve for zigzag CNT presented by Tserpes et al. [117] based on their experimental results and curve fitting as given by Eq. (3.12) in Chapter 3 (section 3.5.2). Equation (3.12) has been used for stress-strain relation of a zigzag CNT in the present multi-scale FE modeling of CNT-reinforced composites.

5.2.1 Single-CNT RVE model where CNT is surrounded by epoxy matrix

5.2.1.1 Finite element modeling

The front view of a single-CNT RVE surrounded by epoxy is shown in Fig. 5.1(a). The pictorial view of single-CNT RVE model with FE mesh is shown in Fig. 5.1(b), where the *x*-*y* plane is the transverse plane and the *z*-axis is the axial direction. SOLID45 element embodied in ANSYS has been used for FE modeling of the RVE. At the small length of debonded interface near the broken CNT, the top and bottom nodes are connected by bi-linear contact element (CONTAC52 in ANSYS) in order to prevent the interpenetration of the debonded surfaces during FE analysis. A highly refined FE mesh using very small size elements have been used in order to capture the high stress gradient near the broken CNT and the sizes of the elements are gradually increased towards the end and away from the break. A very fine mesh has been used near the debonding to capture the high stress gradient in the vicinity of the broken CNT and coarse meshes are used away from the break along the length.

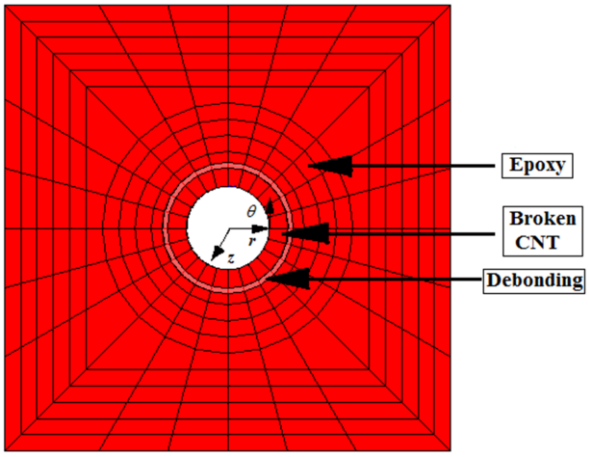

Figure 5.1(a) Front view of single-CNT RVE with FE mesh.

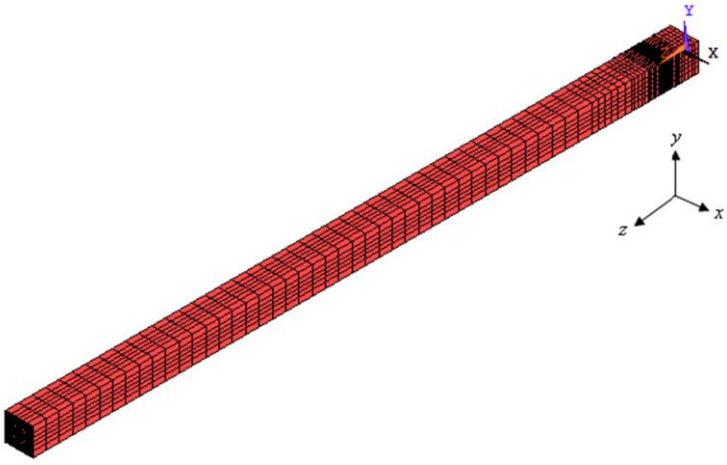

Figure 5.1(b) Pictorial view of single-CNT RVE model with FE mesh.

The pictorial view, front view and the zoomed sectional side view of the broken CNT with surrounding matrix are shown in Figs. 5.2(a), 5.2(b) and 5.2(c), respectively.

In the present analysis, the length of the RVE is considered as 200 nm and the length of the debonding near the fiber break has been taken as 10 nm. The diameter of CNT has been taken as 1.88 nm (which is equal to the diameter of zigzag (24, 0) CNT) and the thickness (*t*) of CNT is considered 0.34 nm [6-7]. After convergence study, the number of nodes and elements are 26712 and 24768 respectively in the FE model and there are 288 contact elements between 288 pairs of nodes for a constant volume fraction of 3.06% as shown in Fig. 5.1(b**)**. The ratio of the length $\Delta a/a$ is considered equal to 0.1.

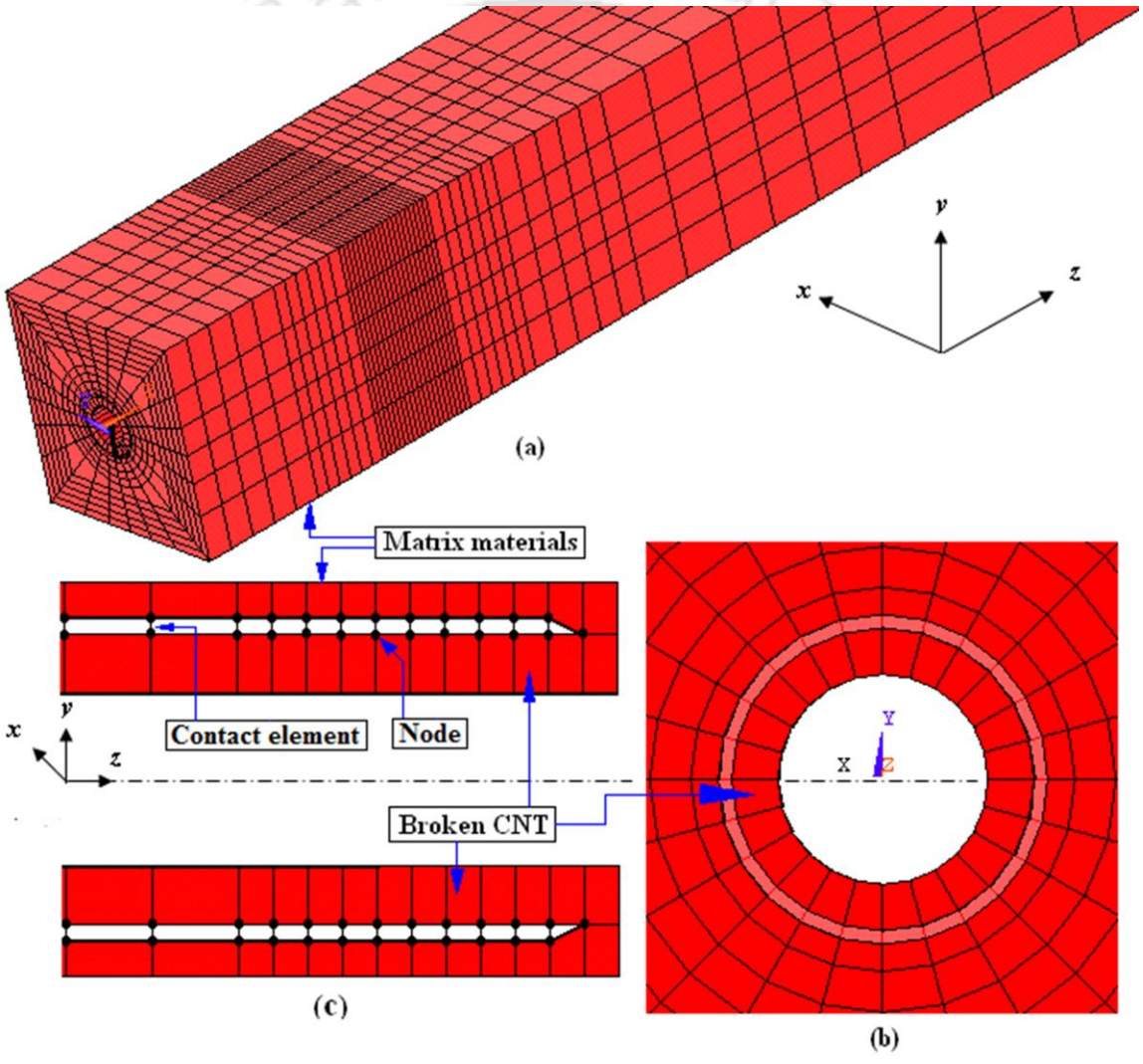

Figure 5.2 The broken CNT of 1-CNT RVE with FE mesh (a) pictorial view, (b) front view and (c) zoomed sectional side view of the interfacial debonding.

5.2.1.2 Boundary conditions

All the nodes at $z = 0$ are fully restrained except the nodes belonging to the broken fiber. The axial mechanical loading is applied by a uniform displacement in the axial direction at the far end of the model. The total applied axial strain is considered as 1.5%.

5.2.1.3 Properties of CONTAC52

Characteristic of SOLID45 has been described in Chapter 3 (section 3.2.2.1) and the characteristic of CONTAC52 is presented here. The element CONTAC52 is a 3D point-to-point contact element and the element is defined by two nodes having three degrees of freedom at each node: translations in the nodal *x*, *y* and *z* directions. The element CONTAC52 represents two surfaces which may maintain or break physical contact and may slide relative to each other. The element may be initially preloaded in the normal direction or it may be given a gap specification. A specified stiffness acts in the normal and tangential directions when the gap is closed and not sliding. The element is capable of supporting only compression in the direction normal to the surfaces and shear in the tangential direction.

5.2.2 Single-CNT RVE model where CNT is surrounded by CNT/epoxy matrix

The single-CNT RVE model presented in the previous sections where the CNT is considered broken essentially means that all the CNTs of the composite are broken at the same location which is practically not possible. Even if more than one CNT break simultaneously it is unlikely that the break will be in the same location. Therefore analysis results of this model may not be useful from present design point of view. Therefore a more realistic RVE model for a CNT composite where one CNT is broken is to consider the single CNT surrounded by matrix and other CNTs represented by the equivalent properties of CNT-matric composites. To understand the importance of such modeling, the single-CNT RVE is now analyzed when the CNT is surrounded by the composite instead of matrix.

The same model and boundary condition have been used as described in the previous. But here the matrix material surrounded by broken CNT is replaced by CNT/epoxy composites.

5.2.2.1 Properties of CNT/epoxy composite

Properties of the CNT are input using Eq. (3.12) as described in Chapter 3 (section 3.5.2). The elastic moduli of composite can be expressed in terms of the elastic properties and volume fractions of the fiber and matrix. These five elastic moduli of the composite can be calculated using mechanics of materials approach i.e. using ROM [141] as follows -

$$E_1 = E_f V_f + E_m V_m \tag{5.1}$$

$$\frac{1}{E_2} = \frac{V_f}{E_f} + \frac{V_m}{E_m} \tag{5.2}$$

$$\nu_{12} = \nu_f V_f + \nu_m V_m \tag{5.3}$$

$$\frac{1}{G_{12}} = \frac{V_f}{G_f} + \frac{V_m}{G_m} \tag{5.4}$$

$$G_{23} = \frac{E_2}{2(1+\nu_{23})} \tag{5.5}$$

where, notation '1' indicate fiber direction and the plane '2-3' is the plane of isotropy. In the present FE model the direction of fiber is considered as '*z*' and the plane '*x-y*' is the plane of isotropy.

E_1 and E_2 are longitudinal and transverse Young's modulus of composite, respectively;

E_f and E_m are the Young's modulus of CNT fiber and matrix, respectively;

V_f and V_m are the fiber and matrix volume fraction, respectively;

ν_{12} and ν_{23} are the longitudinal (major) and transverse Poisson's ratio of composite, respectively; ν_f and ν_m are the Poisson's ratios of fiber and matrix, respectively;

G_{12} and G_{23} are the longitudinal and transverse shear modulus of composite, respectively;

G_f is the shear modulus of fiber;

Effective properties of the CNT/epoxy composite are calculated for a constant volume fraction of 3.06%. The Young's modulus and Poison's ratio of epoxy are considered as 3.09 GPa and 0.372 [147], respectively. The Young's modulus and Poison's ratio of CNT are considered as 1000 GPa and 0.28 [7, 13, 145], respectively. In the present case, the axial and

transverse Young's moduli, shear modulus, and Poisson's ratio of CNT/epoxy composite are calculated using Eqs. (5.1 – 5.5) and listed in the following Table 5.1

Table 5.1 Properties of CNT/epoxy composite for V_{nt} = 3.06%.

Axial Young's modulus [GPa]	Transverse Young's modulus [GPa]	Shear modulus [GPa]	Poisson's ratio
44.73	3.19	1.16	0.369

5.2.3 VCCI for determination of SERR components

Considering the initial small debonding near the fiber break as a crack front, Irwin's [136] well known virtual crack closure integral (VCCI) has been used to calculate the strain energy release rate (SERR) components near the fiber break. SERR components can be evaluated in terms of the nodal stresses ahead of the crack tip and the displacement distributions in terms of the nodal displacements behind the crack tip using the FE method. The debonding at the interface is considered as a crack spanning over a small length ahead of the fiber break and throughout the circumference as shown in Fig. 5.3.

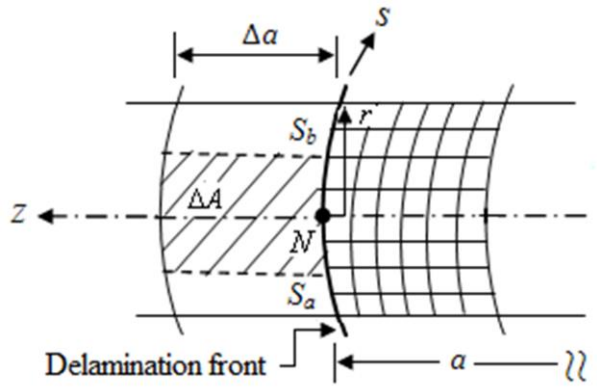

Figure 5.3 Calculation of SERR using 3D VCCI at node *N*.

The components of mode-I SERRs (G_I), mode-II SERR (G_{II}) and mode-III SERR (G_{III}) are as follows (Fig. 5.3):

$$G_I = \lim_{\Delta A \to 0} \frac{1}{2\Delta A} \int_{s_a}^{s_b} \int_{0}^{\Delta a} \sigma_{rr}(z,s) u_r(\Delta,s) \mathrm{d}z\mathrm{d}s \tag{5.6}$$

$$G_{II} = \lim_{\Delta A \to 0} \frac{1}{2\Delta A} \int_{s_a}^{s_b} \int_{0}^{\Delta a} \tau_{rz}(z,s) u_z(\Delta,s) \mathrm{d}z\mathrm{d}s \tag{5.7}$$

$$G_{III} = \lim_{\Delta A \to 0} \frac{1}{2\Delta A} \int_{s_a}^{s_b} \int_{0}^{\Delta a} \tau_{rs}(z,s) u_s(\Delta,s) \mathrm{d}z\mathrm{d}s \tag{5.8}$$

where, $\sigma_{rr}(z,s)$ is the interfacial normal stress (IFNS), $\tau_{rz}(z,s)$ and $\tau_{rs}(z,s)$ are the interfacial shear stress (IFSS) components ahead of the crack tip responsible for mode-I, mode-II and mode-III growth, respectively. $u_r(\Delta,s)$, $u_z(\Delta,s)$ and $u_s(\Delta,s)$ are the relative opening, sliding and tearing displacements between the corresponding top and bottom nodes on the crack surfaces behind the crack front, respectively. The parameters *r*, *z* and *s* are the local coordinates along radial, axial and tangential directions with respect to the crack front, respectively. ΔA is the virtual extension area of the crack.

The total SERR (G_T) is given by

$$G_T = G_I + G_{II} + G_{III} \tag{5.9}$$

5.2.4 Comparison between single-CNT RVE surrounded by epoxy and CNT/epoxy composite

The distributions of axial normal stress in the broken CNT and interfacial stresses at the interface of the broken CNT and the matrix have been studied for a constant volume fraction of 3.06%. SERR has been determined for the single-CNT RVE composite for a constant volume fraction of 3.06%. Two types of model have been considered for the RVE viz (i) the CNT is surrounded by pure epoxy (1-CNT/epoxy model) and (ii) the CNT is surrounded by CNT/epoxy composite (1-CNT/composite model) and accordingly the properties of the element are input in the FE model.

5.2.4.1 Axial normal stresses in the broken CNT

Figure 5.4 shows the variation of the axial normal stress (ANS) in the broken fiber (CNT) along the fiber length of 1-CNT/epoxy model and 1-CNT/composite model for a constant volume fraction of 3.06%. Figure 5.4 shows that the axial normal stress in the broken fiber is different in two cases which are due to the difference in effective stiffness in these two models. However more importantly, the ineffective lengths estimated by the two models are also different.

It could be observed from Fig. 5.4 that the ineffective length of the 1-CNT/epoxy model and 1-CNT/composite model are 24 nm and 55 nm, respectively. Therefore, the ineffective lengths of the broken CNT are 12% and 27.5% for 1-CNT/epoxy model and 1-CNT/composite model, respectively. Ineffective length estimated using 1-CNT/epoxy model is almost half of that estimated using 1-CNT/composite model. This is again due to the stiffness difference between the CNT and the surrounding materials.

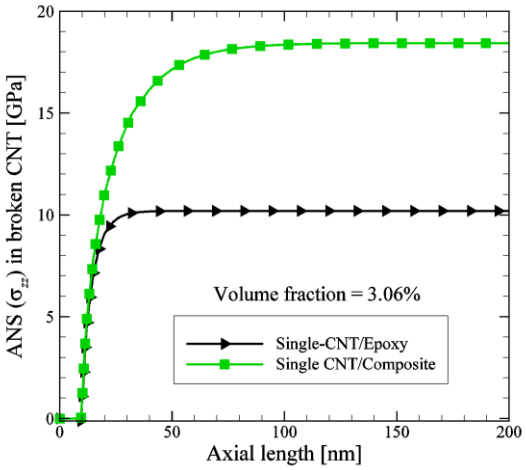

Figure 5.4 Axial normal stress in the broken CNT for 1-CNT/epoxy and 1-CNT/composite models.

5.2.4.2 Interfacial shear stresses at the interface of broken CNT and matrix

Figure 5.5 shows the variation of the interfacial shear stress (τ_{rz}) at the interface of the broken CNT and the matrix for 1-CNT/epoxy RVE and 1-CNT/composite RVE for a constant volume fraction of 3.06%.

It could be observed from Fig. 5.5 that the magnitudes of τ_{rz} of 1-CNT/epoxy model and 1-CNT/composite model are 0.48 GPa and 0.454 GPa, respectively. Therefore it could be concluded that there is no significant difference between the magnitudes of τ_{rz} between the two models for a constant volume fraction of 3.06%.

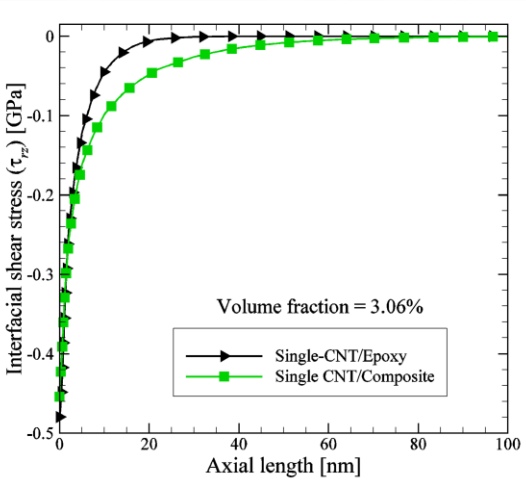

Figure 5.5 Interfacial shear stress in front of debonding for 1-CNT/epoxy and 1-CNT/composite models.

5.2.4.3 Strain energy release rate

Following the FE modeling and formulation describe in previous section 5.2.3, strain energy release rate components have been calculated using VCCI for both the 1-CNT RVE composites at a constant volume fraction of 3.06%. Mode-II normalized strain energy release rates (G_{II}/ε^2) of 1-CNT/epoxy and 1-CNT/composite model have been estimated for a constant volume fraction of 3.06% and listed in Table 5.2. It could be observed that the estimated value of normalized SERR of 1-CNT/epoxy model is 2.5 times higher than that of 1-CNT/composite model. The reason for the same is that the displacement of 1-CNT/epoxy model composite is more than that of the 1-CNT/composite model for same RVE as well as for same applied strain which once again shows that the first model is too conservative.

Table 5.2 Mode-II SERR of 1-CNT/epoxy and 1-CNT/composite for V_{nt} = 3.06%.

1-CNT/epoxy (G_{II}/ε^2) [J/m^2]	1-CNT/composite (G_{II}/ε^2) [J/m^2]
463.21	140.27

5.3 Analysis using nine-CNT RVE model

Even though the single-CNT RVE model is simple and provides the understanding of the stress distribution and SERR, in this section the same analysis is carried out considering a 9-CNT RVE with an objective of understanding the limitation of 1-CNT RVE (if any) in predicting SERR. Single-CNT RVE considered in the previous section 5.2 is a simple model showing the effect of fiber break. However it does not provide a true representation in the sense that it is not possible to study the effect of fiber break on the adjacent fibers. Therefore, a more realistic model with nine-uniformly spaced CNTs (9-CNTs RVE) in the matrix is considered, which represent a CNT-composite where one out of 9-CNTs are broken.

5.3.1 Finite element modeling

The nonlinear stress-strain relation of CNT has been considered for modeling the square 9-CNTs RVE and Eq. (3.12) has been used for modeling stress-strain relation of a zigzag CNT in the present multi-scale modeling of CNT-reinforced composites as described in Chapter 3 (section 3.5.2).

The front view and pictorial view of the 3D FE model with a square RVE are shown in Figs. 5.6(a) and 5.6(b), respectively, where the *x*-*y* plane is the transverse plane and the *z*-axis is the axial direction for a constant volume fraction of CNT (V_{nt}) equal to 30.6%. In the 9-CNTs RVE, the central CNT is considered to be broken. A small length of debonding at the interface of the broken CNT and the matrix has been considered as a crack front. Eight noded solid element with 3-degree of freedom (DOF) at each node (SOLID45 in ANSYS) has been used for FE modeling of the 9-CNTs RVE. The length of the RVE is considered as 200 nm and the length of the debonding near the fiber break has been taken as 10 nm

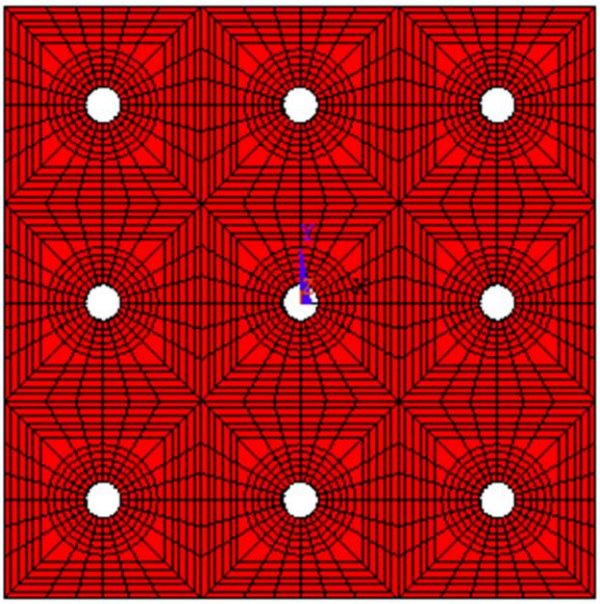

Figure 5.6(a) Front view of FE mesh for 9-CNT RVE model.

VCCI has been used for determination of the components of SERRs for mode-I (G_I), mode-II (G_{II}) and mode-III (G_{III}) as described in previous section 5.2.3 (Fig. 5.3).

5.3.2 Boundary conditions

Referring to Fig. 5.6(b), all the nodes at $z = 0$ are fully restrained except the nodes belonging to the broken CNT of the 9-CNTs RVE. Uniform axial displacements are applied on the nodes at $z = L_a$ (here, L_a is the axial length of the model). Applied axial strain of 1.5% is considered for calculation of axial normal stress, interfacial shear stress and SERR of CNT/epoxy composites.

5.3.3 Results and discussion for CNT/epoxy composite

The distribution of axial normal stress in the broken CNT, interfacial normal stress and interfacial shear stress at the interface of the broken CNT and the matrix, and axial normal stress in the adjacent intact CNTs have been determined for different volume fractions of CNT using the 3D FE analysis. The three components of SERR ahead of the debonding at the interface have also been determined using VCCI method. In the present analysis, the range of the volume fractions of CNT is considered between 0.56% - 10.31%. The diameter of CNT has been taken as 1.88 nm (which is equal to the diameter of zigzag (24, 0) CNT) and the thickness (t) of CNT is considered as 0.34 nm (which is equal to the atomic diameter of carbon). Thermoplastic epoxy [147] has been considered in the present analysis for which Young's modulus and Poisson's ratio of the epoxy are 3.09 GPa and 0.372, respectively.

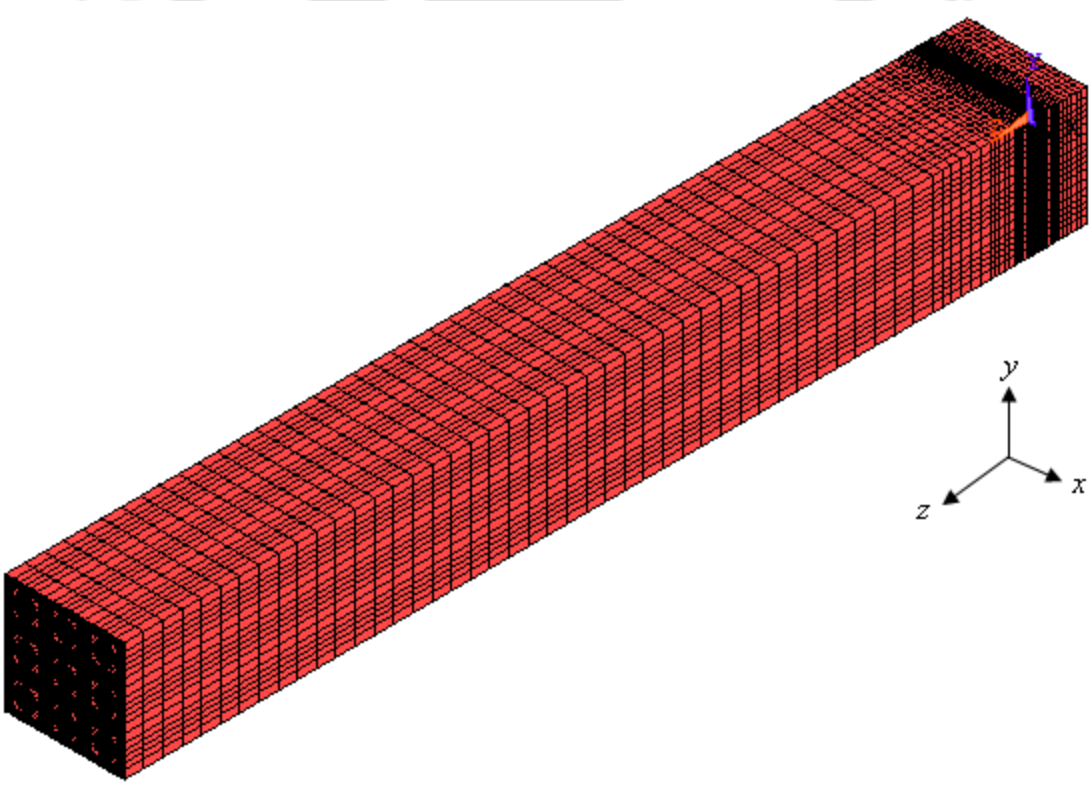

Figure 5.6(b) Pictorial view of 3D FE mesh for 9-CNT RVE model.

5.3.3.1 For a constant volume fraction of 3.06%

5.3.3.1.1 Axial normal stress in the broken CNT

Figure 5.7 shows the distribution of the axial normal stress (ANS) along the length of the broken fiber (CNT) in CNT/epoxy composites. The ANS is zero at the point of break but it could be observed that the broken CNT regained the nominal stress value at a CNT length of 85 nm for CNT/epoxy composites. Therefore, it could be concluded that the ineffective lengths (where 95% of the strength is regained) of the broken CNT is 42.5% in CNT/epoxy composites.

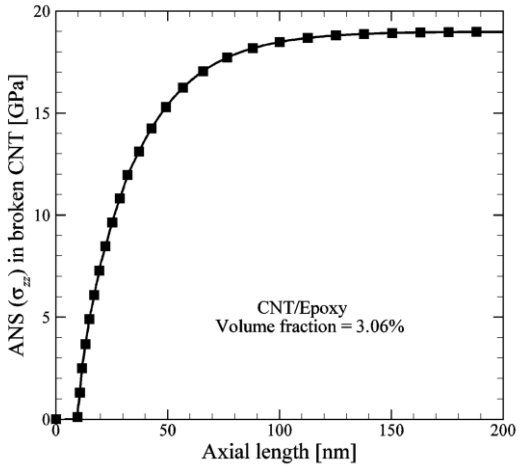

Figure 5.7 Axial normal stress in the broken CNT in CNT/epoxy composite.

5.3.3.1.2 Interfacial stresses at the interface of broken CNT and matrix

Since, IFNS (σ_{rr}) and IFSS (τ_{rz} and τ_{rs}) are responsible for debonding of the CNT from the matrix, therefore determination of these stresses in the vicinity of the broken CNT is important. Figure 5.8 shows the distribution of σ_{rr}, τ_{rz} and τ_{rs} at the interface of the fiber and the matrix along the length of fiber in CNT/epoxy composite. Even though the length of the CNT is 200 nm, stresses are shown only up to 100 nm for better clarity and beyond this length there is no change in interfacial stresses.

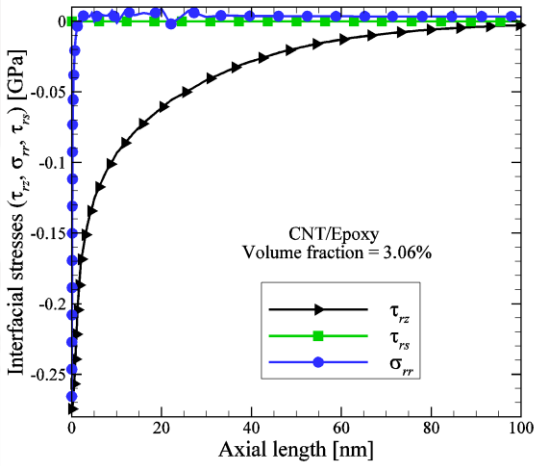

Figure 5.8 Interfacial stresses in front of debonding in CNT/epoxy composite.

It can be seen in Fig. 5.8 that the magnitude of τ_{rz} is maximum near the vicinity of broken fiber and the magnitude of τ_{rs} is zero along the length of fiber. It has also

been observed that the value of σ_{rr} is negative near the debonding even though it shows a negligible positive value slightly away from the crack tip but the magnitude of negative stress is higher than the positive stress. From the above results a high magnitude of τ_{rz} is observed to have developed at the interface and in the vicinity of fiber break. It could be concluded that τ_{rz} is responsible for debonding, σ_{rr} has negligible effect on debonding and τ_{rs} has no effect on debonding of CNT from the matrix in the case of axial loading. It could be observed that while the axial normal stresse distribution of 9-CNT and 1-CNT/epoxy RVE model (ref. Figs. 5.7 and 5.4) agree well, there is different in the magnitude of interfacial stress. While 1-CNT/epoxy RVE predicts τ_{rz} = 0.48 GPa and 9-CNT RVE estimates τ_{rz} = 0.274 GPa.

5.3.3.1.3 Axial normal stress in the adjacent intact CNTs

Figure 5.9 shows the distribution of ANS in the adjacent intact CNTs along the length of fiber in CNT/epoxy composite. It could be observed that due to the presence of a broken CNT, the adjacent intact CNTs experience a stress concentration in the vicinity of the break. Even though the length of the CNT is 200 nm, stresses are shown only up to 100 nm for better clarity and beyond this length there is no change in axial normal stress.

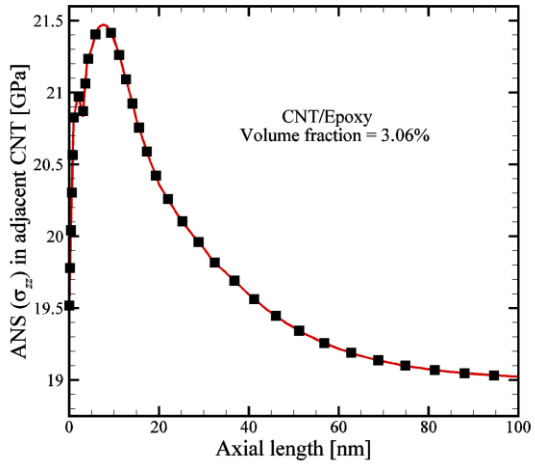

Figure 5.9 Axial normal stress in the adjacent intact CNT in CNT/epoxy composite.

It can be seen in Fig. 5.9 that the stress concentration factors (maximum stress/nominal stress) of CNT/epoxy composite is 1.13 for a constant volume fraction of 3.06%. So, it could be concluded that there is a possibility that the adjacent intact CNT may break as a consequence of over loading. When one fiber breaks, it may lead to the breaking of the adjacent fibers, leading to successive failure of fibers and finally the failure of the nanocomposites.

5.3.3.2 Effect of volume fraction

5.3.3.2.1 Axial normal stress in the broken CNT

Figure 5.10 shows the distribution of the ANS in the broken fiber along the length of the broken fiber with volume fraction in CNT/epoxy composite. It can be seen in Fig. 5.10 that the ineffective lengths of the broken CNT in CNT/epoxy composites are 46% and 34% corresponding to volume fraction of 0.56% and 10.31%, respectively. Therefore, it could be concluded that the ineffective lengths decrease with increase in volume fractions. But the ineffective lengths are 44% and 46% corresponding to volume fraction of 3.06% and 0.56%, respectively. Therefore it could also be concluded that there is not much difference in ineffective length for the volume fractions of 30.6% to 0.56% in CNT/epoxy composites.

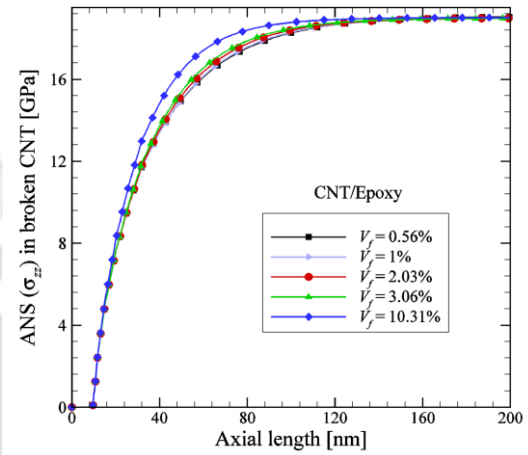

Figure 5.10 Axial normal stress in the broken CNT with volume fraction in CNT/epoxy composites.

5.3.3.2.2 Interfacial shear stress at the interface of the broken CNT and the matrix

Figure 5.11 shows the distribution of τ_{rz} at the interface between the broken fiber and the matrix along the fiber length with volume fraction in CNT/epoxy composite. The magnitudes of τ_{rz} are 0.279 GPa and 0.275 GPa corresponding to the volume fraction of 0.56% and 10.31%, respectively. It could be concluded that the magnitude of τ_{rz} decreases with the increase in volume fraction in the CNT/epoxy composite though the change is not significant. Even though

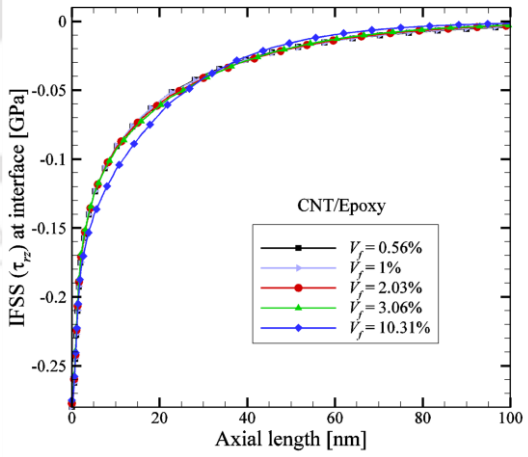

Figure 5.11 Interfacial shear stress in front of debonding with volume fraction in CNT/epoxy composite.

the length of the CNT is 200 nm, stresses are shown only up to 100 nm for better clarity and beyond this length there is no change in interfacial shear stress (IFSS).

5.3.3.2.3 Axial normal stresses in the adjacent intact CNTs

Figure 5.12 shows the distribution of ANS in the adjacent intact fiber along the length with volume fraction in CNT/epoxy composite. It can be seen in Fig. 5.12 that the magnitudes of ANS in the adjacent intact fiber near the vicinity of the broken fiber increase with the increase in volume fraction of CNTs. It has been found that the stress concentration factors (SCFs) of CNT/epoxy composites are 1.05, 1.08, 1.11, 1.13 and 1.17 corresponding to the volume fractions of 0.56%, 1%, 2.03%, 3.06% and 10.31%, respectively. So, it could be concluded that the SCFs increase with the increase in volume fraction for the CNT/epoxy composites. Even though the length of the CNT is 200 nm, stresses are shown only up to 100 nm for better clarity and beyond this length there is no change in axial normal stress.

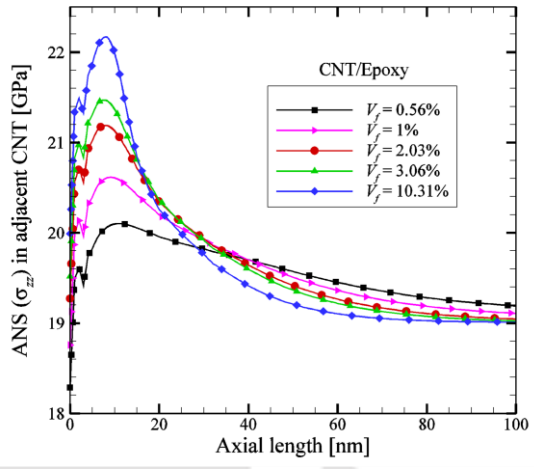

Figure 5.12 Axial normal stress in the adjacent intact CNT with volume fraction in CNT/epoxy composite.

The trends of the distribution of ANS in the broken CNT as well as adjacent intact CNTs in CNT/epoxy composite studied in the present work are in good agreement with the distribution of ANS in conventional carbon fiber/epoxy composites as reported by Nedele and Wisnom [143].

5.3.3.3 Variation of SERR with volume fraction

From the 3D FE analysis, components of SERR G_I, G_{II} and G_{III} are calculated using Eqs. (5.6), (5.7) and (5.8), respectively. Since, the IFNS (σ_{rr}) and IFSS (τ_{rs}) near the fiber break are insignificant, therefore G_I and G_{III} are also negligible (i.e. G_I ~ 0 and G_{III} ~0)

hence only G_{II} is significant for such an axial loading of CNT/epoxy composite having a fiber (i.e. CNT) break.

Figure 5.13 shows the variation of normalized SERR (G_{II}/ε^2) of CNT/epoxy composite with volume fraction. Here ε is the applied axial strain (1.5%). Figure 5.13 also shows that initially the value of (G_{II}/ε^2) increases with the increase in volume fraction, attains the maximum value at a particular volume fraction and then decreases with further increase in volume fraction. So, it could be concluded that the maximum SERR could be obtained for 1 vol% CNT in CNT/epoxy composites. It can also be seen from Fig. 5.13 that the maximum value of (G_{II}/ε^2) is equal to 146.09 J/m^2 for 1 vol% CNT in CNT/epoxy composite.

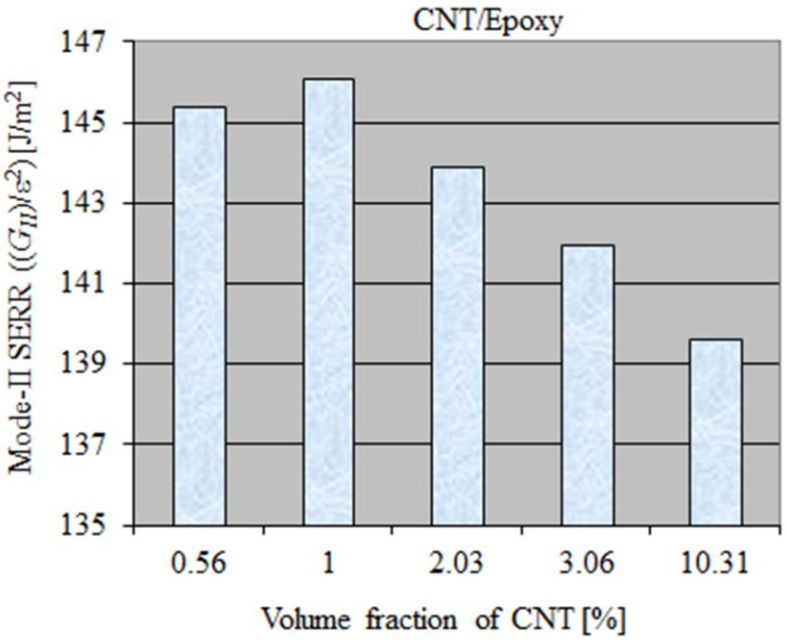

Figure 5.13 Variation of normalized SERR with volume fraction in CNT/epoxy composite.

The trend of the variation of normalized SERR (G_{II}/ε^2) with volume fraction of CNT/epoxy composite studied in the present work are in good agreement with the normalized critical SERR of CNT reinforced carbon fiber/vinylester composite as reported by Faulkner et al. [140].

Using the same procedure, normalized mode-II SERR (G_{II}/ε^2) is computed for carbon fiber (CF)/epoxy composite with properties taken from [148] and for the same applied strain

= 1.5% and volume fraction = 3.06%. G_{II} / ε^2 for CF/epoxy is obtained as 46.64 J/m^2 which is approximately three times less than that for CNT/epoxy composite.

5.3.4 Result and discussion for CNT/Al composites

A large number of works have been reported on CNT/polymer composites. Even though there are few works reported on the fabrication and characterization of CNT/Al composites but there is no work reported on the fracture behavior of CNT/Al composites with a broken CNT. Therefore, the present analysis is aimed at studying the stress redistribution and calculation of SERRs using VCCI method of CNT/Al composite in presence of a broken CNT. The same FE model and boundary condition is used as described in previous section 5.3.1.

The distribution of axial normal stress in the broken CNT and interfacial stresses at the interface of the broken CNT and the matrix, and axial normal stress in the adjacent intact CNTs have been studied for different volume fractions of CNTs for CNT/Al composites. The three components of SERR ahead of the debonding at the interface have been determined using VCCI method. In the present analysis, the range of the volume fractions of CNT is considered between 0.56% - 10.31% and the total applied axial strain has been considered equal to 1.5%. The Poisson's ratio of CNT has been considered as 0.28. The Young's modulus and Poisson's ratio of aluminum have been considered as 69 GPa and 0.334, respectively.

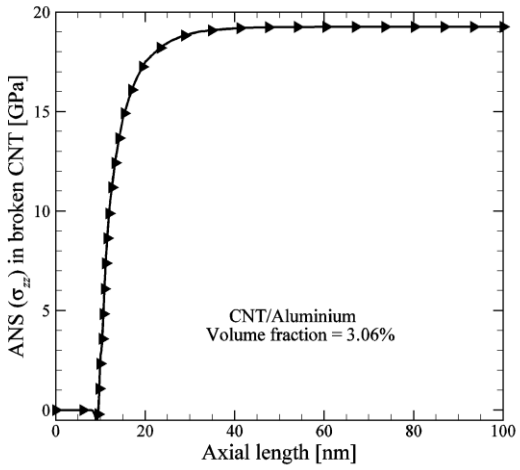

Figure 5.14 Axial normal stress in the broken CNT in CNT/Al composite.

5.3.4.1 For a constant volume fraction

5.3.4.1.1 Axial normal stress in the broken CNT

Figure 5.14 shows the distribution of the axial normal stress (ANS) in the broken CNT along the length of the CNT in CNT/Al composites for a constant volume fraction of 3.06%.

It can be seen in Fig. 5.14 that the broken CNT regained the nominal stress value at a fiber length of 25 nm, therefore, it could be concluded that the ineffective lengths of the broken CNT is 12.5% in CNT/Al composites. Even though the length of the CNT is 200 nm, stresses are shown only up to 100 nm for better clarity and beyond this length there is no change in axial normal stress.

5.3.4.1.2 Interfacial stresses at the interface of the broken CNT and the matrix

Figure 5.15 shows the distribution of interfacial stresses (σ_{rr} , τ_{rz} and τ_{rs}) at the interface of broken CNT and the matrix along the length of CNT in CNT/Al composite for a constant volume fraction of 3.06%. It can be seen in Fig. 5.15 that the magnitude of interfacial normal stress (σ_{rr}) is negative at the point of debonding but there is also small positive values away from the debonding. But the magnitude of negative values of σ_{rr} is more than the magnitude of positive values. The magnitude of interfacial shear stress (τ_{rz}) is maximum near the debonding but the magnitude of τ_{rs} is zero along the fiber length. Therefore, it could be concluded that the interfacial shear stress (τ_{rz}) is responsible for debonding, interfacial normal stress (σ_{rr}) have negligible effect on debonding and the interfacial shear stress (τ_{rs}) has no effect on debonding of CNT from the matrix materials in the case of axial loading for CNT/Al composite. Even though

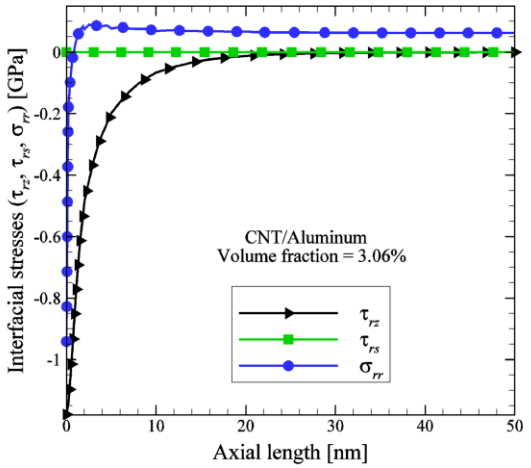

Figure 5.15 Interfacial stresses in front of debonding in CNT/Al composite.

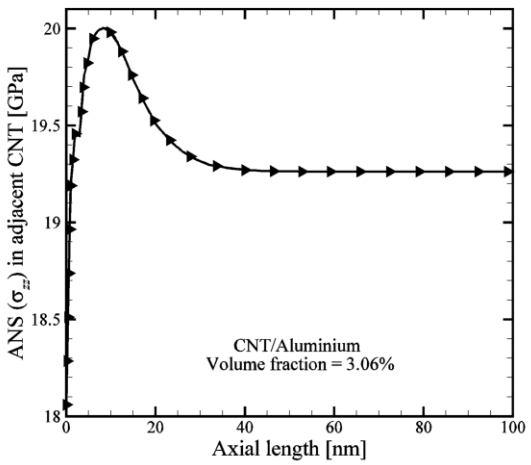

Figure 5.16 Axial normal stress in the adjacent intact CNT in CNT/Al composite.

the length of the CNT is 200 nm, stresses are shown only up to 50 nm for better clarity and beyond this length there is no change in interfacial stresses.

5.3.4.1.3 Axial normal stress in the adjacent intact CNTs

Figure 5.16 shows the distribution of ANS in the adjacent intact CNTs along the length of CNT in CNT/Al composite. It can be seen in Fig. 5.16 that the stress concentration factor of CNT/Al composite is 1.04 for a constant volume fraction of 3.06%. So, it could be concluded that there is a possibility that the adjacent intact CNT may break as a consequence of over loading, leading to successive failure of CNTs and finally the failure of CNT/Al composites. Even though the length of the CNT is 200 nm, stresses are shown only up to 100 nm for better clarity and beyond this length there is no change in axial normal stress.

5.3.4.2 Effect of volume fraction

5.3.4.2.1 Axial normal stress in the broken CNT

Figure 5.17 shows the distribution of the ANS in the broken fiber along the length of the broken CNT with volume fraction in CNT/Al composite. It can be seen in Fig. 5.17 that for all the range of volume fraction from 0.56% - 10.31% the ineffective length of the broken CNT remains almost same in CNT/Al composites. It could be concluded that the ineffective length of the broken CNT does not show significant changes with the change in volume fraction in CNT/Al composite in the case of axial loading. Even though the length of the CNT is 200 nm, stresses are shown only up to 50 nm for better clarity and beyond this length there is no change in interfacial stresses.

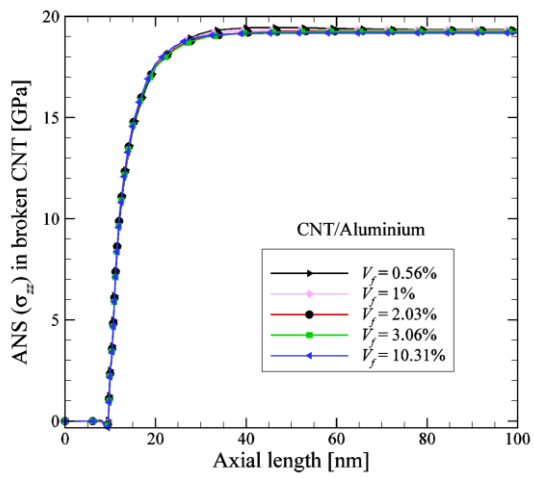

Figure 5.17 Axial normal stress in the broken CNT with volume fraction in CNT/Al composite.

5.3.4.2.2 Interfacial shear stress at the interface of broken CNT and matrix

Figure 5.18 shows the distribution of interfacial shear stress (τ_{rz}) at the interface between the broken CNT and the matrix along the CNT length with volume fraction in CNT/Al composite. It can be seen in Fig. 5.18 that the magnitudes and distribution of τ_{rz} of CNT/Al composite are almost same for the range of volume fraction from 0.56% - 10.31% in the case of axial loading.

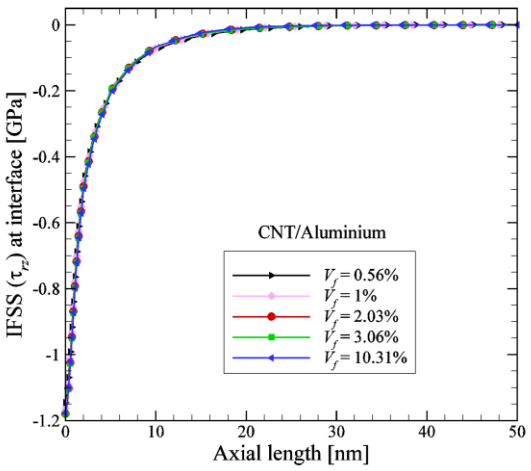

Figure 5.18 Interfacial shear stress in front of debonding with volume fraction in CNT/Al composite.

5.3.4.2.3 Axial normal stresses in the adjacent intact CNTs

Figure 5.19 shows the distribution of axial normal stress (ANS) in the adjacent intact CNT along the length of CNT with volume fraction in CNT/Al composite. It has been found that the stress concentration factors of CNT/Al composite are 1.01 and 1.11 corresponding to the volume fraction of 0.56% and 10.31%, respectively. It could be concluded that the SCF increases with the increase in volume fraction in the CNT/Al composite. Even though the length of the CNT is 200 nm, stresses are shown only up to 100 nm for better clarity and beyond this length there is no change in axial normal stress.

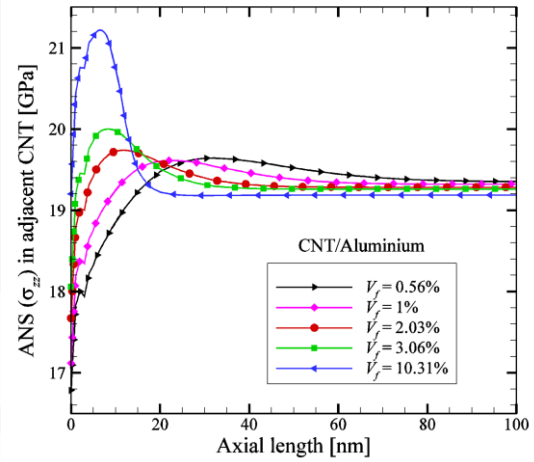

Figure 5.19 Axial normal stress in the adjacent intact CNT with volume fraction in CNT/Al composite.

The trends of the distribution of ANS in the broken CNT as well as adjacent intact CNTs in CNT/Al composite studied in the present work are in good agreement with the distribution of ANS in conventional carbon fiber/epoxy composites as reported by Nedele and Wisnom [143].

5.3.4.3 Variation of SERR with volume fraction

Virtual crack closure integral technique has been used for determination of the components of SERRs for mode-I, mode-II and mode-III (G_I G_{II}, and G_{III}). Since, the σ_{rr} and τ_{rs} near the fiber break are insignificant, therefore G_I and G_{III} are also negligible and hence only G_{II} is significant for such an axial loading of CNT/Al composite having a broken CNT.

Figure 5.20 shows the variation of normalized SERR (G_{II}/ε^2) of CNT/Al composite with volume fraction. Here ε is the total applied axial strain (1.5%). It has been observed that the values of SERR of CNT/Al composites increase with increase in volume fraction in the range of volume fraction considered. It has also been observed that the value of SERR increase rapidly upto 3.06 vol% and beyond that a constant SERR. The values of SERR for CNT/epoxy initially increased and then decreased with the increase in volume fraction as reported in previous section 5.3.3.3. But the value of SERR for CNT/Al composite increase with the increase in volume fraction in the range of volume fraction considered.

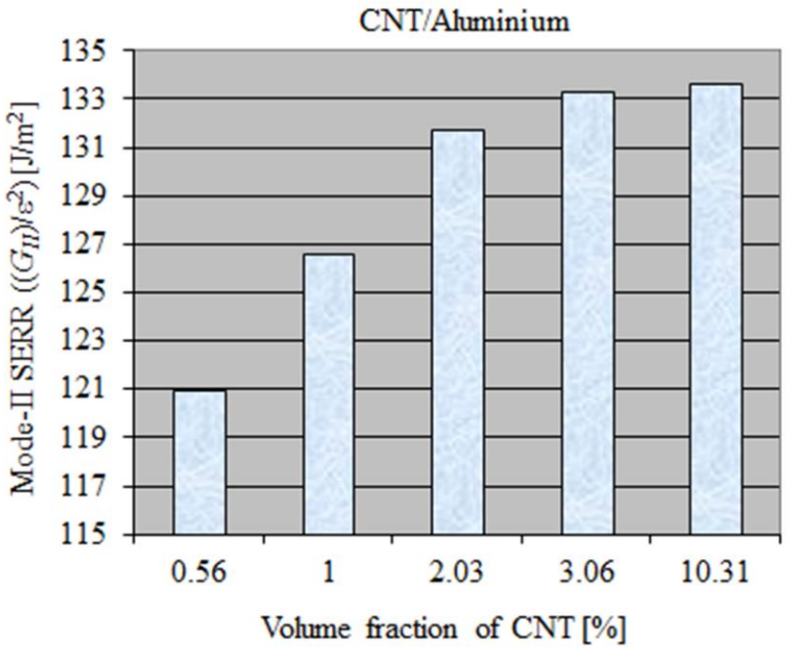

Figure 5.20 Variation of mode-II SERR with volume fraction in CNT/Al composites.

5.4 Comparison between Nine-CNTs RVE and single-CNT RVE surrounded by CNT/epoxy matrix

Epoxy used as matrix material for modeling of 9-CNTs/RVE but for the modeling of single-CNT RVE the epoxy is replaced by CNT/epoxy composites material. Such single-CNT/composites will be much simpler in terms of FE modeling and analysis.

5.4.1 Axial normal stress in the broken CNT

Figure 5.21 shows the variation of the axial normal stress (ANS) in the broken fiber along the fiber length of 1-CNT/composite and 9-CNTs/epoxy composite for a constant volume fraction of 3.06%. Ineffective lengths of 1-CNT/composites and 9-CNT/epoxy composite have already been investigated in earlier sections. It could be observed from Fig. 5.21 that the ineffective length of 1-CNT/composites and 9-CNT/epoxy are 55 nm and 85 nm, respectively. In both the cases a strain of 1.5% has been applied in axial direction.

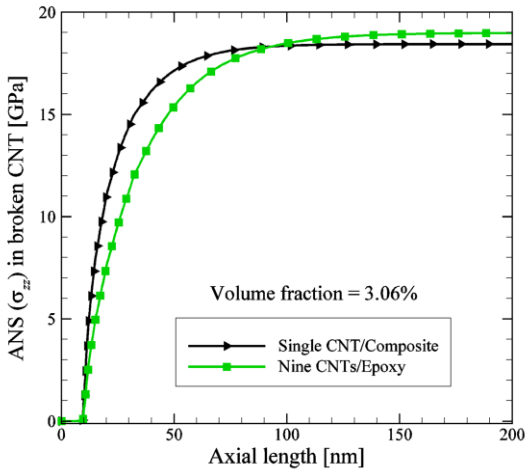

Figure 5.21 Axial normal stress in the broken CNT 1-CNT/composite and 9-CNT/epoxy.

While comparing 1-CNT RVE and 9-CNT RVE model, it could be seen from Fig. 5.21 that ineffective length estimate are different. But the difference in magnitude of nominal stresses for 1-CNT RVE and 9-CNT RVE model are negligible. When the difference in estimates of normal strength is understood due to the difference in stiffness of the two models, it is important to observe that there is substantial difference in the estimate of ineffective length. Ineffective length estimated using 9-CNT RVE model is almost 1.5 times higher than of that of estimated using 1-CNT RVE model showing that use of the ineffective length estimated by 1-CNT RVE model cannot be used for failure analysis of such composites and 9-CNT RVE model needs to be used for design.

5.4.2 Interfacial shear stress at the interface of broken CNT and matrix

Figure 5.22 shows the variation of the IFSS (τ_{rz}) at the interface of the broken fiber and matrix between 1-CNT/composite and 9-CNTs/epoxy composite for a constant volume fraction of 3.06%. It could be observed from Fig. 5.22 that the magnitude of τ_{rz} is higher in the case of 1-CNT/composite compared to that of 9-CNTs/epoxy composite. The magnitudes of τ_{rz} of 1-CNT/composite model and of 9-CNT/epoxy model are 0.454 GPa and 0.274 GPa, respectively. Therefore it could be concluded that the magnitude of τ_{rz} estimated from 1-CNT/composites RVE is almost 1.5 times that estimated from 9-CNTs/epoxy composite for same volume fraction of 3.06%. This is due to mismatch of relative stiffness between types of composites. In both the cases a strain of 1.5% has been applied in axial direction. Even though the length of the CNT is 200 nm, stresses are shown only up to 100 nm for better clarity and beyond this length there is no change in interfacial shear stress.

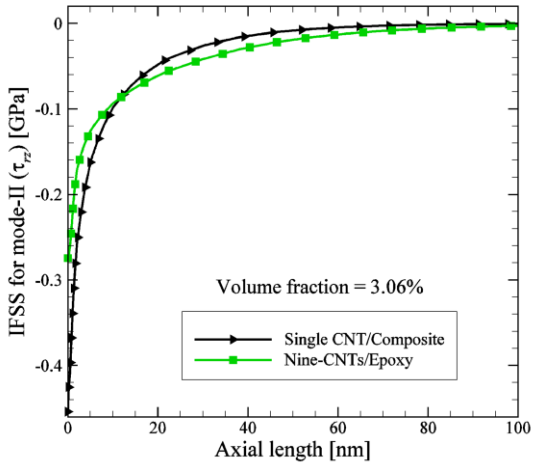

Figure 5.22 Interfacial shear stress in front of debonding in 1-CNT/composite and 9-CNT/epoxy.

5.4.3 Strain energy release rate

The normalized strain energy release rate (G_{II}/ε^2) of 1-CNT/composite and 9-CNT/epoxy composite are evaluated and listed in the following Table 5.3. It could be concluded that the values of normalized SERR (G_{II}/ε^2) obtained using 1-CNT/composite is higher than that obtained from 9-CNT/epoxy composite.

Table 5.3 Mode-II SERR of 1-CNT RVE and 9-CNT RVE for V_{nt} = 3.06%.

1-CNT/composite (G_{II}/ε^2) [J/m^2]	9-CNTs/epoxy (G_{II}/ε^2) [J/m^2]
140.27	141.98

5.5 Determination of critical strain energy release rate (SERR)

5.5.1 Failure criterion of composites

A high shear stress concentration develops at the fiber-matrix interface under in-plane shear in the composites. This high shear stress at the interface can cause shear failure in the matrix and/or fiber-matrix debonding. The in-plane shear strength of the composites based on matrix shear failure can be predicted as [148].

$$F_6 = \frac{F_{ms}}{\kappa_t} \tag{5.10}$$

where F_{ms} and κ_t are the matrix shear strength and shear stress concentration factor, respectively. An approximate expression for the shear stress concentration factor is [148].

$$\kappa_t = \frac{1 - V_f(1 - G_m / G_{12f})}{1 - (4V_f / \pi)^{1/2}(1 - G_m / G_{12f})} \tag{5.11}$$

where V_f , G_m and G_{12f} are the fiber volume fraction, matrix shear modulus and fiber axial shear modulus, respectively.

The quadratic stress criterion [139] states that delamination will initiate when

$$(\frac{\sigma_{rr}}{S_{rr}})^2 + (\frac{\tau_{rs}}{S_{rs}})^2 + (\frac{\tau_{rz}}{S_{rz}})^2 = 1 \tag{5.12}$$

where, σ_{rr} is the interfacial normal stress (IFNS), τ_{rz} and τ_{rs} are the interfacial shear stress (IFSS) components ahead of the debonding responsible for mode-I, mode-II and mode-III growth, respectively. Similarly S_{rr} is the interfacial normal strength for σ_{rr} stress; S_{rs} and S_{rz} are the interfacial shear strengths for τ_{rs} and τ_{rz} stresses, respectively.

In the present work, an attempt has also been made to determine critical SERR (G_c) using VCCI technique in conjunction with quadratic stress criterion. Finite element analysis of the 9-CNTs RVE (described in previous section) is done and debonding growth at the interface of the broken fiber and matrix has been predicted using Eq. (5.12). Interfacial stresses (σ_{rr}, τ_{rs} and τ_{rz}) have been calculated from the FE analysis. It was observed from

FE analysis of CNT/epoxy composites that the values of IFNS (σ_{rr}) and IFSS (τ_{rs}) were negligible and IFSS (τ_{rz}) significantly dominated the failure, which implies that only mode-II is present. Therefore, Eq. (5.12) now reduces to a single term with τ_{rz}. The applied strain is varied till the condition of Eq. (5.12) is satisfied. At that particular strain, using VCCI, G_{II} is calculated and that G_{II} is termed as critical SERR for mode-II (G_{IIc}) since at that value of SERR, debonding growth is predicted by quadratic stress criterion (QSC).

In order to analyze the effect of broken CNT on the CNT/epoxy composites, stresses have been determined using FE analysis. The axial normal stress redistribution along the broken CNT provides an assessment of the ineffective length of the broken CNT. IFSS and IFNS also show the chances of failure at the interface. Axial normal stress on the adjacent intact fibers shows the chances of tensile failure of the adjacent fibers. Concept of fracture mechanics is also used to determine SERR near the broken fiber where a small debonding at the interface is considered as a pre-existing crack. By performing a full 3D FE analysis and using VCCI, the components of SERR corresponding to mode-I, mode-II and mode-III have been determined to study the propensity of the interfacial debonding to grow further. Debonding initiation has been predicted using QSC and critical SERR has also been calculated using VCCI in conjunction with QSC.

5.5.2 Critical SERR of CNT/epoxy composites

Quadratic stress criterion (Eq. (5.12)) has been used to assess the initiation of debonding at the interface of the broken CNT and the matrix. Properties of carbon fiber and epoxy are considered as follows [148]. Young's modulus, Poisson's ratio and shear strength of epoxy are considered 3.09 GPa, 0.372 and 40 MPa, respectively. Therefore shear modulus of epoxy is equal to 1.13 GPa. Axial shear modulus of carbon fiber (G_{12f}) is considered as 27 GPa. Shear stress concentration factor (κ_t) of carbon fiber/epoxy is evaluated as 1.12 using Eq. (5.11) for a constant volume fraction of 3.06%, the in-plane shear strength of CF/epoxy composite is calculated as 33.41 MPa using Eq. (5.10). The interfacial shear strength of CNT/epoxy has been considered to be 10 times that of CF/epoxy composites [149] and the same has been calculated as 334 MPa. Mode II critical SERR (G_{IIc}) at the point of debonding

is calculated using VCCI in conjunction with QSC. Figure 5.23 shows the variation of normalized critical SERR (G_{IIc}/ε^2) of CNT/epoxy composite with volume fraction. Here ε is the applied axial strain.

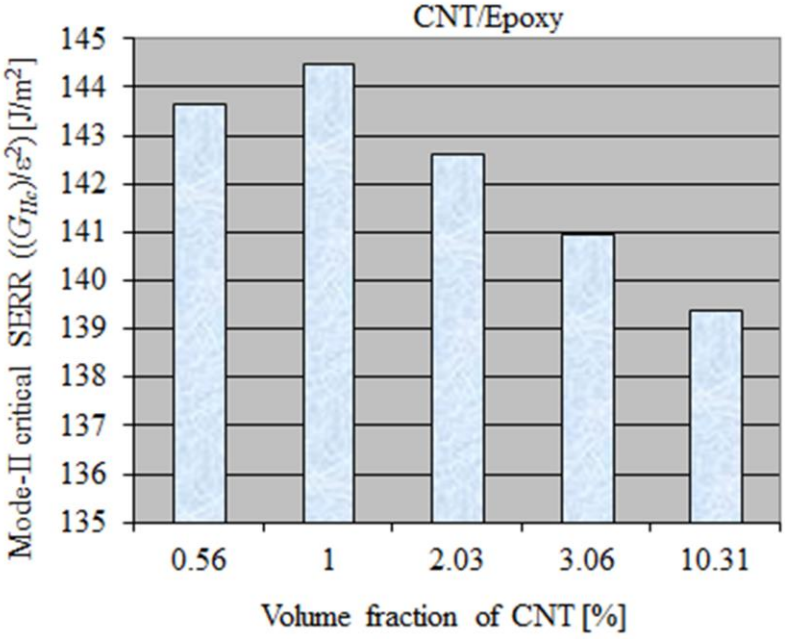

Figure 5.23 Variation of mode-II critical SERR with volume fraction in CNT/epoxy composite.

The trend of normalized critical SERR (G_{IIc}/ε^2) variation with volume fraction of CNT/epoxy composite is same as that for normalized SERR (G_{II}/ε^2) presented in previous section 5.3.3.3 (Fig. 5.13). Figure 5.23 also shows that initially the value of G_{IIc}/ε^2 increases with the increase in volume fraction, attains the maximum value at a particular volume fraction and then decreases with further increase in volume fraction. It can be seen in Fig. 5.23 that the value of G_{IIc}/ε^2 show an initial increment and then decrease with further increase in volume fraction. However, the actual value of mode-II critical SERR (G_{IIc}) shows a continuous decrease with increase in volume fraction in the range of 0.56% to 10.31%. Variation of critical SERR (G_{IIc}) of CNT/epoxy composite with volume fraction are listed in Table 5.4.

Table 5.4 Critical mode-II SERR for different volume fractions of CNT/epoxy composite.

Volume fraction of CNT (%)	0.56	1.0	2.03	3.06	10.31
Critical SERR (J/m^2)	0.066	0.061	0.057	0.051	0.040

The trend of the variation of (G_{IIc}/ε^2) with volume fraction of CNT/epoxy composite studied in the present work are in good agreement with the normalized critical SERR of CNT reinforced carbon fiber/vinylester composite as reported by Faulkner et al. [140].

5.6 Summary

Considering a small debonding near the broken CNT, concept of linear elastic fracture mechanics (LEFM) has been used to determine the SERR to study the propensity of such debonding to grow further. Both single-CNT RVE and 9-CNT RVE model were carried out and it was observed that results from 9-CNT RVE model are more realistic and hence 9-CNT model need to be used for design and analysis. Using LEFM and quadratic stress criterion (QSC), critical SERR has been evaluated numerically for such broken CNT composites. For complete understanding on the analysis of CNT-reinforced composites, the use of 9-CNTs RVE model is important as 1-CNT RVE model neglects the presence of intact fibers surrounding the broken fiber. Distribution of stress near the fiber break, SERR of CNT-reinforced composites have been studied in the present work and same has also been compared with some earlier published literature [140, 143] and a good agreement have been found. Some of the important observations are

- The ineffective length of a broken CNT decreases with the increase in stiffness of the matrix materials. In the present work, the ineffective lengths of the broken CNT are 42.5% and 12.5% of its original length in CNT/epoxy and CNT/Al composites, respectively for a volume fraction of 3.06%.
- Ineffective lengths of the broken CNT in CNT/epoxy composites with a small debonding increase with increase in volume fractions. The increase in ineffective length with volume fraction is significant in the range of volume fraction from 3.06% to 10.31%. However there is not much difference in ineffective length for the volume fractions of 0.56 to 3.06%.
- For a given load the magnitude of the IFSS depends upon the type of the matrix materials and fiber volume fraction. In the present work, corresponding to an applied strain of 1.5%, the magnitudes of IFSS (τ_{rz}) for CNT/epoxy and CNT/Al

composites are 0.274 GPa and 1.178 GPa, respectively for a volume fraction of 3.06%.

- The magnitude of IFSS (τ_{rz}) at the interface increases with the increase in volume fraction for all the CNT-reinforced composites, however the increase is not very significant in the range of volume fraction studied in the present case.
- For a given load the magnitude of axial normal stress in the adjacent fiber depends upon the type of the matrix materials and fiber volume fraction. The SCFs of CNT/epoxy and CNT/Al composites are 1.13 and 1.04, respectively for a volume fraction of 3.06%.
- The SCFs in the adjacent CNT increases with the increase in volume fraction. Corresponding to a volume fraction of 0.5% and 10.31% the magnitudes of SCFs are 1.05 and 1.17 respectively, for CNT/epoxy composites. In the same line corresponding to a volume fraction of 0.5% and 10.31% the magnitudes of SCFs are 1.01 and 1.11 respectively, for CNT/Al composites.
- For a CNT composite subjected to axial loading, presence of broken CNT leads to stress concentrations in the axial stress induced in the adjacent fiber thereby increasing the chances of failure of these fiber due to over loading and hence cumulative fiber failure.
- Calculation of SERR components show that the mode of debonding between the CNT and matrix depends upon the type of loading.
- In the case of axial loading on CNT composite with a fiber break only mode II is the dominant mode and the other two modes are absent. Thus, mode-II SERR G_{II} is only responsible for debonding in the case of axially loaded CNT/epoxy composites.
- The SERRs of CNT/epoxy composites vary with volume fraction. Initially the value of SERR increases with the increase in volume fraction attains the maximum value at a particular volume fraction and then decreases with further increase in volume fraction. In the present case maximum SERR is observed to be at 1 vol% CNT of CNT/epoxy composite. But in case CNT/Al composite the

value of SERR increases with the increase in volume fraction and after a particular volume fraction a constant SERR is observed.

- Critical SERR of CNT composites having a small fiber matrix debonding could be calculated using VCCI and QSC.
- The critical SERRs of CNT composites depend on volume fraction.
- For the case of CNT/epoxy composite critical mode-II SERR initially increase with the increase in volume fraction and then decrease with further increase in volume fraction. However, the actual value of critical mode-II SERR (G_{IIc}) shows a continuous decrease with increase in volume fraction in the range of 0.56% to 10.31%.

भारतीय प्रौद्योगिकी संस्थान गुवाहाटी
Indian Institute of Technology Guwahati

Chapter 6

Conclusions and Scope for the Future Work

Finite element (FE) modeling and analysis have been done first for characterization of CNT reinforced composites and then for understanding the behavior of CNT-reinforced composites having fiber break in the form of a broken CNT. Representative volume element (RVE) has been considered for the analysis where the CNT and surrounding matrix are modeled individually and FE analysis have been used to study the influence of important factors on such CNT composites from design point of view. In analyzing the effect of fiber break, single-CNT RVE and nine-CNT RVE has been compared to understand the limitations and computationally simpler single-CNT model and the advantages of nine-CNT RVE model. Conclusions drawn from the results obtained from the present thesis are presented in this chapter in two sections viz. the general conclusions and the specific conclusions. In general conclusions, some of the findings which are sometimes expected or not so significant are presented. In specific conclusions, important finding which contributes to the better understanding of CNT composites and provides new knowledge in the area are presented. Finally, possible extension of the present work is described in the subsection scope of the future work.

6.1. General conclusions

- Finite element modeling could be used for determination of thermo-mechanical characteristics of CNT composites to avoid the difficulties involved in experimental determination.
- Thermoelastic properties determined using multi-scale FE method shows resemblance with the thermoelastic properties estimated using rule of mixture (ROM) and thermoelastic extremum principle (TEEP).
- Not considering non-linear stress-strain relation of the CNT may lead to inaccurate results especially at higher strains.

- Existence of a broken CNT in the CNT composites leads to significant stress redistribution ahead of such break thus enhancing the chances of failure.
- Existence of a broken CNT leads to stress concentration on the adjacent intact CNTs and thereby initiating the chances of cumulative breakage of CNTs leading to final failure.
- Volume fraction of CNT does have significant effect on the stress concentration factor (SCF) of CNT composites.
- In a CNT-reinforced composite, when a CNT breaks, it does not completely become ineffective. Due to the presence of matrix, the broken CNT becomes ineffective only over a very small length ahead of the break and the remaining length of the CNT can still take part in load bearing.
- Ineffective length depends upon the type of matrix and the volume fraction of the CNT fiber.
- Small debonding ahead of the fiber break may be considered as a crack front and the concept of fracture mechanics could be applied to understand the severity of fiber break in the CNT composites and strain energy release rate (SERR) could be used as parameters to understand the severity of a fiber break.
- Types of matrix material and CNT volume fraction have significant effect on the SERR of CNT composites.
- Finite element analysis in conjunction with stress based failure initiation criterion could be used to determine the critical SERR of CNT composites with a fiber break.
- Mode-II SERR components are observed to be also dependent on the matrix materials and volume fraction of CNT. When compared to conventional carbon fiber/epoxy composite, more-II SERR of CNT/epoxy composite is approximately three times more compared to that in conventional carbon fiber/epoxy composites for CNT volume fraction of 3.06%.

6.2 Specific conclusions

6.2.1 Thermo-mechanical properties of CNT composites

- Even a small volume fraction of CNT sufficiently increases the Young's modulus of CNT composites compared to the matrix. This however depends upon type of matrix materials. For a CNT volume fraction of 3.06%, the axial Young's modulus of CNT/epoxy composites could be increased about nine times compared to the Young's modulus of pure epoxy.
- The transverse Young's modulus of CNT composite show deviation when compared to the theoretical results obtained from ROM.
- The axial Young's modulus of CNT composite increase with the increase in volume fraction.
- The computed longitudinal Young's modulus of CNT composite using non-linear stress-strain relation of CNT show deviation at higher volume fraction when compared to the theoretical results obtained from ROM.
- For CNT/epoxy composite the difference of estimated longitudinal Young's modulus by considering linear and non-linear model is almost 15% for a CNT volume fraction of 3.06% and the linear model overestimates the longitudinal stiffness.
- Estimate of longitudinal Young's modulus using non-linear stress-strain relation of CNT is less than that obtained using linear stress-strain relation of CNT and the differences are more at higher volume fraction of CNT. It is observed that the linear model estimates a higher value of longitudinal Young's modulus and hence using non-linear model will provide a conservative design approach.
- The computed longitudinal coefficients of thermal expansions (CTEs) of CNT/epoxy composite have a difference of almost 42% between the linear and non-linear model of CNT at CNT volume fraction of 3.06% and the non-linear model estimates a higher value of longitudinal CTE.
- Increase in volume fraction of CNT in CNT-reinforced composites lead to decrease in CTE. Therefore, it is possible to decide volume fraction of CNT to achieve the desired CTE. For example the axial CTE of the CNT/epoxy could be reduced to zero

corresponding to a volume fraction of ~10%. It is observed that the linear model underestimates volume fraction of CNT at which axial CTE become zero.

- The transverse CTE of CNT composite shows deviation when compared to the theoretical results obtained from TEEP at higher volume fraction.
- It is important to note that using the non-linear model, the volume fraction of CNT at which the longitudinal CTE is zero is estimated to be higher compared to that estimated by TEEP or linear model and hence in designing components from the view point of thermal stability, it is important to use the non-linear model.

6.2.2 CNT-reinforced composites with a broken CNT

- The ineffective length of a broken CNT decreases with the increase in stiffness of the matrix materials. In the case of CNT-reinforced composites, if a fiber (i.e. CNT) breaks, the ineffective length of the broken fiber has a significance dependence on the stiffness of the matrix materials. Stiffer is the matrix materials, lower is the ineffective length.
- Ineffective length of a broken CNT is also affected by the volume fraction. Ineffective lengths of the broken CNT in CNT/epoxy composites with a small debonding decrease with increase in volume fractions. The increase in ineffective length with volume fraction is significant in the range of volume fraction from 3.06% to 10.31%. However there is not much difference in ineffective length for the volume fractions of 0.56% to 3.06%.
- Incorporation of non-linear stress-strain relation of CNT not only estimates normal stress much less than that from linear model but also estimates lower (two times less for CNT/epoxy composite at CNT volume fraction of 3.06%) ineffective length for the broken fiber. This is true for all the CNT-reinforced composites. Thus not incorporating non-linear model actually overestimates both normal stress and ineffective length especially at higher strain.
- In the vicinity of the broken CNT, stress redistribution take place and interfacial normal and shear stress are induced at the interface of broken CNT and matrix.

- The magnitude of such interfacial stresses depend upon the loading and in the present case of axial loading along the fiber direction, it was observed that interfacial shear stress (τ_{rz}) is only significant (*r*: radial and *z*: longitudinal).
- Not incorporating non-linear stress-strain relation in the model leads to overestimation of interfacial shear stress in both the cases of CNT/epoxy and CNT/Ti composites with a small debonding. Thus once again it could be concluded that to get accurate result the non-linear stress-strain relation of CNT must be incorporated in the CNT-reinforced composites.
- Interfacial shear stresses (IFSS) induced are sensitive to the stiffness of the matrix materials. As stiffness of matrix materials increase the magnitude of IFSS (τ_{rz}) increase. In the same line as volume fraction increase the magnitude of IFSS (τ_{rz}) also increase.
- As expected the breaking of one CNT leads to overloading of the adjacent CNT and stress concentration factor (SCF) in the adjacent CNT depends on the stiffness of matrix and volume fraction. As stiffness of matrix material increases the SCF increases for a strain of 14%. In the same line as volume fraction increase the SCF also increase.
- Degree of over loading is also decided by the stiffness of the matrix materials and in consistence with the ineffective length as stiffness increases the SCF decreases for a strain of 1.5%.
- In the case of a CNT composite with a fiber break, the debonding of the fiber from the matrix is a mixed mode problem and which mode will dominate depends upon the relative values of SERR in each mode. In the present problem of axial loading only mode II is the dominant mode and the other two modes are absent. As a consequence, mode I SERR $G_I = 0$, mode III SERR $G_{III} = 0$ and mode II SERR G_{II} is only responsible for debonding in the case of axially loaded CNT/epoxy composites.
- Adjacent intact CNTs experience a stress concentration as a consequence of over loading which may lead to breaking of the adjacent intact CNTs, leading to progressive failure of CNTs and finally the failure of nanocomposites.
- The magnitude of SERR depends upon the type of the matrix materials.

- The SERRs of CNT/epoxy composites vary with volume fraction. Initially the value of SERR increases with the increase in volume fraction attains the maximum value at a particular volume fraction and then decreases with further increase in volume fraction. But in case CNT/Al composite the value of SERR increases with the increase in volume fraction and after a particular volume fraction a constant SERR observed.
- In the present case maximum SERR is observed to be at CNT volume fraction of 1% in CNT/epoxy composite.
- Critical SERR of CNT composites having a small fiber matrix debonding could be calculated using virtual crack closure integral and quadratic stress criterion.
- The critical SERRs of CNT composites depend on volume fraction.
- For the case of CNT/epoxy composite the value of critical SERR initially increases with the increase in volume fraction and then decreases with further increase in volume fraction. However, the actual value of critical SERR shows a continuous decrease with increase in volume fraction in the range of 0.56% to 10.31%.

6.3 Scopes for the future work

This thesis presents the determination of elastic properties, stress distribution and calculation of critical strain energy release rate to predict failure of CNT-reinforced composites. But the present analysis is limited to

(i) long and continuous CNTs,

(ii) the cases where orientation of CNTs in matrix are aligned and

(iii) only mechanical loading.

Therefore the present work could be extended to

(i) the cases of different orientations of the CNTs in CNT reinforced composite

(ii) the stress analysis of CNT composites under combined thermo-mechanical loading

(iii) the analysis of CNT-reinforced laminated composites considering different types of defects like delamination and debonding

(iv) the fabrication and testing of CNT-reinforced laminated composites.

References

[1] Feynman RP (1992). There's plenty of room at the bottom. *Journal of Microelectromechanical systems* 1(1), 60-66.

[2] Taniguchi N (1974). On the Basic Concept of 'Nano-Technology'. In *Proc. Intl. Conf. Prod. Eng.*, Tokyo, Part II, Japan Society of Precision Engineering, pp.18-23.

[3] Iijima S (1991). Helical microtubules of graphitic carbon. *Nature* 34, 56-58.

[4] Lau K-T and Hui D (2002). The revolutionary creation of new advanced materials - carbon nanotube composites. *Composites: Part B* 33(4), 263-77.

[5] Thostenson ET, Ren Z and Chou T-W (2001). Advances in the science and technology of carbon nanotubes and their composites: a review. *Composites Science and Technology* 61(13), 1899-1912.

[6] Dresselhaus MS, Dresselhaus G and Saito R (1995). Physics of carbon nanotubes. *Carbon* 33(7), 883-891.

[7] Lu JP (1997). Elastic properties of carbon nanotubes and nanoropes. *Physical Review Letters* 79(7), 1297-1300.

[8] A computer generated model of multiwalled carbon nanotube. Available at: http://www.essentialchemicalindustry.org/materials-and-applications/nanomaterials.html (Accessed: 04 July, 2016).

[9] Lund JR and Byrne JP (2001). Leonardo da Vinci's tensile strength tests: implications for the discovery of engineering mechanics. *Civil Engineering and Environmental System* 18(3), 243-250.

[10] Odegard GM, Gates TS, Nicholson LM and Wise KE (2002). Equivalent-continuum modeling of nano-structured materials. *Composites Science and Technology* 62(14), 1869-1880.

[11] Li C and Chou T-W (2003). A structural mechanics approach for the analysis of carbon nanotubes. *International Journal of Solids and Structures* 40(10), 2487-2499.

[12] Tserpes KI and Papanikos P (2005). Finite element modeling of single-walled carbon nanotubes. *Composites: Part B* 36(5), 468-477.

[13] Kirtania S and Chakraborty D (2007). Finite element based characterization of carbon nanotubes. *Journal of Reinforced Plastics and Composites* 26(15), 1557-1570.

[14] Lu X and Hu Z (2012). Mechanical property evaluation of single-walled carbon nanotubes by finite element modeling. *Composites: Part B* 43(4), 1902-13.

[15] Kwon Y-K, Berber S and Tomanek D (2004). Thermal contraction of carbon fullerenes and nanotubes. *Physical Review Letters* 92(1), 015901-1- 015901-4.

[16] Jiang H, Liu B, Huang Y and Hwang KC (2004). Thermal expansion of single wall carbon nanotubes. *Journal of Engineering Materials and Technology* 126, 265-270.

[17] Maniwa Y, Fujiwara R, Kira H, Tou H, Kataura H, Suzuki S, Achiba Y, Nishibori E, Takata M, Sakata M, Fujiwara A and Suematsu H (2001). Thermal expansion of single-walled carbon nanotube (SWNT) bundles: X-ray diffraction studies. *Physical Review B* 64(24), 241402-1-241402-3.

[18] Yengejeh SI, Kazemi SA and Oechsner (2016). Advances in mechanical analysis of structurally and atomically modified carbon nanotubes and degenerated nanostructures: A review. *Composites Part B* 86, 95-107.

[19] Belytschko T, Xiao SP, Schatz GC, and Ruoff RS (2002). Atomistic simulation of nanotube fracture. *Physical Review B* 65(23), 235430-1-8.

[20] Tserpes KI, Papanikos P and Tsirkas SA (2006). A progressive fracture model for carbon nanotubes. *Composites: Part B* 37(7-8), 662-669.

[21] Thostenson ET and Chou TW (2006). Fracture mechanisms in carbon nanotube-reinforced composites. In *Fracture of Nano and Engineering Materials and Structures*, Springer, Netherlands, Part B (Subpart IT9), pp. 95-96.

[22] Vaez A Jalili S (2012). *Ab initio s*tudy of defected single walled carbon nanotubes. *Journal of Computational and Theoretical Nanoscience* 9(8), 1059-1062.

[23] Feng C and Liew KM (2011). Fracture properties of defective carbon nanorings. *Journal of Computational and Theoretical Nanoscience* 8(1), 1-7.

[24] Talukdar K and Mitra AK (2011). Changes in mechanical properties and fracture behavior of single wall carbon nanotubes on bundle formation. *Journal of Computational and Theoretical Nanoscience* 8(9), 1882-1887.

[25] Tuzun B and Erkoc S (2012). Structural and electronic properties of unusual carbon nanorods. *Quantum Matter* 1(2), 136-148.

[26] Moelhave K, Gudnason SB, Pedersen AT, Clausen CH, Horsewell A and Boeggild P (2006). Transmission electron microscopy study of individual carbon nanotube breakdown caused by Joule heating in air. *Nano Letters* 6(8), 1663-1668.

[27] Xiao JR, Gama BA and Gillespie Jr JW (2005). An analytical molecular structural mechanics model for the mechanical properties of carbon nanotubes. *International Journal of Solids and Structure* 42(11-12), 3075-3092.

[28] Yu MF, Lourie O, Dyer MJ, Moloni K, Kelly TF and Ruoff RS (2000). Stregth and breaking mechanism of multiwalled carbon nanotubes under tensile load. *Science* 287, 637-640.

[29] Endo M, Hayashi T and Kim Y-A (2006). Large-scale production of carbon nanotubes and their applications. *Pure Applied Chemistry* 78(9), 1703-1713.

[30] Volder MLF De, Tawfick SH, Baughman RH and Hart J (2013). Carbon nanotubes: Present and future commercial applications. *Science* 339, 535-539.

[31] Vohrera U, Kolaricb I, Haqueb MH, Rothc S and Weglikowskac UD (2004). Carbon nanotube sheets for the use as artificial muscles. *Carbon* 42(5-6), 1159-1164.

[32] Chen WX, Tu JP, Wang LY, Gan HY, Xu ZD and Zhang XB (2003). Tribological application of carbon nanotubes in a metal-based composites coating and composites. *Carbon* 41(2), 215-222.

[33] Sinha N, Ma J and Yeow JTW (2006). Carbon nanotube-based sensors. *Journal of Nanoscience and Nanotechnology* 6(3), 573-590.

[34] Li C, Thostenson ET and Chou TW (2008). Sensors and actuators based on carbon nanotubes and their composites: A review. *Composites Science and Technology* 68(6), 1227-1249.

[35] Peigney A, Laurent Ch, Flahaut E, Bacsa RR and Rousset A (2001). Specific surface area of carbon nanotubes and bundles of carbon nanotubes. Carbon 39, 507-514.

[36] Harris PJF (2009). *Carbon Nanotube Science: Synthesis, Properties and Applications*. Cambridge University Press.

[37] Nahas MN (2012). Finite element modeling of carbon nanotubes and their composites. In *computational finite element methods in nanotechnology*, CRC Press, Chapter 8, pp. 291-310.

[38] Lau K-T, Hui D (2002). Effectiveness of using carbon nanotubes as nano-reinforcements for advanced composites structures. *Carbon* 40(9), 1605-06.

[39] Jia Z, Wang Z, Xu C, Liang Ji, Wei B, Wu D and Zhu S (1999). Study on poly(methyl methacrylate)/carbon nanotube composites. *Materials Science and Engineering A* 271, 395-400.

[40] Pal G and Kumar S (2016). Modeling of carbon nanotubes and carbon nanotube-polymer composites. *Progress in Aerospace Sciences* 80, 33-58.

[41] Bakshi SR, Lahiri D and Agarwal A (2010). Carbon nanotube reinforced metal matrix composites – a review. *International Matererials Review* 55(1), 41-64.

[42] Cho J, Boccaccini AR and Shaffer MSP (2009). Ceramic matrix composites containing carbon nanotubes. *Journal of Materials Science* 44(8), 1934-51.

[43] Tjong SC (2009). Carbon Nanotube Reinforced Composites – Metal and Ceramic Matrices. Wiley-VCH Verlag GmbH & Co. Germany.

[44] Wagner HD, Lourie O, Feldman Y and Tenne R (1998). Stress-induced fragmentation of multiwall carbon nanotubes in a polymer matrix. *Applied Physics Letters* 72(2), 188-90.

[45] Andrews R, Jacques D, Rao AM, Rantell T, Derbyshire F, Chen Y, Chen J, and Haddon RC (1999). Nanotube composite carbon fibers. *Applied Physics Letters* 75(9), 1329-1331.

[46] Bastwros MMH, Esawi AMK and Wifi A (2013). Friction and wear behavior of Al-CNT composites. *Wear* 307, 164-173.

[47] Guo Y, Cho H, Shi D, Lian J, Song Y, Abot J, Poudel B, Ren Z, Wang L and Ewing C (2007). Effect of plasma surface modification on interfacial behaviors and mechanical properties of carbon nanotube-Al_2O_3 nanocomposites. *Applied Physics Letters*. 91(26), 261903-1-261903-3.

[48] Fan J-P, Zhuang D-M, Zhao D-Q, Zhang G, Wu M-S, Wei F, and Fan Z-J (2006). Toughening and reinforcing alumina matrix composite with single-wall carbon nanotubes. *Applied Physics Letters* 89(12), 121910-1-121910-3.

[49] Shimizu Y (2011). High strength magnesium matrix composites reinforced with carbon nanotube. In: *Magnesium Alloys - Design, Processing and Properties*, Edited by Czerwinski F, InTech, pp.491-500.

[50] Ashrafi B, Hubert P and Vengallatore S (2006). Carbon nanotube-reinforced composites as structural materials for microactuators and microelectromechanical system. *Nanotechnology* 17(19), 4895-4903.

[51] Kausar A, Rafique I and Muhammad B (2016). A review on applications of polymer/carbonnanotube and epoxy/CNT composites. *Polymer-Plastics Technology and Engineering* 55(11), 1167-1191.

[52] Hayashi T and Endo M (2011). Carbon nanotube as structural material and their application in composites. *Composites Part B* 42, 2151-2157.

[53] Park C, Ounaies Z, Watson KA, Pawlowski K, Lowther SE, Connell JW, Siochi EJ, Harrison JS and St. Clair TL (2002). Polymer-single Wall Carbon Nanotube Composites for Potential Spacecraft Applications. Making Functional Materials with Nanotubes Symposium (Materials Research Society Symposium Proceedings) 706, 91–96.

[54] Liu T, Sreekumar TV, Kumar S, Hauge RH and Smalley RE (2003). SWNT/PAN composites film-based supercapacitors. *Carbon* 41(12), 2440-2442.

[55] Isaza C, Sierra G and Meza JM (2016). A novel technique for production of metal matrix composites reinforced with carbon nanotubes. *Journal of Manufacturing Science and Engineering* 138, 024501-1-024501-4.

[56] Tang Y, Cong H, Zhong R and Cheng HM (2004). Thermal expansion of a composite of single-walled carbon nanotubes and nanocrystalline aluminum. *Carbon* 42(15), 3260-3262.

[57] Chu K, Wu Q, Jia C, Liang X, Nie J, Tian W, Gai G and Guo H (2010). Fabrication and effective thermal conductivity of multi-walled carbon nanotubes reinforced Cu matrix composites for heat sink applications. *Composites Science and Technology* 70(2), 298-304.

[58] Ohnabe H, Masakia S, Onozukaa M, Miyaharab K and Sasab T (1999). Potential application of ceramic matrix composites to aero-engine components. *Composites: Part A* 30(4), 489–496.

[59] Nam TH, Goto K, Yamaguchi Y, Premalal EVA, Shimamura Y, Inoue Y, Arikawa S, Yoneyama S and Ogihara S (2016). Improving mechanical properties of high volume fraction aligned multi-walled carbon nanotube/epoxy composites by stretching and pressing. *Composites: Part B* 85, 15-23.

[60] Thostenson ET and Chou TW (2002). Aligned multi-walled carbon nanotube-reinforced composites: processing and mechanical characterization. *Journal of Physics D: Applied Physics* 35(16), L77-L80.

[61] Cheng QF, Wang JP, Wen JJ, Liu CH, Jiang KL, Li QQ and Fan SS (2010). Carbon nanotube/epoxy composites fabricated by resin transfer molding. *Carbon*, 48(1), 260-66.

[62] Jin L, Bower C and Zhou O (1998). Alignment of carbon nanotubes in polymer matrix by mechanical stretching. *Applied Physics Letters* 73(9), 1197-1199.

[63] Wardle BL, Saito DS, Garcıa EJ, Hart AJ, Villoria RG De and Verploegen EA (2008). Fabrication and characterization of ultrahigh-volume-fraction aligned carbon nanotube–polymer composites. Advance Materials 20, 2707-2714.

[64] Bradford PD, Wang X, Zhao H, Maria JP, Jia Q and Zhu YT (2010). A novel approach to fabricate high volume fraction nanocomposites with long aligned carbon nanotubes. *Composites Science and Technology* 70(3), 1980-1985.

[65] Kwon H, Estili M, Takagi K, Miyazaki T and Kawasaki A (2009). Combination of hot extrusion and spark plasma sintering for producing carbon nanotune reinforced aluminum matrix composites. *Carbon* 47(3), 570-577.

[66] Esawi AMK, Morsi K, Sayed A, Taher M and Lanka S (2010). Effect of carbon nanotube (CNT) content on the mechanical properties of CNT-reinforced aluminium composites. *Composites Science and Technology* 70(16), 2237-2241.

[67] Chen Q, Chai G and Li B (2005). Exploration study of multifunctional metallic nanocomposite utilizing single-walled carbon nanotubes for micro/nano devices. *Proceedings of the Institute of Mechanical Engineers, Part N: Journal of Nanoengineering and Nanosystems* 219(2), 67-72.

[68] Goh CS, Wei J, Lee LC and Gupta M (2006). Simultaneous enhancement in strength and ductility by reinforcing magnesium with carbon nanotubes. *Materials Science and Engineering A* 423(1-2), 153-156.

[69] Uddin SM, Mahmud T, Wolf C, Glanz C, Kolaric I, Vilkmer C, Holler H, Wienecke U, Roth S and Fecht H-J (2010). Effect of size and shape of metal particles to improve hardness and electrical properties of carbon nanotube reinforced copper and copper alloy composites. *Composites Science and Technology* 70(16), 2253-2257.

[70] Chai G, Sun Y, Sun JJ and Chen Q (2008). Mechanical properties of carbon nanotube-copper nanocomposites. *Journal of Micromechanics and Microengineering* 18(3), 035013-1-4.

[71] Kuzumaki T, Ujiie O, Ichinose H and Ito K (2000). Mechanical characteristics and prepation of carbon nanotubes fiber-reinforced Ti composite. *Advanced Engineering Materials* 2(7), 416-418.

[72] Pal A, Mukherjee S, Das GC and Mitra MK (2011). Synthesis and characterization of CNT reinforced alumina based nanocomposites. *Transactions of Indian Ceramic Society* 70(4), 215-20.

[73] Zhan G-D, Kuntz JD, Wan J and Mukherjee AK (2003). Single-wall carbon nanotubes as attractive toughening agents in alumina-based nanocomposites. *Nature Matererials*, 2(1), 38-42.

[74] Zhang T, Kumari L, Du GH, Li WZ, Wang QW, Balani K and Agarwal A (2009). Mechanical properties of carbon nanotube-alumina nanocomposites synthesized by chemical vapor deposition and spark plasma sintering. *Composites: Part A* 40(1), 86-93.

[75] Qian D, Dickey EC, Andrews R and Rantell T (2000). Load transfer and deformation mechanisms in carbon nanotube-polystyrene composites. *Applied Physics Letters* 76(20), 2868-2870.

[76] Liu YJ and Chen XL (2003). Evaluations of the effective material properties of carbon nanotube-based composites using a nanoscale representative volume element. *Mechanics of materials* 35(1-2), 69-81.

[77] Chen XL and Liu YJ (2004). Square representative volume elements for evaluating the effective material properties of carbon nanotube-based composites. *Computational Materials Science* 29(1), 1-11.

[78] Alamry ANS, Prusty BG, Mada MR and Bandyopadhyay S (2014). Improved crack resistance and fracture toughness using MWCNT modified epoxy for delaminated composite structures *Procedia Materials Science* 3, 805–810.

[79] Nahas MN and Alzahrani, MA (2012). Finite element analysis of the effective mechanical properties of a nano scale cubic element of epoxy reinforced with monolayer graphene. *Journal of Computational and Theoretical Nanoscience* 9(5), 707-710.

[80] Zuberi MJS and Esat V (2015). Investigating the mechanical properties of single walled carbonnanotube reinforced epoxy composite through finite element modeling. *Composites: Part B* 71, 1–9.

[81] Han Y and Elliott J (2007). Molecular dynamics simulations of the elastic properties of polymer/carbon nanotube composites. *Computational Materials Science* 39(2), 315-323.

[82] Lau KT, Shi SQ and Cheng HM (2003). Micro-mechanical properties and morphological observation on fracture surfaces of carbon nanotube composites pre-treated at different temperatures. *Composites Science and Technology* 63(8), 1161-1164.

[83] Lusti HR and Gusev AA (2004). Finite element predictions for the thermoelastic properties of nanotube reinforced polymers. *Modelling and simulation in Materials Science and Engineering*. 12, S107-S119.

[84] Sul JH, Prusty BG and Kelly DW (2014). Application of molecular dynamics to evaluate the design performance of low aspect ratio carbon nanotubes in fibre reinforced polymer resin *Composites: Part A* 65, 64-72.

[85] Sul JH, Prusty BG and Crosky A (2015). Effect of the addition of multi-walled carbon nanotubes on the thermomechanical properties of epoxy resin. *Polymer Composites* DOI 10.1002/pc.23757.

[86] Kundalwal SI and Meguid SA (2015). Micromechanics modeling of the effective thermoelastic response of nano-tailored composites. *European Journal of Mechanics A/Solids* 53, 241-253.

[87] Dong C (2014). Mechanical and thermo-mechanical properties of carbon nanotube reinforced composites. *International Journal of Smart and Nano Materials* 5(1), 44-58.

[88] Guo H, Sreekumar TV, Liu T, Minus M, Kumar S (2005). Structure and properties of polyacrylonitrile/single wall carbon nanotube composites films. *Polymer* 46, 3001-3005.

[89] Alian AR, Kundalwal SI and Meguid SA (2015). Multiscale modeling of carbon nanotube epoxy composites. *Polymer* 70, 149-160.

[90] Chwal M and Muc A (2016). Transversely isotropic properties of carbon nanotube/ olymer composites. *Composites Part B* 88, 295-300.

[91] Si-nian L, Shou-zhi S, Tian-qing YU, Hui-min C, You-shou Z and Jin-long S (2004). Properties and structure of magnesium matrix composite reinforced with CNTs. *Journal of Wuhan University and Technology – Mater. Sci. Ed.* 19(1), 65-68.

[92] Thotsaphon T, Katsuyoshi K, Junko U and Hisashi I (2008). Friction and wear behavior of titanium matrix composite reinforced with carbon nanotubes under dry conditions. *Transactions of JWRI* 37(2), 51-56.

[93] Hassan MTZ, Esawi AMK and Metwalli S (2014). Effect of carbon nanotube damage on the mechanical properties of aluminium–carbon nanotube composites. *Journal of Alloys and Compounds* 607, 215–222.

[94] Kaewsai D, Watcharapasorn A, Singjai P, Wirojanupatump S, Niranatlumpong P and Jiansirisomboon S (2010). Thermal sprayed stainless steel/carbon nanotube composite coatings. *Surface and Coatings Technology* 205(7), 2104–2112.

[95] Rahmat M and Hubert P (2011). Carbon nanotube–polymer interactions in nanocomposites: A review. *Composites Science and Technology* 72(1), 72–84.

[96] Liao K and Li S (2001). Interfacial characteristics of a carbon nanotubes-polystyrene composite system. *Applied Physics Letters* 79(25), 4225-4227.

[97] Cooper CA, Cohen SR, Barber AH and Wagner HD (2002). Detachment of nanotubes from a polymer matrix. *Applied Physics Letters* 81(20), 3873-3875.

[98] Barber AH, Cohen SR and Wagner HD (2003). Measurement of carbon nanotube-polymer interfacial strength. *Applied Physics Letters* 82(23), 4140-4142.

[99] Chowdhury SC and Okabe T (2007). Computer simulation of carbon nanotube pull-out from polymer by the molecular dynamics method. *Composites: Part A* 38(3), 747–754.

[100] Montazeri A, Javadpour J, Khavandi A, Tcharkhtchi A and Mohajeri A (2010). Mechanical properties of multi-walled carbon nanotube/epoxy composites. *Materials and Design* 31, 4202-4208.

[101] Schadler LS, Giannaris SC and Ajayan PM (1998). Load transfer in carbon nanotube epoxy composites. *Applied Physics Letters* 73(26), 3842-3844.

[102] Zhu Y-F, Chen W-J, Jiang Y and Wand FY (2012). Effects of structure characteristics of carbon nanotubes on properties of composites. *Journal of Reinforced Plastics and Composites* 31(16), 1097-1102.

[103] Wang H, Meng F and Wang X (2010). Transfer characteristics of interfacial stresses between carbon nanotubes and matrix. *Journal of Reinforced Plastics and Composites* 29(15), 2262-78.

[104] Romanov VS, Lomov SV, Verpoest I and Gorbatikh L (2015). Modelling evidence of stress concentration mitigation at the micro-scale in polymer composites by the addition of carbon nanotubes. *Carbon* 82, 184-194.

[105] Xiong QL and Meguid SA (2015). Atomistic investigation of the interfacial mechanical characteristics of carbon nanotube reinforced epoxy composites. *European Polymer Journal* 69, 1-15.

[106] Frankland SJV, Harik VM, Odegard GM, Brenner DW and Gates TS (2003). The stress-strain behavior of polymer-nanotube composites from molecular dynamics simulations. *Composites Science and Technology* 60(11), 1655-1661.

[107] Tzeng SH and Tsai JL (2011). Investigating the stress distribution of single walled carbon nanotubes embedded in polyimide nanocomposites. *Journal of Reinforced Plastics and Composites* 30(11), 922-931.

[108] Mora RJ, Vilatela JJ and Windle AH (2009). Properties of composites of carbon nanotube fibres. *Composites Science and Technology* 69(10), 1558-1563.

[109] Xiao KQ and Zhang LC (2004). The stress transfer efficiency of a single-walled carbon nanotube in epoxy matrix. *Journal of Materials Science* 39(14), 4481-86.

[110] Gao X-L and Li K (2005). A shear-lag model for carbon nanotube-reinforced polymer composites. *International Journal of Solids Structures* 42(5-6), 1649-1667.

[111] Li K and Saigal S (2007). Micromechanical modeling of stress transfer in carbon nanotube reinforced polymer composites. *Materials Science and Engineering A* 457(1-2), 44-57.

[112] Meguid SA, Sun Y (2004). On the tensile and shear strength of nano-reinforced composites interfaces. *Materials and Design* 25, 289-96.

[113] Ci L and Bai J (2006). The reinforcement role of carbon nanotubes in epoxy composites with different matrix stiffness. *Composites Science and Technology* 66(3-4), 599-603.

[114] Mohammadpour E, Awang M, Kakooei S and Md Akil H (2014). Modeling and tensile stress-strain response of carbon nanotube/polypropylene nanocomposites using nonlinear representative volume element. *Materials and Design*. 58, 36-42.

[115] Li C and Chou T-W (2003). Multiscale modeling of carbon nanotube reinforced polymer composites. *Journal of Nanoscience and Nanotechnology* 3(6), 423-430.

[116] Haque A and Ramasetty A (2005). Theoretical study of stress transfer in carbon nanotube reinforced poly matrix composites. *Composite Structures* 71(1), 68-77.

[117] Tserpes KI, Papanikos P, Labeas G and Pantelakis Sp. G (2008). Multi-scale modeling of tensile behavior of carbon nanotube-reinforced composites. *Theoretical and Applied Fracture Mechanics* 49(1), 51-60.

[118] Shokrieh MM and Rafiee R (2010). On the tensile behavior of an embedded carbon nanotube in polymer matrix with non-bonded interphase region. *Composite Structure* 92(3), 647-652.

[119] Spanos KN, Georgantzinos SK and Anifantis NK (2014). Investigation of stress transfer in carbon nanotube reinforced composites using a multi-scale finite element approach. *Composites: Part B* 63, 85-93.

[120] Boesl B, Lahiri D, Behdad S and Agarwal A (2014). Direct observation of carbon nanotube induced strengthening in aluminum composite via in situ tensile tests. *Carbon* 69, 79-85.

[121] Choi BK, Yoon GH and Lee S (2016). Molecular dynamics studies of CNT-reinforced aluminum composites under uniaxial tensile loading. *Composites Part B* 91, 119-125.

[122] Choi H, Shin J, Min B, Park J and Bae D (2009). Reinforcing effects of carbon nanotubes in structural aluminum matrix nanocomposites. *Journal of Material Research* 24(8), 2610-2616.

[123] Fereidoon A, Rajabpour M and Hemmatian H (2013). Fracture analysis of epoxy/SWCNT nanocomposite based on global-local finite element model. *Composites Part B* 54, 400-408.

[124] Ayatollahi MR, Shadlou S and Shokrieh MM (2011). Fracture toughness of epoxy/multi-walled carbon nanotube nano-composites under bending and shear loading conditions. *Materials and Design* 32, 2115-2124.

[125] Rafiee R, Fereidoon A and Heidarhaei M (2012). Influence of non-bonded interphase on crack driving force in carbon nanotube reinforced polymer. *Computational Materials Science* 56, 25–28.

[126] Kuronuma Y, Shindo Y, Takeda T and Narita F (2009). Fracture behavior of cracked carbon nanotubes-based polymer composites: Experiments and finite element simulations. *Fatugue and Fracture of Engineering Materials and Structures* 33, 87-93.

[127] Joshi UA, Sharma SC and Harsha SP (2012). Analysis of fracture in carbon nanotube based composites using extended finite element method. *Journal of Computational and Theoretical Nanoscience* 9(6), 872-878.

[128] Jia Y, Chen Z and Yan W (2015). A numerical study on carbon nanotube pullout to understand its bridging effect in carbon nanotube reinforced composites. *Composites Part B* 81, 64-71.

[129] Lei S, Zhu Y-F, Chan Z and Ji L (2008). Heterocoagulation system assisted adsorption of carbon nanotubes on alumina for toughening ceramics. *Journal of Reinforced Plastics and Composites* 27(3), 245-253.

[130] Li C and Chou TW (2009). Failure of carbon nanotube/polymer composites and the effect of nanotube waviness. *Composites: Part A* 40(10), 1580-1586.

[131] Chen YL, Liu B, He XQ, Huang Y and Hwang KC (2010). Failure analysis and the optimal toughness design of carbon nanotube-reinforced composites. *Composites Science and Technology* 70(9), 1360-1367.

[132] Chen Y, Wang Z, Wang S, Zhou Z, Zhang J and Liu B (2015). Carbon nanotube reinforced composites: the smaller diameter, the higher fracture toughness? *Journal of Applied Mechanics* 82(8), 081009-081009-14.

[133] Chen B, Li S, Imai H, Umeda J, Takahashi M and Kondoh K (2015). Inter-wall bridging induced peeling of multi-walled carbon nanotubes during tensile failure in aluminum matrix composites. *Micron* 69, 1-5.

[134] Yamamoto G, Shirasu K, Hashida T, Takagi T, Suk JW, An J, Piner RD and Ruoff RS (2011). Nanotube fracture during the failure of carbon nanotube/alumina composites. *Carbon* 49(12), 3709-16.

[135] Tay TE, Liu G, Tan VBC, Sun XS and Pham DC (2008). Progressive failure analysis of composites. *Journal of Composite Materials* 42(18), 1921-1946.

[136] Irwin GR (1957). Analysis of stresses and strains near the end of a crack traversing a plate. *Journal of Applied Mechanics* 24, 361-363.

[137] Xie D and Jr. Biggers SB (2006). Strain-energy release rate calculation for a moving delamination front of arbitrary shape based on the virtual crack closure technique. Part I: Formulation and validation. *Engineering Fracture Mechanics* 73(6), 771-85.

[138] Venkatesha KS, Ramamurthy TS and Dattaguru B (1996). Generalized modified crack closure integral (GMCCI) and its application to interface crack problems. *Computers Structures* 60(4), 665-676.

[139] Brewer JC and Lagace PA (1988). Quadratic stress criterion for initiation of delamination. *Journal of Composite Materials* 22(12), 1141-1155.

[140] Faulkner SD, Kwon YW, Bartlett S and Rasmussen EA (2009). Study of composite joint strength with carbon nanotube reinforcement. *Journal of Materials Science* 44(11), 2858-64.

[141] Herakovich CT (1998). *Mechanics of Fibrous Composites*. New York: John Wiley & Sons, pp.406.

[142] Schepery RA (1968). Thermal expansion coefficient of composite materials based on energy principle. *Journal of Composite Materials* 2(3), 380-404.

[143] Nedele MR and Wisnom MR (1994). Three-dimensional finite element analysis of the stress concentration at a single fiber break. *Composites Science and Technology* 51(4), 517-524.

[144] Meyyappan M (2005). *Carbon Nanotubes: Science and Applications*. CRC Press LLC.

[145] Treacy MMJ, Ebbesen TW and Gibson JM (1996). Exceptionally high Young's modulus observed for individual carbon nanotubes. *Nature* 381, 678-80.

[146] Mukerji J (1993). Ceramic matrix composites. *Defence Science Journal* 43(4), 385-95.

[147] Taniguchi N, Nishiwaki T, Hirayama N, Nishida H and Kawada H (2009). Dynamic tensile properties of carbon fiber composite based on thermoplastic epoxy resin loaded in matrix dominant directions. *Composites Science and Technology* 69(2), 207-2013.

[148] Daniel IM and Ishai O (2006). *Engineering Mechanics of Composite Materials*. 2nd ed. New York: Oxford University Press, pp.114-115 and pp.374-378.

[149] Han B, Yu X and Know E (2009). A self-sensing carbon nanotube/cement composite for traffic monitoring. *Nanotechnology* 20(44), 445501 (5pp).

भारतीय प्रौद्योगिकी संस्थान गुवाहाटी
Indian Institute of Technology Guwahati

Publications from the Present Thesis Work

International Journals

1. Kirtania S and Chakraborty D (2015). Failure analysis of carbon nanotube/epoxy composites having a broken carbon nanotube. ***Journal of Reinforced Plastics and Composites*** **34(19), 1639-1647.**
2. Kirtania S and Chakraborty D (2014). Analysis of carbon nanotube-reinforced alumina matrix nanocomposites with a broken fiber. ***Journal of Reinforced Plastics and Composites*** **33(3), 389-398.**
3. Kirtania S and Chakraborty D (2014). Fracture behavior of carbon nanotube-based composites with a broken fiber using multi-scale finite element modeling. ***Journal of Computational and Theoretical Nanoscience*** **11(3), 676-684.**
4. Kirtania S and Chakraborty D (2012). Multi-scale modeling of carbon nanotube reinforced composites with a fiber break. ***Materials and Design*** **35, 498-504.**

International Conferences

1. Kirtania S and Chakraborty D (2015). Investigation of stress distribution and strain energy release rate in CNT/Aluminum composites having a broken CNT. In **the *4th International Conference on Advanced in Nanomaterials and Nanotechnology*;** December 8-11, 2015; IIT Guwahati, India.
2. Kirtania S. and Chakraborty D (2013). Multi-scale analysis of carbon nanotube (CNT)-reinforced metal matrix composites with a broken fiber. In **the *4th International Conference on Recent Advanced in Composites Materials*;** February 18-20, 2013; Goa, India.
3. Kirtania S. and Chakraborty D (2009). Evaluation of thermoelastic properties of carbon nanotube-based composites using finite element method. In **the *8th International Conference on Mechanical Engineering***; December 26-28, 2009; Dhaka, Bangladesh. Paper No. AM-13.

Book Chapters

1. Kirtania S and Chakraborty D (2013). Stress transfer characterizations at fiber break in carbon nanotube-reinforced composites. In ***Advanced Nanomaterials and Nanotechnology - Springer Proceedings in Physics*; Springer-Verlag,** Heidelberg: Vol. 143, pp. 333-346.
2. Kirtania S and Chakraborty D (2009). Finite element based determination of effective Young's modulus and coefficient of thermal expansion of carbon nanotube-based composites. In ***Modelling and Simulation in Computational Mechanics: Engineering Applications*;** LAP Lambert Acad. Publ., Germany: pp. 76-90.

भारतीय प्रौद्योगिकी संस्थान गुवाहाटी
Indian Institute of Technology Guwahati

BIOGRAPHY

Mr. Sushen Kirtania completed class X and class XII in the year 1993 and 1995 respectively both from West Bengal State Boards. He received his Bachelor of Engineering in Mechanical Engineering from Bengal Engineering College (Deemed University), Shibpur, West Bengal, India in the year 2001 and was placed in the first class. He did his Maters of Technology (MTech) in Machine Design from Mechanical Engineering Department of Indian Institute of Technology (IIT) Guwahati, Assam, India in the year 2006. Since August 2008, Mr Kirtania has been working as an Assistant Professor in the Mechanical Engineering Department of Tezpur University (Central University under Government of India) and since then he has also been continuing as a part-time PhD student in Mechanical Engineering Derpartment at IIT Guwahati.